Variation of Fission Fragment Kinetic Energy Distribution and Yield of Long Range Alpha Particles in the Resonance Neutron Induced Fission of U^{235}.

$\alpha's$

Girijesh K. Mehta

ABSTRACT

The ratio of fission yields from thick and
thin U^{235} targets was measured in the energy region
where resonances can be resolved in order to measure
the variation in the kinetic energy distribution of
fission fragments from resonance to resonance. Also,
the ternary alpha yield from a thick U^{235} sample was
compared with the thin U^{235} foil binary fission yield
for several resonances as a measure of the variation
of the yield of ternary alphas per fission from level
to level. In each set of results differences in the
ratios were observed far outside the errors. The
data were found to be incompatable with a single
average value on the basis of a Chi-square test.
The data for each set were compatable with two
values of the ratios suggesting a grouping which
may correspond to the two possible J values of the
resonances.

Our assignments of the resonances to two groups,
made on the basis of variation in kinetic energy
distribution of fission fragments, agree well with
the assignments made by Cowan, et. al. from the radio-

chemical measurements on symmetric fission for those levels with definite assignments in both sets of data. A definite physical interpretation of the results of relative variation of ternary alpha yield from resonance to resonance could not be made because of the lack of measurements on ternary alpha yield with a thin U target.

ACKNOWLEDGMENTS

CONTENTS

I. Introduction

The term fission embraces a number of associated processes. The most common and systematically studied of these is binary fission, in which the nucleus divides into two fragments of comparable size. Binary fission does not occur with a unique division of the masses; on the contrary, a wide range of fragment masses is observed. In low energy neutron induced fission, the most probable mass splitting is that into two unequal fragments, and the yield for fragments of equal mass is very low. There are thus two groups of fragments formed, a light group and a heavy group, which give rise to the double-humped mass distribution curve. The valley between the two peaks represents symmetric fission, corresponding to the equal mass split.

Although the Bohr and Wheeler[1] liquid drop model of fission does not rule out the possibility of fission into three fragments of roughly equal masses, as suggested by Present[2], indications are that only rarely (perhaps once in 10^4 or less) is there division into three large fragments[3]. Another kind of tripartite fission was observed by Alvarez[4] in the case of slow neutron fission of U^{235} where a long range light nucleus is

emitted in coincidence with two heavy fragments
of the conventional type. The work of Allen and
Dewan[5], and Fulmer and Cohen[6] established that
the long range particles produced in fission are
alpha particles in the overwhelming majority of cases.
It has been reported that other particles (p, d, H^3,
He^3) also occur as the third particle in tripartite
fission, but there is a great deal of evidence[7] to
show that such fission is extremely rare.

The mode of fission, where a long range alpha
particle is emitted along with the two heavy frag-
ments, will be referred in this work as "ternary
fission", and the long range alpha particles as
"ternary alphas". The emission of ternary alpha
particles in fission has been studied by many
investigators, and the results are summarized in
the reviews by Hyde[8], Halpern[9] and Perfilov[10].
The alpha particles emitted in U^{235} fission have an
energy spectrum extending up to 29 MeV, with a broad
peak at 15 MeV. The angular distribution of the
alpha particles shows a strong peaking at an angle
a few degrees less than 90° with respect to the
direction of the lighter of the two fragments.
These observations on the energy and the angular
distributions are consistent with the picture[11]
in which the alpha particle is emitted from a

region between the fragments and not emitted by
the moving fragments.

Ternary fission has so far not been studied
as extensively as other aspects of fission, perhaps
because of its low probability (typically one alpha
particle in several hundred fissions). Nevertheless,
because of the time and place at which the alpha
particles are supposed to be emitted, an investi-
gation of ternary fission is expected to contribute
to our understanding of the actual scission stage
in nuclear fission.

All of this is by way of introduction to the
motivation for this work which was the search for
methods of determining J values of resonance levels.
All nuclei having non-zero spin (I), can form, with
the addition of an S wave neutron, compound nuclei
with two possible values of angular momentum, de-
noted by $J = I \pm \frac{1}{2}$. For example, U^{235}, with a
nuclear spin of $7/2^-$, can form a compound nucleus
with $J = 3^-$ or $J = 4^-$. The measurement of the
angular momenta associated with slow neutron reson-
ances is desirable in order to study any property
of a series of levels of a given nucleus, e.g. to
investigate the statistical properties of nuclear
levels, or to test the spin assignments made in
multilevel fits to the cross-section data. Two

basic methods of determining J values are available: (1) measurement of the total cross-section of polarized nuclei with polarized neutrons, and (2) measurement of the resonance scattering and the total cross-section at the resonance peak. The first is limited to neutron energies at or near the thermal region. No application of this technique to fissile nuclides has yet been reported. Measurements of neutron resonance scattering have been successfully carried out on Pu^{239} [12], where spins have been assigned to eight levels. Though this method can be applied in principle to any fissile target, in practice the small amount of resonance scattering and large number of fast neutrons produced in fission make it very impractical. Therefore, it was desirable to look for a more practical method.

It was proposed by Bohr[13] that the nucleus at the saddle point configuration should be cold as the major part of its energy is bound in potential energy of deformation and so it should have well defined nuclear states similar to ones of nuclei at their equilibrium deformation. This would imply that the fission process is a few channel process rather than the many channel process which had previously been assumed. Thus, many of the

characteristics of fission should be strongly
influenced by the specific fission channel through
which fission occurs. This was followed by a
suggestion from Wheeler[14] that the ratio of
asymmetric to symmetric fission yields might
depend upon the J values of the resonances. This
suggestion initiated a large number of experiments
to study the shape of the mass yield curve when
fission is induced with neutrons of resonance
energy. Radiochemical measurements did show
differences in the ratio of asymmetric to symmetric
fission for the few resonances studied[15], com-
pared to the same ratio for thermal neutrons; the
largest by far is a factor of five in the case of
the 0.3 ev level of Pu^{239}. This measurement was
confirmed by the Oak-Ridge group[16] using a
back-to-back fission chamber arrangement. For U^{235}
the effect was only about 20%. All of these measure-
ments were confined to neutron energies of a few
electron volts. The only extensive information
on mass asymmetry is provided by Cowan, et. al.[17]
for U^{235} from the "spinning-wheel" experiment,
utilizing a nuclear bomb explosion as an intense
neutron source. A rotating wheel faced with U^{235}
was exposed to the neutrons from the explosion
290.5 meters away and later analized radio-

chemically. In this work a number of resonances were definitely assigned to two groups, one having a smaller and one having a larger peak-to-valley ratio (asymmetric to symmetric fission ratio) than is observed in thermal fission of U^{235}. This grouping could correspond to two different spin states.

With the advent of solid state detectors, and the availability of high intensity of neutron bursts from the Nevis synchrocyclotron, we thought it might be feasible to observe the mass distribution for a large number of levels in the resonance region, using large arrays of detectors in a back-to-back fission chamber arrangement. However, it was found subsequently by other groups that solid state detectors were not adequate for detecting the small changes expected for U^{235}. The reason for this arises from the fact that symmetric fission (which comprises the valley of the double humped mass-distribution curve) is usually a small fraction of the total number of events. A low energy tail in the resolution function (along with the inherent resolution), as well as absorption in the source and in the dead layer* distorts this valley. It is hard to observe small changes in symmetric

---

* Explained in Appendix 5.

fission yields in the presence of these extraneous effects. Nevertheless, some preliminary measurements were made with the intention of applying the method to Pu^{239}, where the expected effects are larger, and to apply some other ideas, to be discussed below, which call for looking at the extreme asymmetric fission region in order to achieve the same objective.

Symmetric fission has frequently been considered[18] to be a different mode of fission from asymmetric so that the relative proportion of the two modes may vary with the J value. An alternative explanation of this variation, at low excitation energies, can be given without postulating two fission modes. If we examine the distribution of total kinetic energy (the sum of the kinetic energies of the two fragments) and the mass distribution of the fragments for various values of total kinetic energy, as shown in figure 1, we see that the widths of the mass distribution curves and hence the relative yield of symmetric fission increases with decreasing total energy. Thus the symmetry of fission should be correlated with the total kinetic energy distribution of fission fragments. For example, if the total kinetic energy distributions for the different

J values had the same shape but the peak energy were
slightly displaced from each other, the distribution
of lower mean energy would have a larger contribution
of low energy fission and hence a higher proportion
of symmetric fission. Also, the effects on the
total kinetic energy distribution should reflect
themselves on single fragment kinetic energy dist-
ribution. These ideas were proposed by Dr. Edward
Melkonian at the Washington A.P.S. Meetings of 1963.

Guided by the above considerations, measurements
were made to look for a possible J dependence in the
kinetic energy distribution of fission fragments,
using the following fact. The yields of fission
fragments from a thick foil of uranium (thickness
much greater than the range of fission fragments)
is proportional to the range of the fragments (as
shown in Appendix 2). Thus, if the mean of the
kinetic energy distribution shifts towards higher
energy and/or the distribution becomes broader,
for the resonances corresponding to one particular
J value, it would show an effect of increased
fission yield from thick uranium target, as
compared with the yield from a thin target where
the fission fragment energy does not effect the
yield. This approach has two advantages: (1) it
calls for measurements on a thick U target and thus
gives high yield, and (2) it requires only one

detector set. Although matching of individual detectors in the set is necessary to ensure a uniform energy discrimination on all detectors, resolution requirements are not so severe as in back-to-back arrangement.

The ideas, outlined above, have another implication which can be useful. Although increased symmetric fission does indeed arise from an increase in low energy fission, the yield of extreme asymmetric fission should also increase, due to the broadening of the low energy mass yield curves. Radiochemically deduced mass yield curves for various isotopes at different incident particle energies show a trend in this direction. The practical application of this idea is that while the symmetric region is very narrow and easily contaminated, the extreme regions are better separated, and thus may be easier to study experimentally. This particular application will best be demonstrated by the planned measurements on Pu^{239} using back-to-back chamber, which were not implemented in the present set of measurements.

As a completely different approach it appeared as an interesting possibility that the ternary alpha emission might show some correlation with spin of the resonances. There was some

indication that the alpha yield is higher for symmetric than for asymmetric fission[19]. The ternary alpha yield was measured as a function of neutron energy in the resonance range where we could cover several resonances, presumably of different spin values, thus studying the effect of spin on ternary alpha emission and the connection of alpha emission with the symmetry of fission.

Three measurements were made, as functions of neutron time-of-flight:

(1) the yield of fission fragments from a thin (200 μgm/cm^2) source of U^{235}, giving a measure of the fission cross-section.

(2) the yield of fission fragments from a thick foil of U^{235} (0.005", much thicker than the range of fission fragments in U), giving when combined with (1), an indication of a possible variation of the fission fragment energy distribution from level to level, and

(3) the yield of long range alpha particles from the same thick source as in (2) but covered with 6.5 mg/cm^2 Aℓ to absorb the fission fragments and the natural alphas from U, giving when combined with (1), a measure of the variation of the yield of long range alpha particles per fission from level to level.

The variations in (3) could be expected because of two possibilities:

(a) the ternary fission probability may vary from resonance to resonance.

(b) the ternary alpha energy spectrum may differ from one resonance to other. Although at the time of this experiment there was no experimental clue for this, a very recent measurement of Michaudon, et. al.[31] has given some indication of this type of variation. This effect will produce a variation in the ternary alpha yield for thick U target, the reason being the same as explained above for fission fragments. The disentanglement of these two effects requires an additional measurement of ternary alpha yield for a thin uranium target, which was not carried out because the intensity was too low.

The pulse height information was also recorded for each of these three measurements. Along with the yield measurements, some preliminary work was also done with two sets of solid state detectors, in back-to-back arrangement, recording the energies of both the fission fragments from U^{235} (deposited on one set), as a function of the energy of the neutron inducing the fission event.

II. Experimental Equipment

A. Neutron Spectrometer

Time-of-flight neutron spectroscopy was
used to study binary and ternary fission yields as
a function of neutron energy. A schematic diagram
of the apparatus used in the experiment is shown
in Figure (2). The Columbia University Nevis
Synchrocyclotron, which is pulsed at 60 cycles
per second, was used as the pulsed neutron source.
The 350 MeV proton beam is deflected into a 3/4
inch lead target, which boils of several "evap-
oration" neutrons of about 1-10 MeV energy per
proton, producing a burst of neutrons (the bulk
of the intensity is concentrated into 20 nano-
second burst). The instantaneous evaporation
neutron intensity is about 5×10^{18} neutrons
per second. The neutrons are moderated using a
~1" thick polyethylene sheet. The system has been
described in detail[20]. A short flight path
(~10 meters) was used to achieve reasonable
counting rates.

B. Detector

Semiconductor detectors were used because
they have several advantages over other detectors.
To obtain maximum efficiency the detectors have to

cover the whole beam area, which is 4" X 8" at
~10 meters. As yet, effective junction areas
have been limited largely by the dimensions of
available silicon crystals of adequate purity.
The biggest ingot size available ($1\frac{1}{4}$ inch dia-
meter discs) was procured and the large effective
detector area was obtained through use of a form
of mosaic. Considering the problems and compli-
cations associated with having all detectors in
parallel, or all detectors in series a compromise
between the two was used. The detectors were
connected electrically in six sets of three
detectors in parallel and the resulting sets
were then connected in series. One particular
detector assembly connected this way with leads
taken out from the six sets is shown in Figure
(3). Our detector array simulates a single
large detector and only one preamplifier was used
with it. The problem of assembling the array to
cover the whole beam area was not trivial and great
care was devoted to obtain a reasonable uniformity
of response throughout the effective area. This
required matching of all the detectors in the
array, so that the output signal obtained for a
monoenergetic source is independent of the det-
ector receiving the particle. The detector
fabrication technique, response to α-particles

and fission fragments, different type of
arrays, and the matching is discussed in details
in Appendices (3), (4) and (6).

C. Fission-Chamber

A fission chamber was constructed to use
the full 4 in. X 8 in. size of the neutron beam
at the detector position at ~10 meters. The
chamber consists of an evacuated enclosure 9 in.
high, 15 in. wide, and 12 in. along the beam
direction, made of aluminum with thin windows
in front and back. It is flanked by two
electrically shielded enclosures for making
electrical connections, attaching preamplifiers,
etc. as shown in Figure (4). Inside the chamber
there is provision for mounting several banks of
surface barrier detectors. One bank of detectors
mounted in the chamber is shown in Figure (4).
The leads from the detector are taken from vacuum
to the electrically shielded enclosures through
stupikoff vacuum seals, Figure (5).

The chamber is surrounded with cadmium
to reduce the background due to low energy
neutrons, scattered by nearby objects in the
experimental area.

A "Voltage-sensitive" preamplifier was
used with the detector array instead of a

"charge-sensitive" one (which are generally used
with the semiconductor detectors) because the
charge-sensitive configuration loses its charac-
teristic (output independent of the detector
capacitance) when the detectors connected in
series are used (Appendix 7).

An RIDL Three Parameter Data Acquisition
System, hereafter called a Three Parameter System
or 3PS, was used to record the energies of the
fission fragments (or ternary alphas) as well
as the time-of-flight of the neutron which caused
the fission event. This system is described in
Appendix (9). The system uses a "Address-recording"
where the information is punched on paper tape
event by event using a mechanical punch.

D. Timing Circuit

One unit of the 3PS is used to measure
neutron time-of-flight. For this purpose the
A.D.C. of this unit is disconnected and only the
scalers are used. The time interval between the
neutron burst "START" and detector "STOP" pulses
is measured. This is done by counting the number
of cycles of some fixed frequency that occur between
"START" and "STOP" pulses.

The technique involves the use of a free
running oscillator, of a frequency higher than the

desired frequency, for fundamental timing (an 80 mc crystal oscillator is used). This in conjunction with a gated frequency dividing circuit[21], (Figure 6), which provides the gating feature and integrally divided output of the desired frequency, yields a train of stable timing pulses (in our case 20 mc pulses). The result is a "quasi-pulsed crystal oscillator" which has the frequency stability of the crystal oscillator and starts coherently with a gating signal to within one period of the crystal oscillator frequency.

The block diagram of the circuit is shown in Figure (7). The start pulse triggers a univibrator U1. The output from U1 passes through the gate G2, if there is no busy signal from the analyzer, and flips the gating flip-flop F4. When the detector stop pulse arrives, it fires U2, which then fires U3. The output from U3 resets the gating flip-flop. If desired, the neutron burst start and detector stop pulses can be delayed by choosing the widths and polarities of the U1 and U2 output pulses. The widths of the pulse from the gating flip-flop determines the time for which the gated frequency divider sends out 20 mc pulses. These

20 mc time signals pass through three flip-flop stages and the 2.5 mc output thus obtained goes to the 3PS scalers to be counted in four scaler boards providing 10^4 channels. The information collected on the three flip-flops is transferred to the spare scaler board in the 3PS and is punched on the paper tape along with the information collected on other scaler boards. If the information from these three flip-flop stages is ignored the analyzer provides .4 μsec channel width. The additional timing information collected on the flip-flops reduces the channel width to 50 nsecs.

If a neutron burst does not produce any fission event the overflow signal from the 3PS acts as an artificial stop pulse, 4 msec after the start pulse (the 4 msec arises from 10,000 channels in the system, each corresponding to .4 μsec).

Besides providing timing information as explained above, the circuit performs several other functions:

(a) It insures inactivity of the "pulsed-oscillator" while the 3PS is busy with pulse analysis or data punching. During this time the busy signal inhibits the operation of G2, so that

no start pulses get through the circuit.

(b) It provides a reset pulse to all the scalers. Since the reset pulse is taken from the output of G2, resetting is done just before the arrival of the start pulse.

(c) It provides a prompt gate signal for the 3PS, as indicated in the diagram.

(d) It provides a "strobe" pulse, which enables the parallel transfer from the flip-flops to the spare scaler board in the three-parameter system.

III. Experimental Details

A. Measurements

The measurements made fall into three groups:

(1) Measurement of the yield of fragments in the fission of U^{235}, as a function of neutron energy, for a thick uranium target (.005" thick, which is equivalent to ~240 mg/cm^2).

(2) Measurement of the yield of the long range particles emitted in the fission of U^{235}, as a function of energy of neutron producing ternary fission. The same uranium target was used for this measurement as in (1).

(3) The yield of fission fragments from a thin (200 $\mu gm/cm^2$) source of U^{235}, giving a measure of the fission cross-section as a function of neutron energy.

The schematic diagram of the experimental arrangement is shown in Figure (2). The fission chamber contained a bank of surface barrier detectors facing a 200 $\mu gm/cm^2$ U^{235} deposit, on aluminium (.015"), followed by another bank of surface barrier detectors facing the thick uranium target. The set-up in the figure shows the arrangement used during the thick uranium fission yield measurements. When a fission

fragment was detected, the detector bank gave
a pulse which was amplified by a gain 200 voltage
sensitive preamplifier. Then the signal was
diverted into two channels. The signal in one
channel was amplified and sent to ADC 2 for the
recording of pulse height information, while in
the other channel it was sent to a fast distributed
amplifier through an emitter follower. The ampli-
fied signal was sent to the timing circuit as a
detector stop pulse. When it received the detec-
tor stop pulse, the timing circuit produced a
gating signal which was sent to the 3PS as a
"Prompt-Gate".

During this time interval when the prompt
gate signal was present, the 3PS recorded the
time-of-flight of the neutron which induced the
event, in the first parameter (as explained in
the description of the timing circuit) and the
pulse height of the fission fragment in A.D.C. 2.
The third A.D.C. was not used in these measurements.
When the next neutron burst started, a pulse
supplied from the timing circuit reset all the
scalers in the 3PS, thus making it ready to
receive the next fission event.

The discriminator bias in both channels was
adjusted to be the same. It was set at a very

high level, for these thick U measurements ($\sim$80 MeV), to keep the counting rates low enough to be handled by the Tally punch and avoid the problem of dead time correction. Thus, only very high energy fission fragments were recorded.

For the ternary alpha yield measurements an aluminium foil, 6.5 mg/cm^2 thick, was placed between the detectors and the uranium foil. This thickness of aluminium was enough to absorb the fission fragments and the natural alpha particles from uranium, so that the detectors saw only the long-range particles emitted in the fission. In our measurement we counted all the particles which were not absorbed in 6.5 mg/cm^2 thick aluminium and did not distinguish between various kinds of particles. However, as was mentioned before, these are predominantly ternary alphas. These ternary alpha particles were recorded in the same manner as the fission fragments. The only difference was that the discriminating level was set at about 2 MeV, just above the noise level. The detectors were run at the highest bias they could take, 90 volts. This was enough to stop only 12 MeV alpha particles. Because of this, the pulse height spectrum of alpha particles as a function of neutron energy could not be too

meaningful. Nevertheless, the pulse height information was recorded to observe the variation of the mean position of the distribution.

For the thin uranium fission yield measurements, connections were made to the preamplifier from detector B, instead of detector A, Figure (2). The discriminator bias levels were set just above the level of the natural alpha particles from the uranium source. Under these conditions all the fission fragments emerging from the source in the direction of detectors were counted.

B. γ-Burst

The bremsstrahlung from the lead target produces a very intense beam of γ-rays. Although some 60 cm thickness of lead and zinc was placed in line between the lead target and the detectors to reduce the γ-rays, a burst of pulses still appeared in the first few channels. The signals were shorted to ground for first few microseconds to eliminate spurious counts.

C. Time Resolution

The time resolution of the system depends upon three factors:

(1) Instrumental resolution: This is the time uncertainty in nanoseconds divided by the

flight path length in meters. The timing width depends upon the pulse length of the burst and the channel width of the analyzer. Although the data were recorded with 50 nanoseconds channel width (τ) such fine instrumental resolution was not needed except at high energies, so that for the final analysis purposes of this report, it was integrated to $\tau = 0.2\ \mu$ sec in the computer to obtain better statistical accuracy (i.e. more counts per channel). The contribution of the instrumental resolution to the width (Full width at half maximum abbreviated as FWHM) of resonance is given by the relation

$$\frac{\Delta E}{E} = \frac{2\Delta T}{T}$$

The flight time, T, is related to energy, E, as

$$T = \frac{72.3}{\sqrt{E}}\ \mu\text{sec/meter}$$

Thus, for the 10.5 meter flight path used

$$(\Delta E)_{INST.} \cong 5.3 \times 10^{-4}\ E^{3/2}$$

(2) Moderation Effect: The slowing down time of the neutrons coming from the moderator introduces a smearing of the path length which was calculated for the beam used for 200 meters flight path work, to be 3.72 cm[22]. Our measurements were made using a side beam hole looking at

the target at an angle. This increased the smearing and estimations indicated this effect to be more like 6 cm. The contribution of this to the width (FWHM) is given as

$$\frac{\Delta E}{E} = \frac{2\Delta D}{D}$$

where D is the flight path (10.5 meters)

$$(\Delta E)_{MOD.} = 11.4 \times 10^{-3} E$$

(3) Doppler Broadening: The broadening of the resonances because of the thermal motion of the uranium nuclei is given as (Appendix 1)

$$(\Delta E)_{DOPP.} = .034 \ E^{1/2}$$

(This is the full width at half maximum)

These effects broaden the widths of the resonances. The actual width observed is the square root of the sum of the squares of these three contributions and the inherent total width of the resonance, Γ. Thus, for a resonance, at an energy E, the expected width is

$$\Delta E = \sqrt{(\Delta E)^2_{INST.} + (\Delta E)^2_{MOD.} + (\Delta E)^2_{DOPP.} + \Gamma^2} \ (ev)$$

which is

$$\Delta E = \sqrt{2.81 \times 10^{-7} E^3 + 1.30 \times 10^{-4} E^2 + 1.16 \times 10^{-3} E + \Gamma^2}$$

Typically the inherent widths of resonances are negligible, in our work, in comparison to the other contributions. These are plotted independently as a function of energy in Figure (8) to show their relative importance in different energy regions.

D. Data Taking and Processing

The measurements presented here were made in January, 1963, over a period of five weeks runnnng time on the Nevis cyclotron. The actual data accumulation time was close to 300 hours. During the experiment the data were recorded, event by event, on paper tape, each tape ~1000 feet long. The data on one roll of tape, which records ~10,000 events, represented a run. The approximate time taken for the runs were $1\frac{1}{2}$ hours, $2\frac{1}{2}$ hours and 3 hours for thick U fission, thin U fission and ternary alpha measurements respectively. Altogether one hundred and thirty two runs were recorded, which includes about fifteen exploratory runs of the three parameter measurements (the time taken for these was ~5 hours per run).

Some preliminary measurements were made previously in 1961 and 1962 to study the ternary alpha emission relative to binary fission in the

resonance energy region. The results showed variation of relative ternary alpha emission from resonance to resonance[23]. To get reasonable intensities only thick uranium targets were used, which made the results open to some questions which were examined in detail in the 1963 run.

The data of each run was totalized individually on the IBM 1620 and examined for drifts, etc. Along with the totalization process the data on tape was converted to cards. Finally, it was transferred to the magnetic tape using the IBM 1401. The intermediate step of cards enabled us to make certain checks without using 7090 computer time, and also to get partial results during the run to monitor the taking of data. The final totalization and the computations were done on the IBM 7090. The whole process is shown symbolically in Figure (9).

E. Correction for Timing Drifts

While comparing individual runs, some shifts in the peak positions were observed which were attributed to drifts in the "Timing Circuit." These drifts were found to be a combination of a linear shift (a shift in channel zero (A)) and a proportional shift (shift in channel width (τ)).

The data were first corrected for these drifts
and then all equivalent runs were added together.
The correction procedure was the following:

The mean positions of five isolated resonances
(8.8, 12.39, 19.3, 32.13, 39.5 ev) were determined
and a least squares fitting made to a function
$A + \tau x$ to get the two constants A and τ for each
individual run. The most consistent set of these
two constants was chosen to be a standard and the
rest of the runs were normalized to match the
standard run. (This was done on the IBM 7090
computer). To improve the accuracy of the normal-
ization process the original ~50 ns channel width
data was broken up further into ten grids and the
events were apportioned uniformly among the new
grid channels. This procedure enabled us to work
with an enlarged time scale of artificially pro-
duced channel width of 5 ns.

After adding the normalized runs together the
high energy fission yield spectrum (200 ev to 1 kev)
was compared with the high resolution measurements
of Michaudon, et. al.[24], to check whether the
normalization procedure produced any distortion
effects in our spectrum. No distortion effects were
found and our fission yield curves were in close
agreement with the Michaudon, et. al. curves.

IV. Analysis and Results

A. Overall Results

Figures (10) to (13) show the overall results of the three measurements. In each case, the yield is plotted as a function of channel number (time-of-flight of neutrons). Since the Doppler broadening and time moderation effects are the limiting factors on the overall resolution and not the instrumental resolution (Figure 7), for the region between 2 ev to 16 ev, it is shown with detection channel $\tau = 1.0$ μs, Figure (10). The other three graphs, which cover the resonances up to ~ 1 KeV, are plotted with $\tau = 0.2$ μs. Although the data were taken up to the KeV region, the resonances above ~ 60 ev are not resolved, so the analysis was not extended beyond that. On the low energy side the data extend only to the cadmium cut off point.

B. Background

The background is the sum of all counts not produced by neutrons which should have arrived in the time interval considered. The background can thus be caused by stray slow and fast neutrons which arrive after being scattered from the surroundings, by cosmic radiation, and by spurious noise pulses in the detectors and amplifier, etc.

The chamber was covered with cadmium on all
sides to stop the neutrons which are thermalized
during the process of scattering on surrounding
objects.

The background was determined by looking at
the energy positions where there is negligible
contribution from resonances and a few regions
where strong cadmium levels produced dips in the
yield curves. The background counts determined
this way were plotted as a function of the inverse
of the time-of-flight which fitted a straight line
very well. This is reasonable because the neutron
flux also has a similar time dependence[22].
So the background function used is

$$A + \frac{B}{\text{Channel Number}}$$

Where A and B are constants determined from the
plot. One set of constants was used for the
region greater than 4 ev. For the region below
4 ev a constant background was chosen. The back-
ground for different regions is shown along with
the experimental data and the computed curves in
Figures (15-25).

C. Analysis of the Yield Measure-
ments and the Final Results.

It was required to find the areas under the
individual peaks for all three measurements to
study the variation in yields. The high level
density of U^{235} made it desirable to use an approach
which considers all levels uniformly and gives
contribution of individual peaks to the yield curves.
A program was written by Dr. Melkonian, for the IBM
7090 Computer, which does the least square fitting
of the data to resolution broadened Breit Wigner
peaks. The data supplied to the computer are the
known level positions, the widths of the levels which
are computed from the known parameters discussed
before, and the background function. The outline
of the program is as follows:

' The function* minimized is

$$F = \sum_i^{\text{No.of Points}} P_i \left[\left\{ Y_i - (A + \frac{B}{X_i}) \right\} - \sum_{j=1}^{\text{No.of Levels}} C_j \Psi_j (X_i - X_j) \right]^2 \quad (1)$$

where P_i is the weighting factor ($= \frac{1}{\sigma_i^2}$ where σ_i is
error on Y_i) associated with each data point Y_i, Y_i
represents the number of counts in channel X_i.
$A + \frac{B}{X_i}$ is the background function. The constants A

---

* The interference between the levels was neglected.

and B are supplied. The function[*] Ψ_j is the following:

$$\Psi = \frac{1}{\sqrt{\pi}\beta} \int_{-\infty}^{+\infty} \frac{e^{-(x-y)^2}}{1 + y^2} \, dy \tag{2}$$

where $x = \frac{2(E-E_0)}{\Gamma}$; $y = \frac{2(E'-E_0)}{\Gamma}$ & $\beta = \frac{2\Delta}{\Gamma}$

E is the energy of the incoming neutron; E' is the energy of the neutron relative to the nucleus, Δ is the observed half width of the resonance at 1/e of the maximum, and Γ is the total natural width of the resonance $(\Gamma = \Gamma_f + \Gamma_n + \Gamma_\gamma)$.

This function is written in the following form:

$$\Psi = \frac{1}{\sqrt{\pi}} \int_0^\infty e^{-Z^2} \left[\frac{1}{1 + (x + \beta Z)^2} + \frac{1}{1 + (x - \beta Z)^2} \right] dZ$$

where $Z = \frac{x - y}{\beta}$

and evaluated numerically. The value of constants C_j are determined by minimizing the function F. The constants C_j give the heights of the resonances. The product of the quantities C and Δ (width of the resonance) are used as a parameter proportional to the area of the resonance.

---

[*] The function Ψ has the same form as the Doppler broadened Breit Wigner resonance function (Appendix 1). The only difference is that the observed width, Δ, appears in place of the Doppler width.

The data were divided into several energy intervals for the curve fitting. For each interval a constant width of the resonance was chosen, since the widths do not vary appreciably over the small energy intervals considered. The program was also set up to give a plot of the data and the computed points. One representative computer plot of a small section is shown in Figure (14). Because these plots from the computer could not be compressed much and so were hard to present, the results are plotted in condensed form showing the data and the computed least squares fits in Figures (15) to (25). Each graph contains the results of the three measurements.

The following ratios were computed for the resonances:

$$R_{13} = \frac{\text{Area under the ternary alpha peak}}{\text{Area under the fission yield (Thin U) peak}}$$

$$R_{23} = \frac{\text{Area under the thick uranium fission yield peak}}{\text{Area under the thin uranium fission yield peak}}$$

The numbers 1, 2 and 3 are assigned to the ternary alpha, thick uranium (.005") fission and thin uranium (200 μgm/cm^2) fission data respectively.

The results are listed in Table 1, along with the errors, which were assigned on the basis of the number of events under each peak. In the last column the ratio, R_{21}, of fission yield from thick

uranium and ternary alpha yield from the same target
is also listed.

Although all the resonances from 2 ev to 60 ev
were analized, the results are given only for the
resonances for which the errors were less than ~15%.
All the tabulated ratios are in arbitrary units and
the absolute values of the numbers listed have no
physical significance. We were interested only in
the relative variations from resonance to resonance.

The ratio, R_{23}, in arbitrary units is plotted
for each level as a function of resonance energy in
Figure (26B), to look for the possible variation of
fission fragment energy distribution from resonance to
resonance. The variations observed are far outside
the errors. The data were found to be incompatible
with a single value of the ratio, on the basis of a
Chi-square test. The data can be made statistically
consistent by taking two values of the ratios, ~15%
apart, which might correspond to the two possible J
values of the resonances. These values are indicated
in Figure (26-B). Figure (27) displays these results
only for the resonances for which the ratio R_{23} could
be obtained with a statistical accuracy of better than
6% to show the separation clearly.

The measured areas under the ternary alpha peaks
and thin uranium fission yield peaks were used as a

measure of the variation of the yield of ternary alphas per fission from level to level. This ratio R_{13} is plotted in arbitrary units as a function of resonance energy in Figure (26-A). Here again we find that the data fit two straight lines, on the basis of Chi-square test, but the difference here between the two values of the ratios is ~12%.

Figure (28) shows a similar graph for the ratio R_{21}. Although this ratio does not have any direct physical significance, it is exhibited here because it shows the maximum variation. The variations in this ratio (R_{21}) can be due to the combination of three effects, variation in fission fragment energy distribution, in ternary alpha energy distribution and the variations in the ternary fission probability from level to level.

Thus, both the ratios R_{23} and R_{13} fall into two groups and the ratio R_{21} (which is the ratio of R_{23} and R_{13}) also shows a similar group formation, but with a little more enhanced separation. The study of one of these ratios may be a possible way to assign the resonances to one or the other of the possible J values.

Considering only the time-of-flight data, from the three parameter measurements (described in Appendix 10), we get a fission yield spectrum as a

function of neutron energy for a 50 μgm/cm^2 U

sample. This should be identical with the results

discussed before for fission yield from thin U

(200 μgm/cm^2) because the two thicknesses are

not sufficiently different to produce the type

of effects discussed in the introduction. The

same area analysis was made on this data also

and the ratio of the yield from these two

thicknesses of uranium was computed for all

resonances. The ratios (R_{43}) so obtained fall

on a single straight line, Figure (29). This

gave a good check on our analysis procedure.

V. Conclusions

The results, on the ternary alpha emission as a function of energy of neutron inducing the ternary fission event, have established that the same resonances appear in both the ternary and binary fission cross-section curves. No exception to this has been found.

The variation observed in the ratio of the fission yields from a thick uranium target and a thin uranium target shows that the fission fragment energy distribution differs from resonance to resonance.

The ratio of the ternary alpha yield (from .005" thick uranium) to the binary fission yield (from 200 $\mu gm/cm^2 U^{235}$ deposit) also shows variations well outside the errors, from one resonance to other. In this case a definite physical interpretation of the result can not be made. The observed effect can be caused either by actual variation of the ternary fission probability or by variations in the ternary alpha energy spectrum from resonance to resonance or combination of the two effects. To differentiate between these two effects one has to make ternary alpha measurements with a thin uranium sample also. This was not done because of the very low probability of the process.

Recently, the probability of ternary fission of U^{233} was measured by Panov[25] in the 1-10 ev neutron energy region and he concluded that the probability of ternary fission for U^{233} is constant within statistical error limits ($\sim 8\%$). If this conclusion can be extended

to U^{235}, it suggests that the effects we observed are due to the differences in the energy distribution of the ternary alpha particles. An indication of this type of variation is exhibited in the data shown in Fig. (A-9).

Following the publication of our initial results[23] on the variation of ternary alpha yield from thick U sample, Michaudon and co-workers[26] in Saclay studied ternary alpha emission for 11 resonances between 3 and 21 ev. The conclusions they have reached are: (1) the ternary fission probability varies from resonance to resonance, and (2) the alpha particle spectrum differs from one resonance to other. These conclusions are in agreement with our results, but quantitative figures for Michaudon et.al. measurements were not available for detailed comparison.

It is seen that the variations are much larger when the yields of ternary alphas and fission fragments are both measured for thick uranium sample, Figure (28). This can be explained by postulating that the differences in the energy distributions of the ternary alphas and the fission fragments go in opposite directions.

The pulse height spectrum from thick uranium fission, (Figure A-10) where only the high energy part of the spectrum was recorded, shows some variations, whereas the mean of the total kinetic energy distribution, Figure (A-11) does not show any significant variation outside the statistical errors. This indicates that probably the width of energy distribution changes while the mean position does not. Better measurements are planned to study this in

more detail.

Two straight line fitting of all the three sets
of ratios give an indication that the variations can
be classified into two groups, which could correspond
to two different spin states of the resonances.

Comparison is made with the measurements of
Cowan, et. al.[17] where the ratio of symmetric to
asymmetric fission yield was measured from 8.8 ev
to 40 ev for several resonances. They compared the
probability of symmetric fission in U^{235} for various
resonances with the probability of symmetric fission
at thermal energies. In their results four levels
showed an increase in symmetry and thirteen levels
showed a decrease in symmetry. The assignment of
Cowan, et. al. are marked with letters L and H
(L, H meaning low and high symmetric fission
respectively; primes denote uncertain assignments),
in Figure (26) for comparison. For direct comparison
the ratio, R_{23} (= thick U yield/thin U yield) and
our assignments are also listed in Table 2 along with
Cowan, et. al. assignments, for the resonances
studied by them. There are seven levels for which
both groups (Cowan's and ours) obtained definite
results and for these levels the grouping of levels
into two classes is identical. According to the
picture discussed in the introduction relative yield
of symmetric fission increases with decreasing total

energy. This effect of decrease in total energy will produce the effect of decrease in yield for thick U sample. Thus the increase in symmetric fission corresponds to a lower ratio of thick U to thin U fission in our case.

This agreement justifies the assumption made by Dr. Melkonian in his semiempirical picture that each value of total kinetic-energy release implies a fairly definite relative symmetric mass yield, so that any variation in overall relative symmetric mass yield must arise from variations in the total kinetic-energy distribution.

Our results on ternary alpha yield do not correlate well with the assignments of Cowan, et. al. As was pointed out before that there is some evidence that the alpha particle energy distribution varies from level to level, so that with a thick source as used here for ternary alpha measurements, the results obtained reflect this effect as well as a possible variation in ternary fission probability.

The resonance which we believe have been identified to one or the other group with considerable statistical accuracy (Figure 27) are following:

(1) 3.16, 19.3, 21.1, and 32.13 ev corresponding to a higher mean kinetic energy.

(2) 3.6, 6.4, 8.78, 12.39, 33.6, 34.45, 35.25, and 39.5 ev corresponding to a lower mean kinetic energy.

The two groups possibly correspond to two different spin states ($J = 3$ or 4) of the compound nucleus U^{236}. The absolute values of J can not be assigned unless the J value is known of at least one resonance level.

APPENDIX 1

Single Level Breit-Wigner Formula and the Doppler Broadening

For a single isolated resonance the fission cross-section, σ_f, as a function of neutron energy, E, is given by the Breit-Wigner single level formula

$$\sigma_f = \pi \lambda^2 \frac{g \, \Gamma_n \, \Gamma_f}{(E-E_0)^2 + \Gamma^2/4}$$

where $2\pi\lambda$ is the neutron DeBroglie wavelength, Γ_n and Γ_f the partial widths for scattering and fission respectively, and Γ the total width is the sum of all the partial widths, and E_0 is the energy at exact resonance. The statistical weight factor, g, depends on the angular momentum (I) of the target nucleus and the angular momentum (J) of the compound nucleus $(g = \frac{1}{2} \frac{2 \, J + 1}{2 \, I + 1})$.

This can be written in a slightly different form as:

$$\sigma_f = \frac{\sigma_{of}}{1 + \left((E - E_0)/\frac{\Gamma}{2}\right)^2}$$

where $\sigma_{of} = 4\pi\lambda^2 \, g \, \Gamma_n \, \Gamma_f/\Gamma^2$ gives the cross-section at the resonance energy.

This formula applies properly in the centre of mass system, the Doppler broadening arising from the

thermal motion of the nuclei must be taken into account to get the observed shape of the resonance.

Doppler Broadening

Let the velocity of the neutron in the lab system be U and the component of the nuclear velocity along the neutron beam direction be V. Then the relative velocity of the neutron and the nucleus is (U + V) and the relative kinetic energy is:

$$E_{rel} = \frac{1}{2} m (U + V)^2 = E_n + (2mE_n)^{1/2} V ,$$

neglecting the $\frac{1}{2} mV^2$ term. E_n is the neutron energy in the Lab system.

If the target atoms were that of a gas they would move with the Maxwellian distribution giving for the fraction f of atoms with atomic mass M, having a velocity component V:

$$f(V) \, dV = (\frac{M}{2\pi KT})^{\frac{1}{2}} e^{-mV^2/2KT} \, dV$$

The probability for a given E_{rel} is given as

$$f(E_{rel}) \, dE_{rel} = (\frac{M}{2\pi KT})^{\frac{1}{2}} e^{-\frac{M}{2KT} \frac{(E_{rel}-E_n)^2}{2mE_n}} \frac{dE_{rel}}{(2mE_n)^{\frac{1}{2}}}$$

$$= \frac{1}{\Delta \pi^{\frac{1}{2}}} e^{-(E_{rel}-E_n)^2/\Delta^2} \, dE_{rel}$$

where $\Delta = 2\left(\dfrac{mE_n KT}{M}\right)^{\frac{1}{2}}$ is called the Doppler width (half width at $\dfrac{1}{e}$ of the maximum).

The cross section is given by the single level formula (dropping the subscript f) as

$$\sigma = \frac{\sigma_o}{1 + [(E_n - E_o)/\Gamma/2]^2}$$

The neutron energy, E_n, is to be replaced by the relative energy E_{rel}. We thus obtain for the effective cross section $< \sigma (E_n) >$

$$\langle \sigma(E_n)\rangle = \int \sigma(E_{rel})\, f(E_{rel})\, dE_{rel}$$

$$= \int \frac{\sigma_o}{1 + \dfrac{(E_n - E_o)^2}{\Gamma^2/4}} \; \frac{1}{\pi^{\frac{1}{2}}\Delta} \; e^{-\dfrac{(E_{rel} - E_n)^2}{\Delta^2}}$$

This can be written as

$$\langle \sigma(E_n)\rangle = \frac{\sigma_o}{\pi^{\frac{1}{2}}\beta} \int \frac{e^{-\dfrac{(x - y)^2}{\beta^2}}}{1 + y^2} \; dy$$

Where $\dfrac{E_n - E_o}{\Gamma/2} = x$; $\dfrac{E_{rel} - E_o}{\Gamma/2} = y$ and $\dfrac{\Gamma}{2\Delta} = \dfrac{1}{\beta}$

Thus $\langle \sigma(E_n)\rangle = \sigma_o \, \Psi(\beta,x)$

Where $\Psi(B,x) = \dfrac{1}{\pi^{\frac{1}{2}}\beta} \int \dfrac{1}{1 + y^2} \; e^{-\dfrac{(x - y)^2}{\beta^2}} \; dy$

The resonance has its normal Breit-Wigner shape if the width of the level, Γ, is large compared to the Doppler width. If this is not the case averaging over the thermal motion of the nucleus is necessary. The integrations can not be carried out analytically and use is made of numerical methods and series expansions[27].

APPENDIX 2

Yields from Thick Targets

and Shielding Effects

The estimates made here are to exhibit the dependence of yield on the thickness of the target and the range of the particles.

(A.) Fission Yield from a thick Uranium foil:

Assume that the fission fragments, produced by neutrons, are emitted isotropically from the foil of thickness, t, and the detectors are biased so that all fragments with energy $E > E_B$ are counted. The number of counts from a layer between x and x + dx is given by (Figure A-1(a))

$$dN = K \int_{0}^{\theta_o} 2\pi \sin\theta \, d\theta \, dx \qquad (1)$$

Where K depends upon the neutron flux and the fission cross section. θ_o is that angle at which the particle upon emerging from the foil has just enough energy to be counted. Let the range at this energy be R_B and the range corresponding to its energy R_o, both measured in uranium. Then

$$R_B = R_o - \frac{x}{\cos\theta_o} \qquad (2)$$

Thus

$$\text{Yield } \alpha \; 2\pi \int_0^t dx \int_0^{\theta_0} \sin\theta \; d\theta$$

$$\alpha \; 2\pi \; t \left[1 - \frac{t}{2(R_0 - R_B)} \right] \tag{3}$$

It is assumed here that all fission fragments have the same range R_0, which is of course not true, but for our estimations it is not important. And the thickness t of the foil is assumed to be less than $(R_0 - R_B)$.

The thickness of the foil which is effective in contributing to the yield cannot be greater than $(R_0 - R_B)$, because the particles coming from deeper thickness cannot be detected. Thus, for a virtually infinite thickness of uranium, the yield is given as

$$\text{Yield } \alpha \; 2\pi \left[R_0 - R_B \right]$$

Where thickness t is put equal to $(R_0 - R_B)$, the maximum possible effective thickness.

(B.) Ternary Alpha Yield:

For ternary alpha yield measurements, the uranium foil is covered with an aluminum foil of 6.5 mg/cm^2 thickness. Suppose δ is equivalent thickness of aluminium used in terms of uranium.

Now the angle θ_0 is given by the relation

$$R_B = R_0 - \frac{x + \delta}{\cos\theta_0}$$

Thus giving

$$\text{Yield} \ \alpha \ 2\pi \ t \ [\ 1 - \frac{t + 2\delta}{2(R_O - R_B)} \ ]$$

for a thin foil. For the thick foil we have to put $t = R_O - R_B - \delta$. Ternary alphas have longer range, so the effective thickness is larger.

(C.) Shielding Effect:

So far it was assumed that the neutron beam is unattenuated in the passage through the foil. For the virtually infinite foil used in our measurements, we have to consider the exponential decrease of neutron flux inside the foil.

$$I = I_O \ e^{-n\sigma x}$$

where I_O is the flux which would be present at the position, x, if the sample was absent, n is number of atoms per cm^3 and σ is the absorption cross section. This is referred as shielding effect.

For heavily ionizing fission fragments the shielding effect is negligible in comparison to ternary alphas, for which the range and thus the effective thickness is much larger. The shielding will tend to decrease the ternary alpha yield more for the resonance with large cross section in comparison to ones with smaller cross section. The effects will be maximum at the peak positions

where the absorption cross section is maximum. The percentage decrease in the yield is calculated as a function of the range of alpha particles and the absorption cross section. (To calculate the exact correction factor, it would be necessary to integrate the effect over the entire alpha particle distribution which gets complicated.)

Taking into account the attenuation of neutron flux inside the foil, the expression for the yield can be written as

$$N \propto \sigma' I_0 \int_0^t dx \, e^{-n\sigma x} \int_0^{\theta_0} d\theta \sin\theta$$

Where σ' is the cross section for the production of ternary alphas. Again, the alpha emission is assumed to be isotropic.

As before, the angle θ_0 is given by the expression

$$\cos\theta_0 = \frac{x + \delta}{R'}$$

Where $R' = R_0 - R_B$.

Solving the integral we get

$$N = \frac{2\pi I_0 \sigma'}{(n\sigma)^2 R'} [(1 - e^{-n\sigma t})(n\sigma\{R' - \sigma\} - 1) + e^{-n\sigma t} n\sigma t]$$

For a very thick foil (as explained in part A)

$$t + \delta = [R_0 - R_B] = R'$$

$$N \propto \frac{2\pi I_0 \sigma'}{(n\sigma)2 R'} [e^{-Z} + Z - 1]$$

Where $z = n\sigma t = n\sigma (R' - \delta)$.

Expanding the exponential $[z < 1]$:

$$N \; \alpha \; \frac{2\pi I_o \sigma'}{(n\sigma)^2 R'} \; [\; \frac{z^2}{2!} - \frac{z^3}{3!}]$$

$$z^2 = n^2 \sigma^2 R'^2 (1 - \frac{2\delta}{R'}) \; ; \; \delta \ll R'$$

$$N \; \alpha \; 2\pi I_o \sigma' \; [\; (^{1-} \frac{2\delta}{R'})(\frac{1}{2} - \frac{z}{6} + \frac{z^2}{24} \; - - - - - -)]$$

When the shielding effect is absent (i.e. $\sigma = 0$)

$$N' \; \alpha \; 2\pi I_o \sigma' \; [\frac{1}{2}(1 - \frac{2\delta}{R'})\;]$$

Thus the correction factor for the shielding effect, for a particle of range R_o is given as

$$c = \frac{N - N'}{N} \quad x \; 100\%$$

$$c = \left\{ \frac{z}{3} - \frac{z^2}{12} \right\} x \; 100\%$$

where $Z = n\sigma \; [R_o - R_B - \delta]$

The decrease in yield, because of this shielding effect, expressed as a correction factor, c, is computed for various values of absorption cross section and several energies of ternary alphas and given in Table (3).

Actually the effects observed are the averages over the whole energy distribution of the ternary alphas. When this average is taken, the results are close to the effects corresponding to 16 MeV alpha particles. Thus, for the neutron energy where the absorption cross section is 1000 barns, the shielding effects will decrease the yield by 5%. In U^{235} the highest peak cross section encountered is 1000 barns. However, the results were computed taking the total yield under the resonance, so it is not the peak cross section which is to be considered but the average cross section over the resonance. This reduces the effect considerably. Thus, it was concluded that the shielding effects could not change the results outside the experimental error.

APPENDIX 3

Surface Barrier Detector Fabrication

Our technique of fabricating a surface-barrier detector is as follows:

(1) The crystal is lapped with fine alumina and distilled water, unless already obtained in a lapped form.

(2) The crystal is next put in a polyethylene beaker, to which about 20 cc of etching solution is added. The composition of etching solution used is:

concentrated nitric acid   10 volumes

40% Hydrofluoric acid   1 volume

Analytic reagent purity chemicals are used for the etch. It is mixed in a clean polyethylene bottle and allowed to stand 20 minutes before use.

The etching is done for about ten minutes to produce a mirror like finish on the silicon surface. Bubbles which occur on the surface during etching are removed by occasional agitation with a polyethylene rod.

(3) Demineralized distilled water is run into the etch, and the crystal is washed by alternate dilution and decantation, avoiding exposure of the silicon to air in the early stages. In the presence of a strong etch, exposure to air produces a brownish

black stain on the silicon.

(4) The crystal is transferred to a clean beaker and washed several more times with demineralized distilled water.

(5) Then it is boiled in demineralized distilled water for about five minutes.

(6) The crystal is then mounted with araldite (Epoxy resin) on a thin clean sheet of mica, over a circular hole in the mica slightly smaller than the crystal.

(7) After mounting, the crystal is kept in a dust free box for a few hours to allow the araldite to harden.

(8) The mounted crystal is given a short etch for about 2 minutes, washed again thoroughly with demineralized distilled water, and finally boiled in demineralized distilled water for 5 minutes.

(9) The crystal is mounted in a vacuum evaporator, about 4 inches from the filament (tantalum boat) and gold is evaporated on both sides of the crystal.

To control the amount of gold deposited, a glass plate with electrodes attached about a centimeter apart is mounted at the same distance from the boat as the detectors. The leads from the glass plate are brought outside the vacuum system and used to

measure resistance across the plate. As the evaporation proceeds, the observed resistance of the gold film on the glass plate indicates when the evaporation should be stopped.

(10) Electrical connections are made on both sides using a thin gold wire attached to the silicon surface with silver paste.

It is important to avoid touching the crystal with the fingers at any stage of the fabrication.

After an initial period of trials we were quite successful in making detectors. To quote a figure, once we made twelve 1 cm diameter detectors all of which were good. Of course, in quoting yields, it is necessary to state the level of acceptance in terms of resolution and break-down voltage. Out of these twelve detectors, nine took up to 350 volts, others broke down near 200 volts. For large area detectors ($\sim 1\frac{1}{4}$" diameter), used in arrays, break-down voltage was generally not so high. In all, some 120 such detectors were made. Out of these, 20 detectors took up to 150 volts and higher, others were generally in the range of 20 volts to 100 volts excepting a few which broke down at the bias of less than 20 volts. For the 200 Ω-cm resistivity material used, the depletion layer necessary to absorb the fission fragments requires only 10 volts bias.

APPENDIX 4

Response of the Fabricated Detectors to

Alpha Particles and Fission Fragments

Figure (A-2) shows a pulse height distribution of α-particles (Th^{228} source) for a detector 12 mm in diameter resistivity 200 Ω-cm, operating at 70 volts. For this detector the resolution width (FWHM) was 85 KeV.

A typical pulse-height spectrum of fragments from U^{235} thermal fission, striking a detector 2 cm in diameter and 200 Ω-cm resistivity is shown in Figure (A-3). The observed energy ratio for the two peaks was 1.62 and did not vary appreciably as the detector bias was raised from 20 volts to 180 volts. The observed ratio is much higher than that usually observed (1.50), in time-of-flight measurements[28]. This higher ratio was attributed to a pulse-height-defect discussed in Appendix (5). It was noticed that at higher bias, a tail develops on the higher energy side of the fission spectrum as shown in Figure (A-4). This is probably because the detector depletion layer becomes sensitive enough to absorb other particles, e.g. electrons. Thus, the detectors were run at ∿ 30 V bias except for ternary alphas where deeper depletion layers are required.

No collimation was used for the measurements shown in these graphs. It was generally noticed that the peak-to-valley ratio increases appreciably if a collimator is used to mask off the edges of the detectors.

APPENDIX 5

Investigation of Problems Associated

With the Semiconductor Detectors

(a.) Pulse height variation over the surface:

It was observed that for large area detectors,
the resolution was much worse than one expects from
the measured capacitance values. This was attributed
to the pulse height variation over the surface of the
detector.

We tested many detectors for this effect, using
a collimated Po source to probe the surface of the
detector. The result of one such test is shown in
Figure (A-5). This detector was about 2.2 cm in
diameter and 200 Ω-cm resistivity. It showed a
variation of about 4% in the peak position over the
surface. The various positions used for scanning
are shown in the upper right hand corner of the
figure. The detector had a resolution of 3.5%
with a collimated source close to the surface.
When the same source was mounted far away from
its surface, thus making the whole surface effective,
the resolution obtained was 5%.

In general, it was observed that the maximum
pulse height was given by the central area of the
detector, while the pulse height decreased as the

source was moved towards the edge. The effect
was especially severe very near the edge. These
observations made us decide to mask off the extreme
periphery of the detectors.

These variations may be caused by the presence
of local inhomogenieties and dislocations in the
material. Another possible explanation is the effect
of series resistance in the detector, but this seems
to be unimportant in our detectors, as will be shown
in the following paragraphs.

Depending upon where, in the depletion region,
the particle is detected the charge carriers have to
cross varying thickness of silicon bulk material
and of gold conducting layer before they reach the
electrode. This introduces a variable resistance
in series with the detector, which otherwise is just
a capacitance. This variable series resistance in
the detector produces variations in the rise time of
the pulses. These pulses, when clipped, can give
rise to the variation in the pulse height over the
surface.

For a 3 cm diameter detector, 1 mm thick with
resistivity 200 Ω-cm, the series resistance of the
bulk material (at zero bias) will be 20 ohms; this
will decrease slightly as the bias is increased.

However, this is not the only source of resistance.
Let us look at the surface of the detector which has
gold evaporated on it and a gold wire connected at
the edge to carry the collected charge. Since the
carriers have to pass through the surface in order
to reach the gold wire electrode, the conducting gold
layer presents some resistance. In order to obtain
the order of magnitude of this resistance, we can
make the rough approximation that the path length
is 1.5 cm, half the detector diameter. The resist-
ance of the gold layer is at our disposal, but we
have to compromise between a good conducting layer
and a thick window. We evaporate about 100 $\mu gm/cm^2$
which gives a resistance of $\sim$ 100 ohms across the
surface. In this case, the sheet resistance is 50Ω
and dominates over the bulk material resistance for
the low resistivity material we use.

We investigated the effect of series resistance
for many detectors by connecting additional charge
collecting leads at several different spots of the
detector to decrease the series resistance and
using several clipping constants to check the effect
of bulk material resistance. The results showed
convincingly that this effect was not serious for our
detectors.

(b.) Window Effect:

All semiconductor detectors have a surface layer through which the incident ionizing particles pass before reaching the sensitive depletion region. This is technically referred to as "window". A portion of the energy of the incident particle is lost in passing through this layer. The window is an integral part of the diode structure in junction detectors. In surface barrier detectors, the window consists mainly of the conducting gold layer, though there is evidence that the oxide layer under the gold coating also contributes to the energy loss.

Window thickness were determined for many detectors by observing the reduction of alpha particle pulse height as the angle of incidence was decreased from 90°. For a typical detector, estimating $\frac{dE}{dx}$ to be 300 KeV/micron, we measured a window thickness of .08 microns. If this were due entirely to the gold, this would correspond to 150 μgm per cm^2. Actually, the amount of gold evaporated on the detector is less than this, since this figure includes the oxide dead layer.

The pulse height data is corrected for this effect, along with the effect described in the next section, whenever absolute energy measurements are required.

(c.) Pulse Height Defect:

We observed a type of nonlinearity in the response of the detectors to fission fragments. When the kinetic energy spectrum of the fission fragments was calibrated using a alpha particle source, the ratio of energies of the most probable high and low energy peaks was found to be generally of the order of 1.6. The expected value of this ratio based on time-of-flight data is ~ 1.5. This effect was first noted by Melkonian[29]. This is termed as "pulse-height defect" and is superficially similar to the ionization defect observed for fission fragments in ion chambers. Ionization defect, in gas ion-chambers, is primarily due to energy lost in the recoil of gas atoms rather than in the production of electron ion pairs, in semiconductor detectors it is expected to be very small because of the small amount of energy required to produce an electron-hole pair. However, it has been suggested by Brown[30] that the high density of holes and electrons around the fission track would result in a lower collection efficiency due to the inability of the junction field to completely penetrate the plasma of holes and electrons. This can result in an recombination effect producing an effect similar to the ionization defect.

The effect has been studied by many invest-
igators.[31]   The measurements of Britt and Wigner[32]
indicate that the light fragments show a smaller
defect than the heavy fragments. Corrections for
this effect along with the window effect are made to
the pulse height data by calibration against the data
from the time-of-flight measurements[28], whenever
necessary.

APPENDIX 6

Detector Arrays and Matching

To obtain large effective areas we considered two different types of arrays, which are following:

(a.) Parallel Detector Array:

One way is by connecting a large number of detectors in parallel and thus simulating a large detector, but this gives a large intrinsic capacitance and thus low signal to noise ratio. A useful formula for the size of the signal from a detector is

$$V = \frac{Q}{C_D} \cong \frac{50W}{C_D} \text{ (millivolts)}$$

where Q is the charge deposited on the detector by the impinging particle, C_D is detector capacitance in pf and W is the energy of the particle detected in MeV. For several detectors connected in parallel

$$V = \frac{Q}{\sum\limits_i C_i}$$

where C_i are the detector capacitances. Thus, with an increasing number of detectors in parallel, the signal levels become smaller and thus more difficult to work with.

(b.) Series Detector Array:

An alternative approach is to connect individual detectors in series to minimize the

resultant capacitance. It has however, different problems. For example, if a connection to one detector becomes loose or detached the whole chain becomes inoperative, which is not the case for the parallel arrangement. Besides this, for matching we require to bring out the signal leads from the vacuum chamber, for each detector to be connected in series. And if the leads are brought out from each detector the stray capacitance becomes quite appreciable to create trouble.

A compromise between the two was used by making a series-parallel combination. The detectors were connected electrically in sets of three detectors in parallel, and the six resulting sets were then connected in series.

Five such detector assemblies were made. The one used for ternary alpha detection was run at 90 V bias. The other assemblies were used for fission fragments and were usually run at 30 V bias. These figures of 90 V and 30 V mean that each detector in the assembly has this particular bias applied. The arrangement used for the voltage distribution in the ternary alpha detector is shown in Figure (A-6). This type of arrangement connects the six sets in series for A.C. operation and in parallel for D. C. operation. Thus, one 90 V battery was enough to

supply the bias for the whole assembly. For the
fission fragment detectors the bias requirements
were not high, so ordinary series connections were
made as shown in Figure (A-7).

Detector Matching

The matching of the detectors in the array
(used as a single large area detector) to get a
uniform response requires: (1) matching of the
depletion layers and (2) compensating the effects
of stray capacitances to ground.

Figure (A-7) shows the electrical connections
for a detector array. C_1, C_2 ... C_6 refer to the
six sets of detector, each with three detectors in
parallel. Each detector set, C_i, is tested separ-
ately by putting a constant charge with a pulser and
a small input condenser (the other detectors being
bypassed) and the resistors, R_i ($\sim$ 10 K), are
adjusted until the outputs are the same. This makes
the depletion layers approximately the same.

When the six sets were operated in series,
as in Figure (A-7), the resolution was worse than
expected. This effect was traced to stray capaci-
tances from the various detectors to ground (the
K's in figure). These stray capacitances were
reduced to minimum by shortening leads as far as
possible. Then capacitors (the σ's in figure) were

added in parallel with the C's, by trial and error until each set gave the same response to a fixed charge input. A specially constructed double pulser (shown connected across detector No. 4 in figure) was used for this test so that additional grounds were not introduced.

The effect of stray capacitances seemed unusually large. Therefore, the system of capacitances of Figure (A-6) (excluding the σ's) was investigated mathematically. A completely rigorous solution is extremely complicated and only a first order correction was calculated. For a charge Q deposited on detector C_n, the input voltage to the preamplifier is given by (for a total of N states in series)

$$V_n = \frac{Q}{C_n} \left[1 - \sum_{i=1}^{N} K_i \sum_{j=1}^{i} \frac{1}{C_j} \right] \tag{1}$$

showing that there is a variation of output with n even if all the C's are the same.

To obtain an estimate of the magnitude of the effect, assume all C's the same (=C) and all K's the same (=K). Then,

$$V_n = \frac{Q}{c} \left[1 - \frac{(N+n)(N-n+1)}{2} \frac{K}{c} \right] \tag{2}$$

The ratio of output of the top stage to that of the bottom stage is

$$\frac{V_N}{V_1} = 1 + \frac{N(N-1)}{2} \frac{K}{C} \qquad (3)$$

For a representative array, $N = 6$, $C = 5000$ pf and $K = 20$ pf, we get

$$\frac{V_N}{V_1} = 1.06$$

This gives another reason for not putting all eighteen detectors in series, since if k is still the same per stage,

$$\frac{V_N}{V_1} = 2.8$$

(Which is only indicative, once the first order expansion in k/c is no longer valid) and a lot more capacity (σ's) would have to be added to the upper stages, losing some of the advantage in resolution otherwise gained by not connecting detectors in parallel.

APPENDIX 7

Preamplifier Selection

There are two types of preamplifier config-
uration one can use. The first, more commonly used
until the introduction of the solid state detectors,
is the "voltage-sensitive" type, and the second is
"charge-sensitive".

In the "voltage-sensitive" preamplifier of
gain A, the output voltage is given as

$$V_o = A \frac{Q}{C_D}$$

where Q is the charge deposited on the detector and
C_D is the detector capacitance + input capacitance.

The corresponding expression[*] for the "charge-
sensitive" configuration is

$$V_o = \frac{Q}{C_f}$$

where C_f is the feedback capacitance of the pre-
amplifier.

The principle short coming of the voltage
sensitive configuration is its sensitivity to
changes in detector capacitance. This was

---

* See Appendix (8-A).

unimportant until the introduction of the solid
state detectors. Because of this undesirable
dependence of output pulse height on detector cap-
acitance with voltage-sensitive preamplifiers, charge
sensitive preamplifiers are preferably used with
semiconductor detectors. In the charge sensitive
configuration nearly all the charge appears across
the feed-back capacitor, C_f, which can be chosen to
have very low temperature coefficient for high
stability.

Although charge-sensitive preamplifiers are
superior to voltage sensitive ones when used with
single detectors, complications arise when one wishes
to connect several detectors to a single preamplifier.
If one uses detector arrays connected in series, as
we did for our experiment, it turns out that the
charge-sensitive configuration no longer gives
an output independent of detector capacitance[*].

It was pointed out by Fairstein[33] that the
charge sensitive configuration should be slightly
noisier than the voltage sensitive one; also, since
the voltage sensitive preamplifier has a very high
input resistance and a very low input capacitance,
it permits fast rise times from detectors which

---

* See Appendix (8-B).

have an unavoidably large component of series
resistance combined with a high capacitance.

Since the use of detector arrays nullified
the main advantage of the charge sensitive config-
uration, and since voltage sensitive preamplifiers
were otherwise superior for our work, we used voltage
sensitive preamplifiers in these experiments. The
gain 200 preamplifiers we used were designed by
J. Hahn in our laboratory.

APPENDIX 8

A. Charge Sensitive Preamplifier with a Single Detector.

The equivalent circuit of the system is shown in Figure (A-8-a). In the diagram C_D is the detector capacitance, C_g the grid capacitance, C_f the feed back capacitance and A the open loop gain of the amplifier.

Let Q be the charge collected by the detector when the particle hits the detector, q_1 the charge on C_g and C_D together, and q_2 the charge on C_f. Then

$$q_1 + q_2 = Q \tag{1}$$

$$q_1 = (C_g + C_D) V_1 \tag{2}$$

Where V_1, is the voltage across C_D

$$q_2 = Q - q_1 = -C_f (V_{out} - V_1) \tag{3}$$

and $V_{out} = - AV_1$

From eqn (3)

$$Q - (C_g + C_D)V_1 = - C_f V_{out} + C_f V_1$$

$$V_{out} = - \frac{Q}{C_f + \dfrac{C_g + C_D + C_f}{A}}$$

Usually the open loop gain is so large, that the output voltage can be approximated as

$$V_0 = - \frac{Q}{C_f}$$

B. <u>Charge Sensitive Preamplifier in Conjunction with</u>

<u>Two Semiconductor Detectors in Series.</u>

The equivalent circuit for this configuration is shown in Figure (A-8-b). We consider the case of particle being detected in detector 1. The charge distribution in various components is shown in the figure. This gives following equations

$$q_1 = C_1 \, V_1 \tag{1}$$

$$q_2 = Q - q_1 = - C_2 \, (V_2 - V_1) \tag{2}$$

$$q_3 = -C_f \, (V_{out} - V_2) \tag{3}$$

$$V_{out} = - A V_2 \tag{4}$$

$$q_2 - q_3 = Q - q_1 - q_3 = C_g \, V_2 \tag{5}$$

From eqn. (2)

$$V_1 = \frac{Q + C_2 V_2}{C_1 + C_2} \tag{6}$$

and from eqn. (5) we get

$$Q = C_1 \, V_1 + [C_g + C_f \, (1 + A)] \, V_2 \tag{7}$$

Putting eqn. (6) in eqn. (7)

$$V_2 = \frac{Q}{C_1 + \dfrac{[C_f(1 + A) + C_g] \, (C_1 + C_2)}{C_2}}$$

This expression along with eqn. (4) gives the expression

$$V_{out} = - \frac{Q}{C_f\left(1 + \dfrac{C_1}{C_2}\right) + \dfrac{C_1 + (C_g + C_f) \, (1 + C_1/C_2)}{A}}$$

Which is no longer independent of the detector capacitance, even when the open loop gain (A) is big enough to make the second term in the denominator negligible.

APPENDIX 9

Three Parameter System (3PS)

In our work we required recording of:

(1) the energies of the fission fragments as well as the time-of-flight of the neutron which caused the fission.

(2) the energy of the ternary alpha particles emitted in fission along with the time-of-flight of the neutron responsible for fission.

In order to record this information we procured a R.I.D.L. Three Parameter Data Acquisition System, hereafter called a Three Parameter System or 3PS, which provides analog-to-digital analysis of two or three mutually coincident pulses, as desired.

The system consists of three separate analog-to-digital converters, henceforth referred to as ADC's, complete with triple coincidence logic and internal amplifiers, three individual address scalers, two scalers of 10^3 and one scaler of 10^5. The 10^5 scaler is used for time-of-flight measurements. Each unit has an individual conversion gain selector to select 50, 100, 200, 500, or 1000 channels full range, and an overflow selector to produce address overflow and address reset pulses at 20, 50, 100, 200, 500 and 1000 channels.

The time-of-flight data is stored in 80,000 channels with a channel width of 50 nsec by using an external circuit which is described in Chapter II.

The low counting rate permitted us to use a "poor man's" recording system. The data are recorded on paper tape by a mechanical Tally punch as each event occurs. The tape punch can handle up to 60 characters per second.

While the event selected for analysis is being analized or punched, the 3PS gives a busy signal pulse. The punching time required for an event (12 characters) is ~200 milliseconds, which is the dead time of the system.

The system provides pulses suitable for a two dimensional oscilloscope display of any two parameters, during data accumulation.

APPENDIX 10

Pulse Height Information and

Three Parameter Measurements

In general the statistical accuracy of the pulse
height data, which could be added together, was not
sufficient to allow us to reach any definite con-
clusions. Nevertheless, a short section is presented
in Figures (A-9), (A-10), and (A-11) for the three
cases. The lower part of Figure (A-9) shows the
ternary alpha yield as a function of the time-of-
flight of neutrons (channel numbers with channel width
of 0.2 μsec). The points on top of this curve are
the mean positions of the ternary alpha energy dist-
ribution (calculated using the formula given in
Appendix (11)) corresponding to each neutron time-of-
flight interval. As was indicated before, the det-
ector depletion layer was not deep enough to absorb
the alpha particles of energy higher than 12 MeV,
and because of the thick uranium sample used the energy
distribution was distorted. However, some variation
outside the errors can be seen.

Figure (A-10) is a similar curve corresponding
to the fission yield measurements with thick uranium
target. As previously mentioned the discriminator
bias was set quite high (~80 MeV) for these measure-
ments. Thus the pulse height distribution consists

of only the high energy tail of the fission fragments kinetic energy distribution. The variations in the mean position of the distributions exhibit themselves outside the statistical error. However, to decipher any systematic trend appears not to be possible, with this statistical accuracy.

Figure (A-11) is a part of the results from the three parameter measurements which were made as exploratory work for future measurements planned. In these measurements two banks of detectors facing each other with one bank coated with $\sim$ 50 μgm/cm^2 U^{235} were used. For each fission event observed the pulse height produced by each of the two fission fragments was recorded together with the time-of-flight of the neutron causing the fission. The upper part of this figure displays the mean of the total kinetic energy distribution of the fission fragments as a function of neutron energy, for the small section near 35 ev. This does not show any marked variations outside the statistical errors.

Pulse height information from the 200 μgm/cm^2 uranium sample measurements was not examined in detail, because the three parameter measurements, which were much more elaborate, included the results which could be extracted from those measurements.

APPENDIX 11

The Mean Position and the Width of a

Peak and Their Statistical Errors

The mean position of the peak of a distribution
in a parameter X is defined as

$$< X > = \frac{\sum_i X_i N_i}{\sum_i N_i} \qquad (1)$$

Where N_i is the number of times parameter X is equal
to X_i.

The error in this is due to the statistical
standard deviation $(\sqrt{N_i})$

Differentiating w.r.t. to N_j we get

$$\frac{\partial < X >}{\partial N_j} = \frac{X_j}{(\sum_i N_i)} - \frac{\sum_i X_i N_i}{(\sum N_i)^2}$$

The error in $< X >$ is given by

$$[\delta < X >]^2 = \sum \frac{X_j^2 N_j}{(\sum N_i)^2} + \sum \left(\frac{\sum_i X_i N_i}{\sum N_i}\right)^2 \frac{N_i}{(\sum N_i)^2} - \sum 2 \frac{X_j \sum X_i N_i N_j}{\sum N_i (\sum N_i)^2}$$

$\delta N_j = \sqrt{N_j}$ is substituted in this expression.

$$[\delta < X >]^2 = \frac{< X^2 >}{\sum N_i} + \frac{< X >^2}{\sum N_i} - \frac{2 < X >^2}{\sum N_i}$$

$$\delta < X > = \sqrt{\frac{< X^2 > - < X >^2}{\sum N_i}} \qquad (2)$$

The square root of the variance is defined
as the width of the distribution

$$W = <X^2> - <X>^2$$

$$= \frac{\sum X_i^2 N_i}{\sum\limits_i N_i} - \left(\frac{\sum X_i N_i}{\sum N_i}\right)^2 \tag{3}$$

To find the error on the width, we follow
the same procedure

$$\frac{\partial W}{\partial N_j} = \frac{X_j^2}{\sum N_i} - \frac{\sum\limits_i X_i^2 N_i}{(\sum\limits_i N_i)^2} - \frac{2(\sum\limits_i X_i N_i)X_j}{(\sum N_i)^2} + \frac{2(\sum\limits_i X_i N_i)^2}{(\sum N_i)^3}$$

Taking the square and putting $(\delta N_j)^2 = N_j$
as before we get

$$(\delta W)^2 = \frac{<X^4> - 4<X^3><X> + 8<X^2><X>^2 - <X^2>^2 - 4<X>^4}{\sum N_i}$$

Therefore, the error on the width is given as

$$\delta W = \sqrt{\frac{<X^4> - 4<X^3><X> + 8<X^2><X>^2 - <X^2>^2 - 4<X>^4}{\sum N_i}}$$

APPENDIX 12

Pick-up Rejection Circuit

In a low counting rate experiment, spurious pulses arising from electrical pick-up, transients, etc., produce a significant background. In our first preliminary run on the detection of long range α particles in fission, we observed that the background introduces quite a large uncertainty in the analysis. Thus, it was found necessary to find a way of eliminating or at least reducing the acceptance of these spurious pulses.

We looked for properties of the spurious pulses by which they could be distinguished from genuine pulses. It was noticed that the pick-up occured as a train of pulses, resembling a modulated signal of many microsecond duration whereas the genuine pulse rate was of the order of one per second.

The circuit was designed to reject the pulses with repetition rate less than 3 μsec. The pulses coming in at interval greater than 3 μsec were treated as genuine pulses.

Description of the circuit:

The circuit is divided into two parts. The upper part which passes the genuine pulses in the absence of pick-up is called channel A, and the lower part which gets triggered from pick-up pulses

and blocks the pulses from getting through the final gate (G2), channel B. Channel A consists of a univibrator discriminator, a gate (G1), and two univibrators (U2 and U3) followed by the final gate. Channel B consists of a flip-flop circuit followed by four univibrators (U4, U5, U6 and U7).

For the moment we will neglect the gate G1. It passes the pulses just as they come from the discriminator as long as there is no anticoincidence input pulse. This will be discussed later.

First let us discuss the case when a single genuine pulse arrives, at time T = 0, at the discriminator with amplitude greater than the discrimination level. U1 puts out a 100 ns wide pulse. G1 provides exactly similar pulses with both polarities. The leading edge of the negative pulse triggers U2 giving a 3 μsec wide pulse. The positive output pulse from U2 is fed at the input of U3. As the univibrator can only be fired by a negative going pulse, it gives an output pulse after 3 μsec, the width of which is adjusted to be .5 μsec. This passes through G2 and is accepted as a genuine pulse if no inhibitor pulse arrives in time at the anticoincidence input of G2 to block it. The circuit is so arranged that the inhibitor pulse arrives if the first pulse is followed by another pulse in less than 3 μsec. Otherwise, no

inhibitor pulse occurs until 3.5 μsecs which is
.5 μsec after the first pulse has gone through.
This is achieved in the following way.

The positive pulse output from G1 is sent to the
flip-flop input (a positive going signal is required
to fire a flip-flop). This pulse flips it from one
equilibrium state (-5V at the output) to the second
equilibrium state (0V.) and it stays in this state
till either a second pulse arrives at the input or a
reset pulse is applied (the pulse required to reset
the flip-flop is a positive going 5V signal). The
reset pulse is the trailing edge of the negative output
of U3. If no other pulse reaches the flip-flop input
for 3.5 μsec, the reset pulse brings the flip-flop
back to the first equilibrium state, thus producing
a output pulse of 3.5 μsec width. If a second pulse
arrives at the flip-flop input before 3.5 μsec have
passed then reset pulse has no effect, and the width
of the flip-flop output pulse equals the separation
between the pulses.

Now let us consider the case of a train of
pulses with repetition rate t (t < 3 μsec) and
amplitude large enough to fire the discriminator,
and discuss their passage through channel B.

The first two pulses produce an output pulse from the flip-flop of width t μsec (since t is less than 3 μsec the reset pulse is ineffective). U4 is fired after t μsec, whose leading edge fires U5. U6 and U7 are triggered after time intervals as shown in the diagram. The negative outputs of U4 and U7 are used as inhibitor pulses for G2. Thus, the inhibitor pulses are present from t to (t + 6) μsec and from (t + 7.5) μsec to t + 13.5 μsec. The gap of 1.5 μsec is not significant because no pulse can arrive during this time, due to the gate G1. As t is less than 3 μsec the inhibitor pulse reaches G2 in time to block the pulse from channel A. After 7.5 μsec if pick-up is still present the same process repeats itself.

Gate G1.

This gate was inserted to prevent pulses entering the system after the flip-flop has given an output pulse and firing of the flip-flop again before it has had time to recover. The recovery time of these modules is 10 nsec $\pm$ 10% of the width of the output pulse.

After the flip-flop output pulse occurs, anti-coincidence input pulses to G1 from U4 and U6 close the gate. The U4 pulse arrives after t μsec and lasts 6 μsec, while the U6 pulse arrives after t + 4 μsec and lasts for 3.5 μsec. So the gate is closed for

7.5 μsec after t μsec. The two pulses provide an
inhibition time greater than the width of the U4 pulse,
which prevents the triggering of U4 before it has had
time to recover.

If a train of pick-up arrives with odd number of
pulses in it, there is some probability that the last
pulse will come at such a time interval which could
make it appear as a genuine pulse (no other pulse
following it in time interval of less than 3 μsec).
The second inhibitor pulse in G2 gate, which stays on
for 5 μsec after the time interval of t + 7.5 μsec,
is for blocking such a spurious pulse.

In short, the function of the whole circuit
is to take a pulse coming out of the discriminator
and delay it by 3 μsec. In the mean time the job of
channel B is to sense whether another pulse follows
it in less than 3 μsec. If it does, the net-work of
univibrators blocks the final gate and no signal out-
put is given. If it is not followed by any pulse with-
in next 3 μsecs, the G2 is open and the pulse passes
through.

The circuit has an effective dead time of 13.5
μsecs. Because of this, it can not be used for high
counting rate work. For our experiment it was very
useful, while taking data on 2000 channel analizer.
It was not used while taking the data with three para-

meter data acquisition system, because the recording
system has a dead time of 200 milliseconds (time taken
to punch the data on paper tape). Thus, even if a
train of pick-up pulses lasts for several hundred
microseconds, only the first pulse has some chance
of being recorded, which is also reduced considerably
by the coincidence requirements.

REFERENCES

1. N. Bohr and J. A. Wheeler, Phys. Rev. 56, 426 (1939).

2. R. D. Present, Phys. Rev. 59, 466 (1941).

3. N. A. Perfilov, "Physics of Nuclear Fission", Atomnaya Energ., Suppl. 1 (1958).

4. L. W. Alvarez, quoted by Farwell, Segré and Wiegband, Phys. Rev. 71, 327 (1947).

5. K. W. Allen and J. T. Dewan, Phys. Rev. 80, 181 (1950).

6. C. B. Fulmer and B. L. Cohen, Phys. Rev. 108, 370 (1957).

7. (a) H. E. Wegner, Bull. Am. Phys. Soc. II, 6, 307 (1961).
   (b) M. L. Muga, Phys. Rev. Lett. 11, 129 (1963).
   (c) J. C. Watson, Phys. Rev. 121, 230 (1961).

8. E. K. Hyde, Univ. of California Radiation Lab. Report, UCRL 9036 (1960).

9. I. Halpern, Annual Rev. of Nucl. Sci. 9 (1959).

10. N. A. Perfilov, Y. F. Romanov, Z. I. Solov'eva, Soviet Physics Uspekhi 3, 542 (1961).

11. Tsien San-Tsiang, Ho Zah-Wei, R. Chastel and L. Vigneron, J. Phys. Radium 8, 165, 200 (1947).

12. J. S. Fraser and R. B. Schwartz, Nucl. Phys. 30, 269 (1962).

13. A. Bohr, Paper P/911, Proc. Intern. Conf. Peaceful Uses of Atomic Energy, Geneva (1955).

14. J. Wheeler, Physica XXII, 1103 (1956).

15. (a) R. B. Regier, W. H. Burgus and R. L. Tromp, Phys. Rev. 113, 1589 (1959).

(b) R. B. Regier, W. H. Burgus, R. L. Tromp and B. H. Sorensen, Phys. Rev. 119, 2017 (1960).

16. F. J. Walter, J. H. Neiler and H. W. Schmitt, Bull. Am. Phys. Soc. II, 8, 369 (1963).

17. G. A. Cowan, B. P. Bayhurst and R. J. Prestwood, Phys. Rev. 130, 2380 (1963).

18. (a) G. P. Ford, Phys. Rev. 118, 1261 (1960).

(b) J. B. Niday, Phys. Rev. 121, 1471 (1961).

19. M. L. Muga, H. R. Bowman and S. G. Thompson, Phys. Rev. 121, 270 (1961).

20. W. W. Havens, Jr. and J. Hahn, Rev. Sci. Inst. 31, 490 (1960).

21. W. O. Lecroy, Jr., Columbia Univ. Nevis Cyclotron Lab. Report, NEVIS 106.

22. L. J. Rainwater, W. W. Havens, Jr., J. S. Desjardins and J. L. Rosen, Rev. Sci. Inst. 31, 481 (1960).

23. (a) G. K. Mehta and E. Melkonian, Bull. Am. Phys. Soc. 7, 304 (1962).

(b) G. K. Mehta and E. Melkonian, Columbia Univ. Pegram Nuclear Physics Lab. Report, CU(PNPL)-218 (1962).

24. (a) A. Michaudon, R. Genin, R. Joly, and G. Vendryes, Saclay Report, CEA-1093 (1958).

(b) A. Michaudon, R. Bergere, A. Coin and R. Joly, Le Journal de Physique et La Radium 21, 429 (1960).

25. A. A. Panov, Soviet Physics Jetp. 16, 599 (1963).

26. A. Michaudon, A. Lottin and D. Paya, C. R. Acad. Sc., t. 256, p. 1490 Seánce du 11 fevrier (1963).

27. E. Melkonian, W. W. Havens, Jr., and L. J. Rainwater, Phys. Rev. 92, 702 (1953).

28. J. C. D. Milton and J. S. Fraser, Can. Journal of Physics 40, 1626 (1962).

29. E. Melkonian, Nuclear Instr. and Methods 11, 307 (1961).

30. W. L. Brown, Trans. I.R.E., Vol. NS-8, 7 (1961).

31. (a) H. W. Schmitt, Bull. Am. Phys. Soc. 6, 240 (1961).

    (b) F. J. Walter, J. W. T. Dabbs and L. D. Roberts, Nuclear Electronics (International Atomic Energy Agency, Vienna, 1962), p. 391.

32. H. C. Britt and H. E. Wegner, Rev. Sci. Instr. 34, 274 (1963).

33. E. Fairstein, Nuclear Science Series Report No. 32, 210 (1961).

FIGURE CAPTIONS

Figure 1   Lower curve: total kinetic energy distribution
of fission fragments from the thermal neutron
fission of U^{235}. Upper curves: mass distri-
butions of the fission fragments for several
values of total fragment energy (E_T). The
abscissa is the fragment energy (E) which is
proportional to mass through the relationship
Mass = 236 E/E_T. The data are taken from
I. G. Schröder, J. A. Moore and G. J. Safford,
Fission Fragment Mass Distribution, Columbia
University Pegram Nuclear Physics Laboratory
Report No. 208 (1960).

Figure 2   Block diagram of the experimental set-up.

Figure 3   Photograph of a Detector Array.

Figure 4   Photograph of the fission chamber with a
detector array mounted inside.

Figure 5   End-on view of the fission chamber showing
the electrically shielded enclosure used for
electrical connections.

Figure 6   Circuit diagram of the "Gated Frequency
Divider".

Figure 7   Block diagram of the Timing circuit.

Figure 8   Contributions to the width (FWHM) of reson-
ances from (a) Instrumental resolution (b)
Moderation effect, and (c) Doppler broadening.

Figure 9   Symbolic block diagram of various computers
              used for the data processing.

Figure 10   Experimental curves for the three measure-
              ments showing the overall results in the
              energy interval of $\sim$ 2 ev to $\sim$ 16 ev. The
              channel width (τ) used for these is 1.0 μsec.

Figure 11   Experimental curves for the three measure-
              ments showing the overall results in the energy
              interval of $\sim$ 12 ev to $\sim$ 40 ev. The channel
              width of 0.2 μsec is used for this region.

Figure 12   Experimental data in the energy interval $\sim$ 39
              ev to $\sim$ 85 ev for the three measurements.
              The channel width τ = 0.2 μsec is used.

Figure 13   Experimental data displaying the energy inter-
              val of $\sim$ 60 ev to $\sim$ 1300 ev for the three
              measurements with the channel width τ= 0.2 μsec.

Figure 14   A representative computer plot of the experi-
              mental data and the computed curve. The levels
              specified for the curve fitting are marked on
              the curve.

Figures 15-
      25   Experimental data and the least square fitted
              curves for the three measurements. The
              background used is also shown. The energy
              levels, specified in the fitting, are indic-
              ated on one curve.

Figure 26   Ratio of alpha particle yield to thin uran-
             ium fission yield (A) and the ratio of thick
             uranium fission yield to thin U fission yield
             (B). Both ratios are in arbitrary units.
             The assignments of Cowan et. al.[17] are indicated
             by vertical lines with the letters H (L) in-
             dicating high (low) degree of symmetric fis-
             sion. The primed letters indicate similar
             assignments with less certainty. The hori-
             zontal lines drawn are from a least square
             fitting of the data to two ratios.

Figure 27   Ratio R_{23} (thick U fission yield/ thin U
             fission yield) plotted as a function of res-
             onance energy for only those resonances where
             the ratio could be obtained with a statistical
             accuracy of better than 60%. The horizontal
             lines drawn on the data are taken from
             Figure (26-A).

Figure 28   Ratio of thick uranium fission yield to thick
             uranium alpha yield (R_{21}) in arbitrary units,
             as a function of resonance energy. The hori-
             zontal lines are the least square fitting to
             the ratios.

Figure 29   Ratio (R_{43}) in arbitrary units, of fission
             yield from two thin U targets (200 $\mu gm/cm^2$
             and 50 $\mu gm/cm^2$) as a function of neutron

energy. The horizontal line drawn is a least square fitting of the ratios.

Figure A-1   Thickness effect on fission yield (a); and on alpha yield (b).

Figure A-2   Pulse height distribution of alpha particles (Th^{228} source) for a detector 12 mm in diameter, resistivity 200 Ω-cm, operating at 70 volts.

Figure A-3   Pulse height distribution of fission fragments in the thermal neutron fission of U^{235}. The spectrum was taken with a 2 cm diameter surface barrier detector of resistivity 200 Ω-cm at 45 V bias.

Figure A-4 U^{235} fission fragment spectrum recorded for a surface barrier detector, 1 cm in diameter and of resistivity 200 Ω-cm at two different voltages. The spectrum shifted towards right was taken at 180 V bias and the other at 22 V.

Figure A-5   Probing of the surface of a 2.2 cm diameter surface barrier detector (200 Ω-cm) using a collimated Po source. The positions used on the surface are shown along with the peaks obtained. The peak shown in the upper left corner was taken by moving the source to a distance of 2 1/2 cm from the detector thus making the whole surface of the detector effective.

TABLE I

No.	Energy (ev)	Ternary Alpha Yield / Thin U Fission Yield	Thick U Fission Yield / Thin U Fission Yield	Thick U Fission Yield / Ternary Alpha Yield
1	2.02	.623 ∓ .103	.907 ∓ .108	1.456 ∓ .241
2	3.16	.815 ∓ .042	.812 ∓ .040	0.996 ∓ .055
3	3.60	.811 ∓ .030	.760 ∓ .030	0.937 ∓ .038
4	6.18	.953 ∓ .087	.899 ∓ .080	0.943 ∓ .094
5	6.38	.682 ∓ .037	.734 ∓ .037	1.076 ∓ .058
6	7.09	.790 ∓ .051	.774 ∓ .048	0.980 ∓ .063
7	8.78	.750 ∓ .013	.730 ∓ .012	0.973 ∓ .017
8	9.28	.707 ∓ .036	.684 ∓ .034	0.967 ∓ .044
9	11.65	.695 ∓ .082	.755 ∓ .081	1.086 ∓ .128
10	12.39	.741 ∓ .021	.731 ∓ .020	0.946 ∓ .027
11	13.76	.733 ∓ .087	.774 ∓ .083	1.056 ∓ .128
12	14.0	.818 ∓ .059	.688 ∓ .050	0.841 ∓ .062
13	15.4	.660 ∓ .077	.912 ∓ .090	1.382 ∓ .161
14	16.09	.676 ∓ .077	.801 ∓ .083	1.185 ∓ .135
15	16.67	.662 ∓ .059	.768 ∓ .063	1.160 ∓ .103
16	18.05	.797 ∓ .086	.769 ∓ .079	0.964 ∓ .090
17	19.30	.731 ∓ .021	.810 ∓ .022	1.108 ∓ .032
18	21.10	.722 ∓ .037	.823 ∓ .039	1.138 ∓ .058
19	22.98	.945 ∓ .095	.850 ∓ .084	0.899 ∓ .090
20	23.50	.934 ∓ .085	.894 ∓ .077	0.957 ∓ .087
21	23.67	.653 ∓ .080	.662 ∓ .073	1.014 ∓ .124
22	24.32	.799 ∓ .083	.858 ∓ .081	1.074 ∓ .107
23	25.60	.757 ∓ .084	.838 ∓ .081	1.107 ∓ .123
24	27.87	.872 ∓ .081	.881 ∓ .077	1.010 ∓ .094
25	32.13	.734 ∓ .039	.886 ∓ .043	1.207 ∓ .056
26	33.60	.792 ∓ .046	.687 ∓ .040	0.865 ∓ .050
27	34.45	.832 ∓ .038	.749 ∓ .034	0.901 ∓ .041
28	35.25	.718 ∓ .021	.758 ∓ .021	1.072 ∓ .031
29	38.40	.716 ∓ .105	.549 ∓ .084	0.767 ∓ .109
30	39.50	.829 ∓ .045	.740 ∓ .040	0.892 ∓ .048
31	40.65	.677 ∓ .086	.749 ∓ .085	1.106 ∓ .140
32	44.76	.798 ∓ .076	.859 ∓ .075	1.133 ∓ .108
33	47.0	.790 ∓ .062	.899 ∓ .064	1.138 ∓ .089
34	48.3	.626 ∓ .064	.808 ∓ .068	1.291 ∓ .132
35	50.6	.869 ∓ .090	.777 ∓ .079	0.894 ∓ .092
36	51.4	.696 ∓ .048	.735 ∓ .046	1.056 ∓ .072
37	52.4	.791 ∓ .064	.810 ∓ .062	1.024 ∓ .083
38	53.5	.651 ∓ .088	.784 ∓ .089	1.204 ∓ .162
39	55.3	.596 ∓ .071	.647 ∓ .064	1.131 ∓ .135
40	56.1	.776 ∓ .066	.775 ∓ .061	0.989 ∓ .085
41	56.7	.696 ∓ .062	.664 ∓ .055	0.954 ∓ .085

TABLE II

No.	Resonance Energy	Ratio of Thick U to Thin U	Our Assignments of Groupings	Cowan et. al. Assignments
1	8.78 ev	.730 ± .012	H*	L'
2	15.40	.912 ± .090	L	L
3	16.09	.801 ± .083	L	L
4	16.67	.768 ± .063	U	L
5	18.05	.769 ± .079	U	L'
6	19.3	.810 ± .022	L	L
7	21.1	.823 ± .039	L	L
8	22.98	.850 ± .084	U	L
9	23.5	.894 ± .081	L	L
10	25.6	.838 ± .081	U	H
11	27.87	.881 ± .077	L	L'
12	32.13	.886 ± .043	L	L'
13	33.6	.687 ± .040	H	L'
14	34.45	.749 ± .034	H	H'
15	35.25	.758 ± .021	H	H
16	39.5	.740 ± .040	H	H

Notation for our assignments:

$H \rightarrow <E>_{Lower}$ → Lower average energy of the fission fragments.

$L \rightarrow <E>_{Higher}$ → Higher average energy of the fission fragments.

$U \rightarrow$ → Uncertain

Notation for Cowan et. al. assignments:

$L \rightarrow$ Low symmetric fission.

$H \rightarrow$ High symmetric fission.

Primes denote uncertain assignments.

* [Note: To make the two assignments identical, we have indicated by H the group having lower average energy.]

FIG. I

EXPERIMENTAL SET-UP

DETECTOR SET

U^{235} FOIL (0.005")

FISSION CHAMBER

200 μgm/cm^2 U^{235}

~10 METER

NEVIS SYNCHROCYCLOTRON AS A PULSED NEUTRON SOURCE

PREAMPLIFIER

A

B

EMITTER FOLLOWER

AMPLIFIER

DISCRIMINATOR

DISTRIBUTED AMPLIFIER

DISCRIMINATOR

PARALLEL TRANSFER

2.5 mc PULSES

TIMING CIRCUIT

START PULSE

PROMPT GATE

SPARE SCALAR BOARD ADC 2
10^4 3 PARAMETER
SCALER SYSTEM
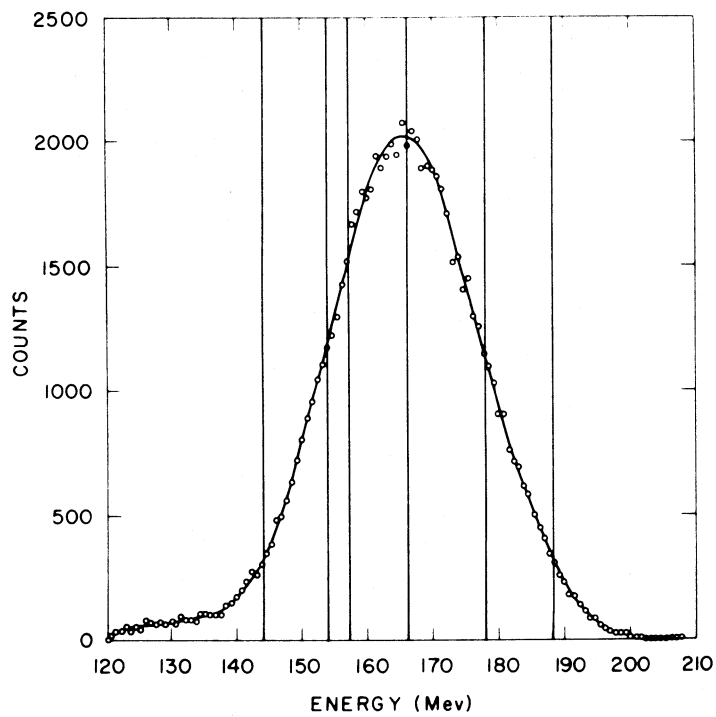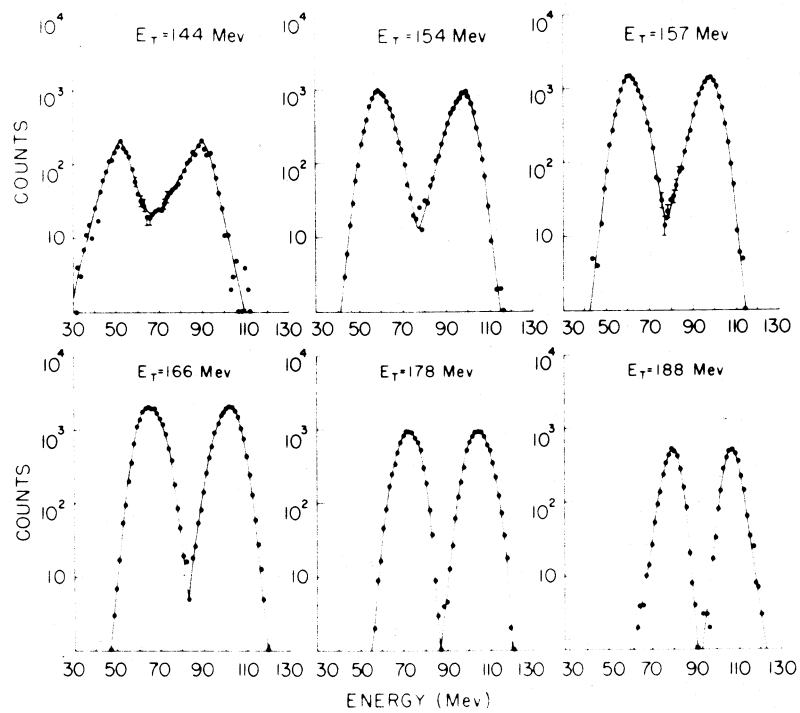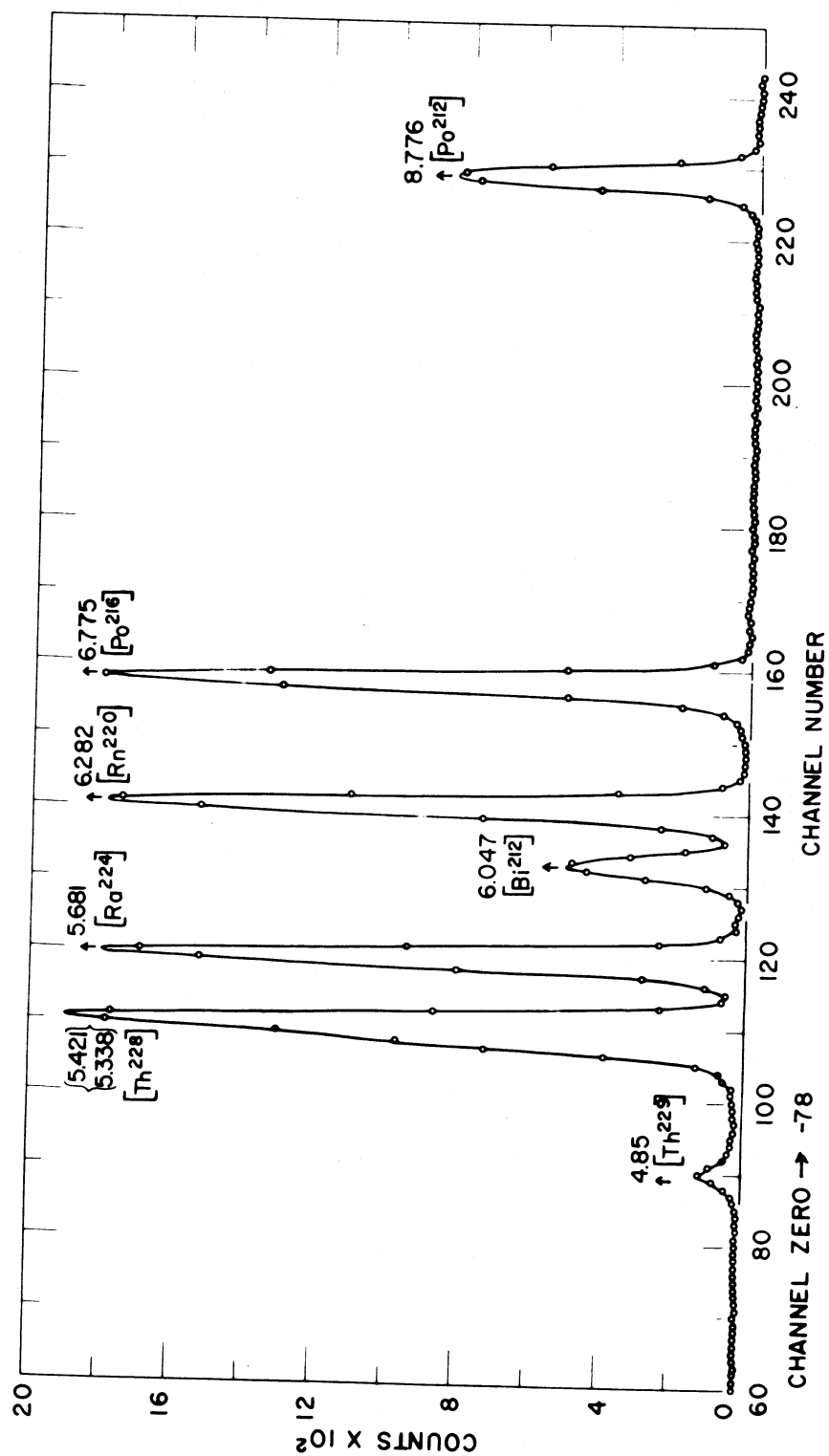
FIG. 2

FIG. 3

FIG. 4

FIG. 5

GATED FREQUENCY DIVIDER
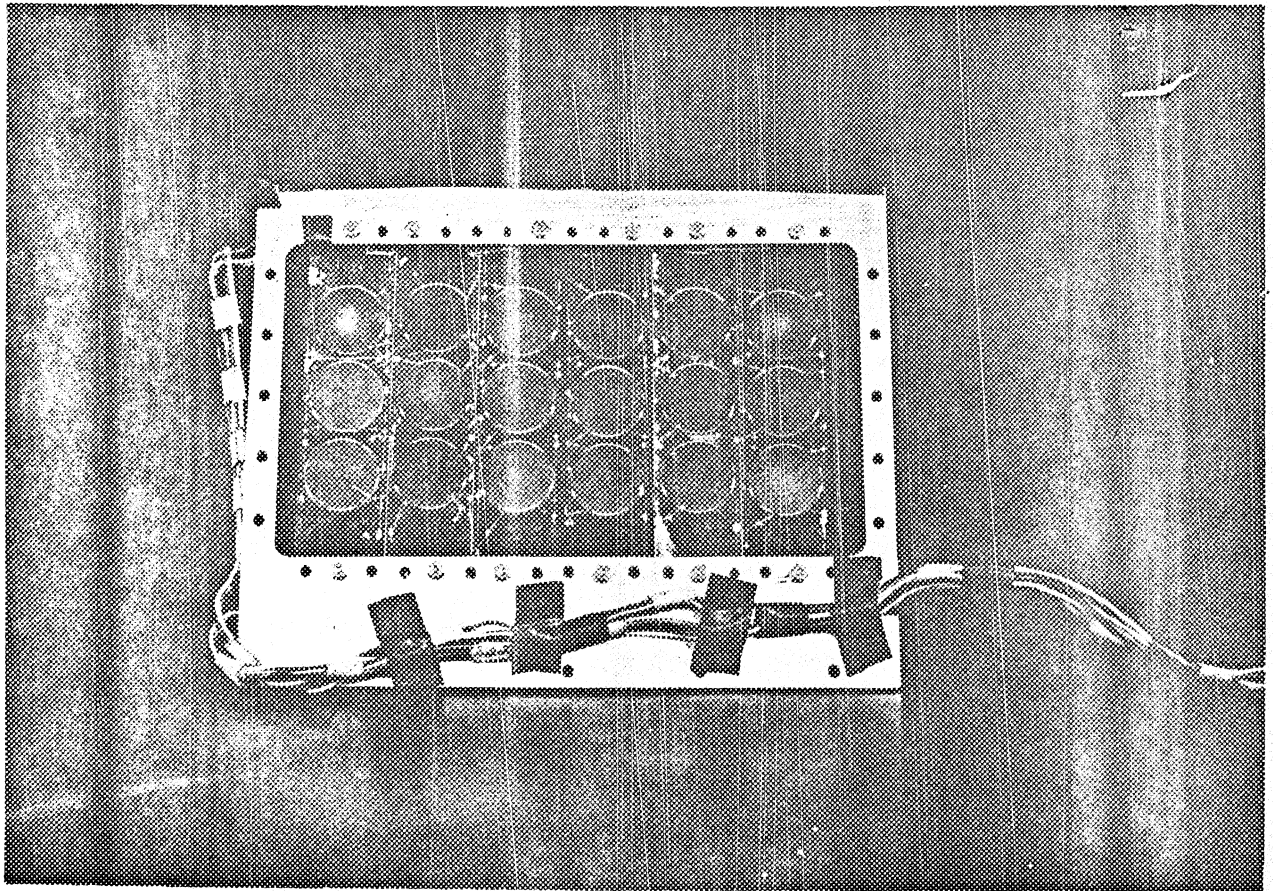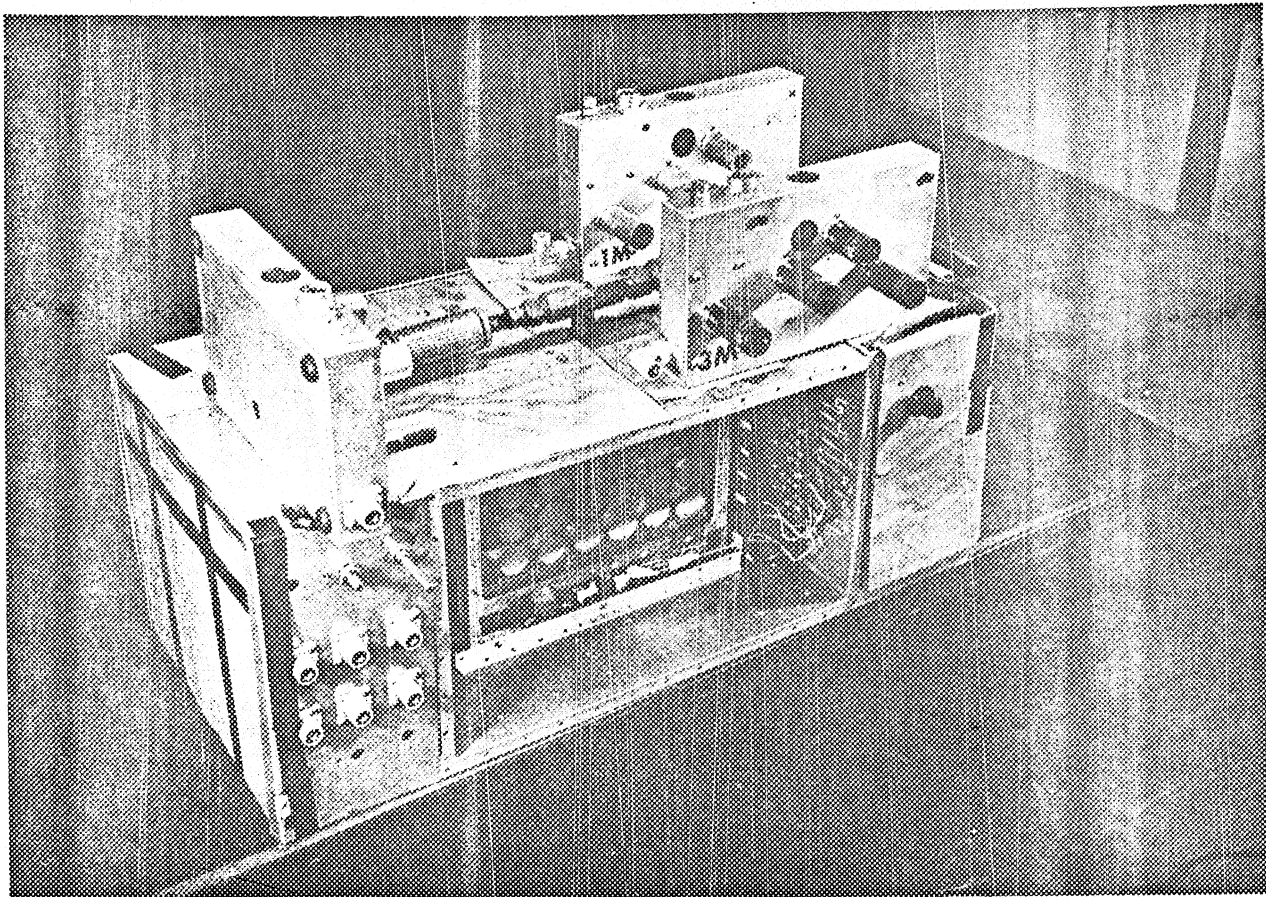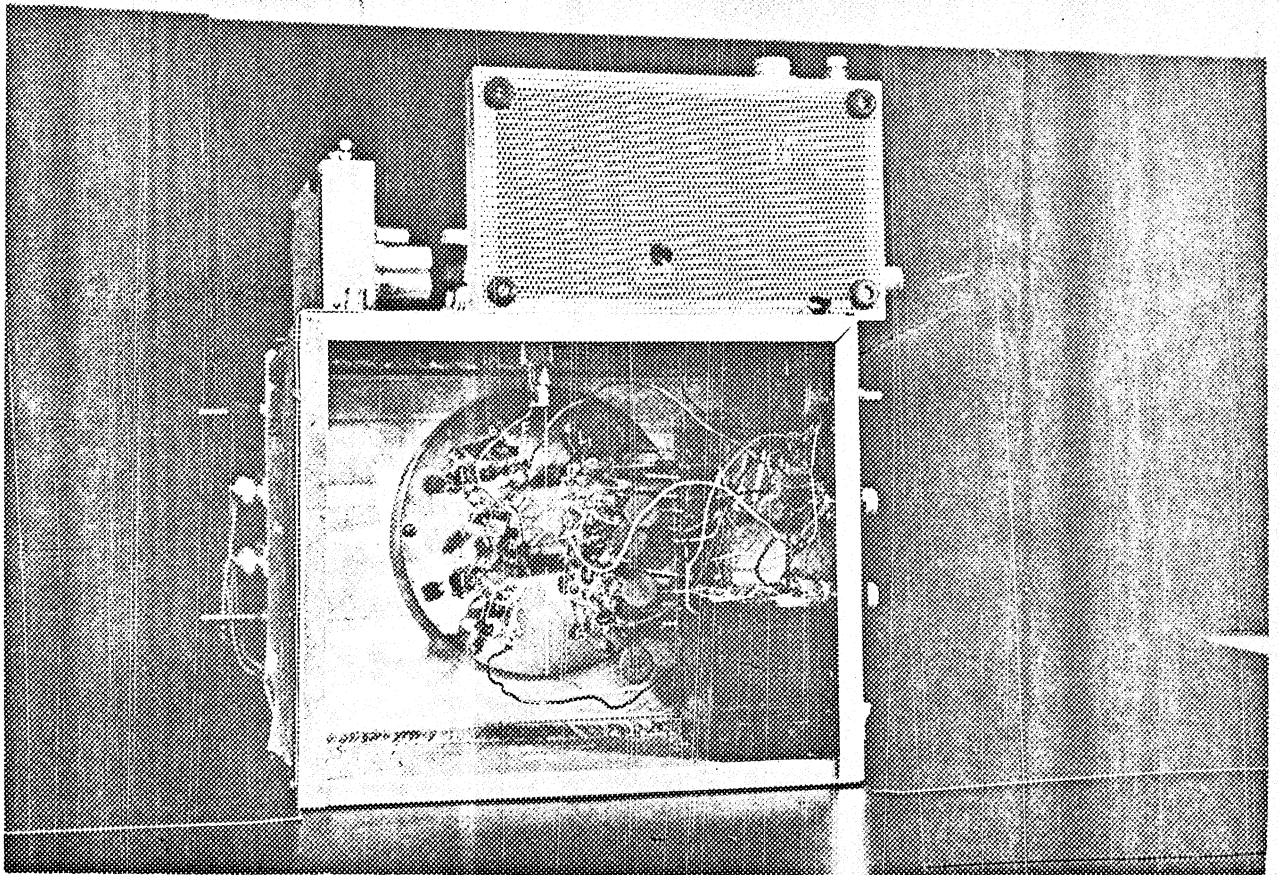
CR1,CR2 D1820 (Sylvania) or HD5000 (Hughes)

TD1 5ma Ge (IN2941) (GE) or T.D.7 (G.I.)

TD2 10ma Ge T.D.6 (G.I.)

ZD1,ZD2 5 V

feed-thru filler, Allen Bradley FIB-A

Q1,Q2 2N2048 (PHILCO)

Q3,Q4,Q5 2N706 or N5382 (NATIONAL)

Q6 2N769, 2N976, or T2122 (PHILCO)

Q7 2N961 (MOTOROLA) or 2N1195

Q8,Q9 2N706 or N5734

(CIRCUIT DESIGNED BY WALTER O. LECROY Jr.)

FIG. 6

TIMING CIRCUIT

FIG. 7

FIG. 8

```
┌─────────────┐
│   PUNCHED   │
│ PAPER TAPE  │
└─────────────┘
       │
┌─────────────┐
│  IBM  1620  │
└─────────────┘
       │
       ▼                    Results of individual runs
    CARDS                   for checks
       │
┌─────────────┐
│  IBM  1401  │
└─────────────┘
       │
 MAGNETIC  TAPE
       │
┌─────────────┐
│  IBM  7090  │
└─────────────┘
       │
       ▼
 FINAL RESULTS
```

FIG. 9

FIG. 10

FIG. 11
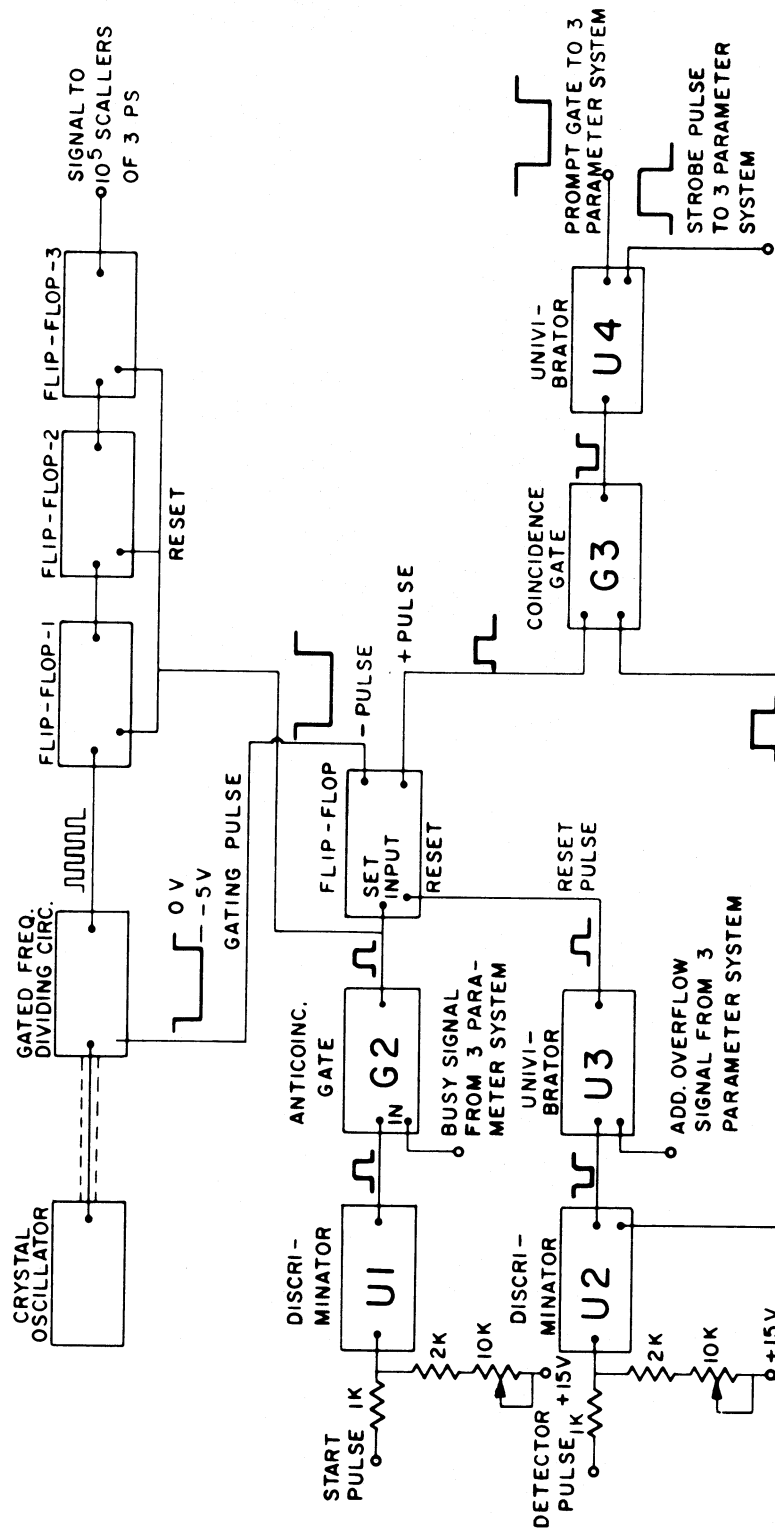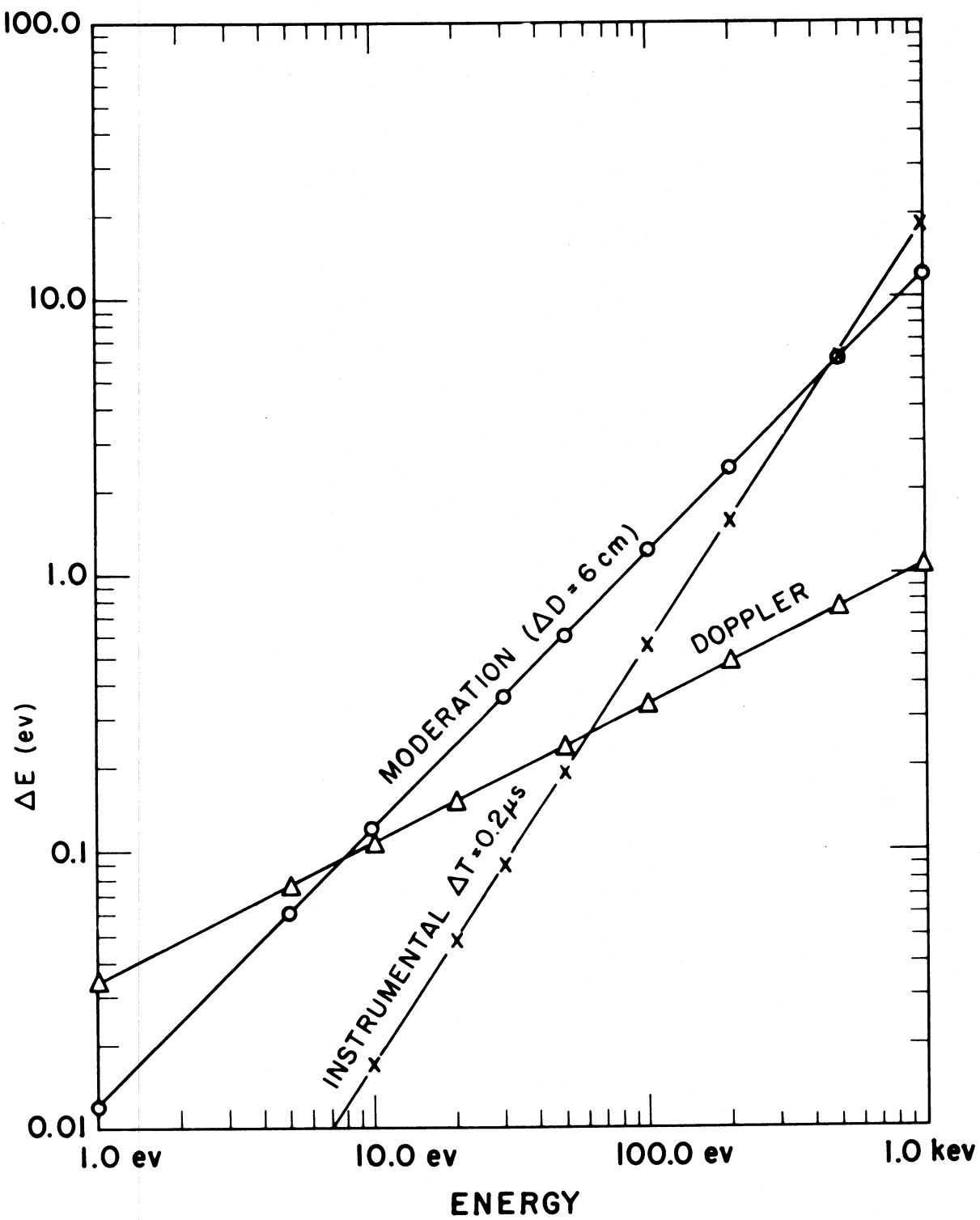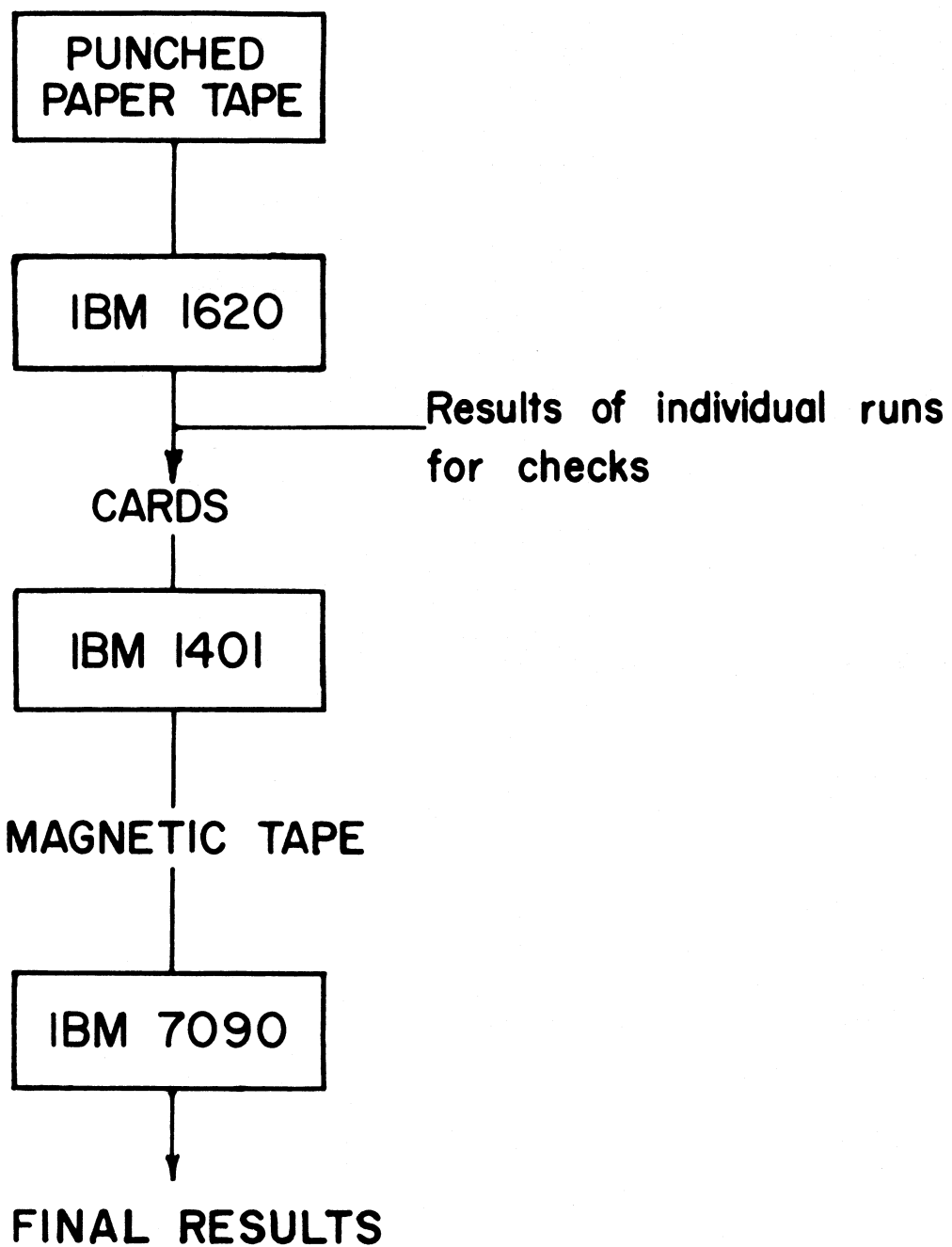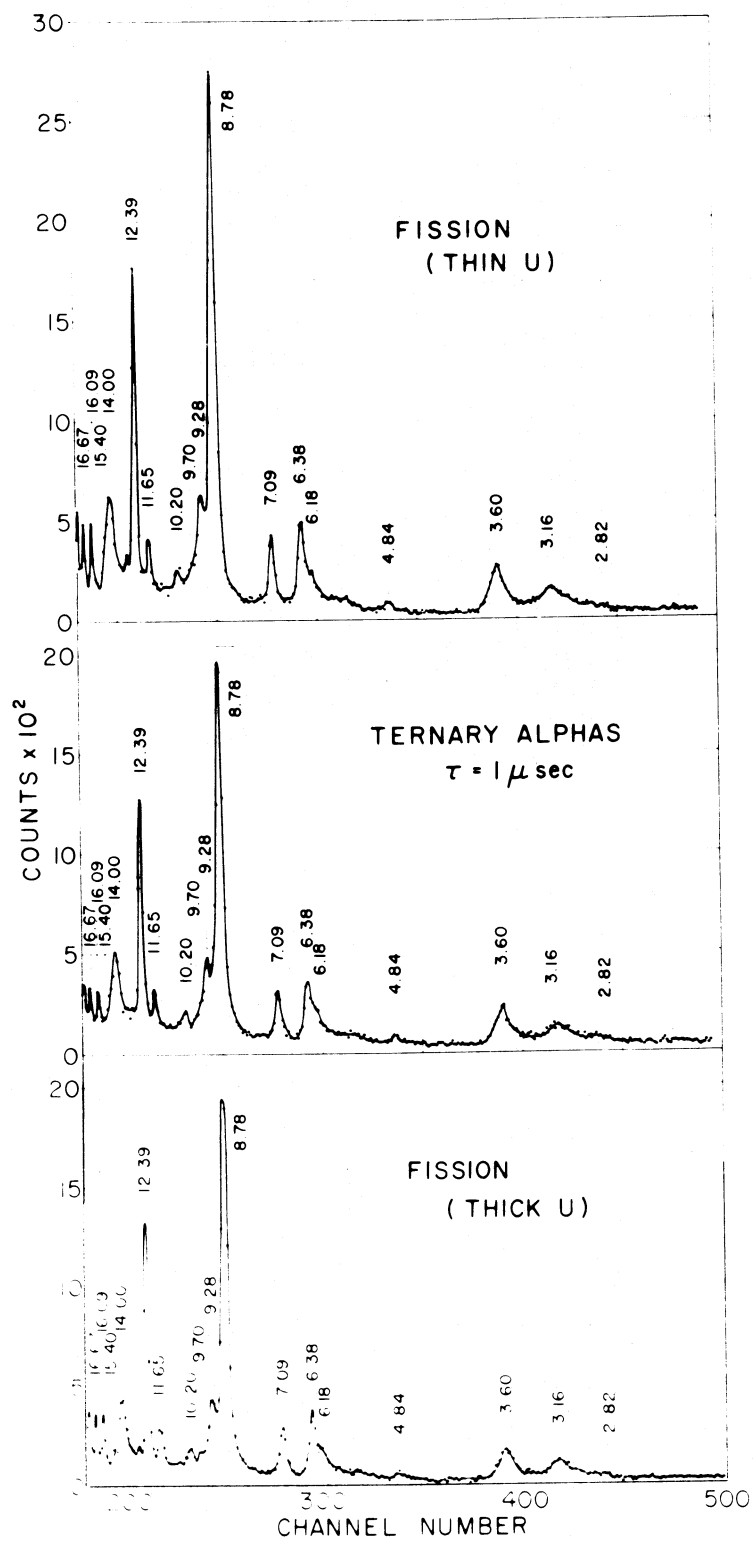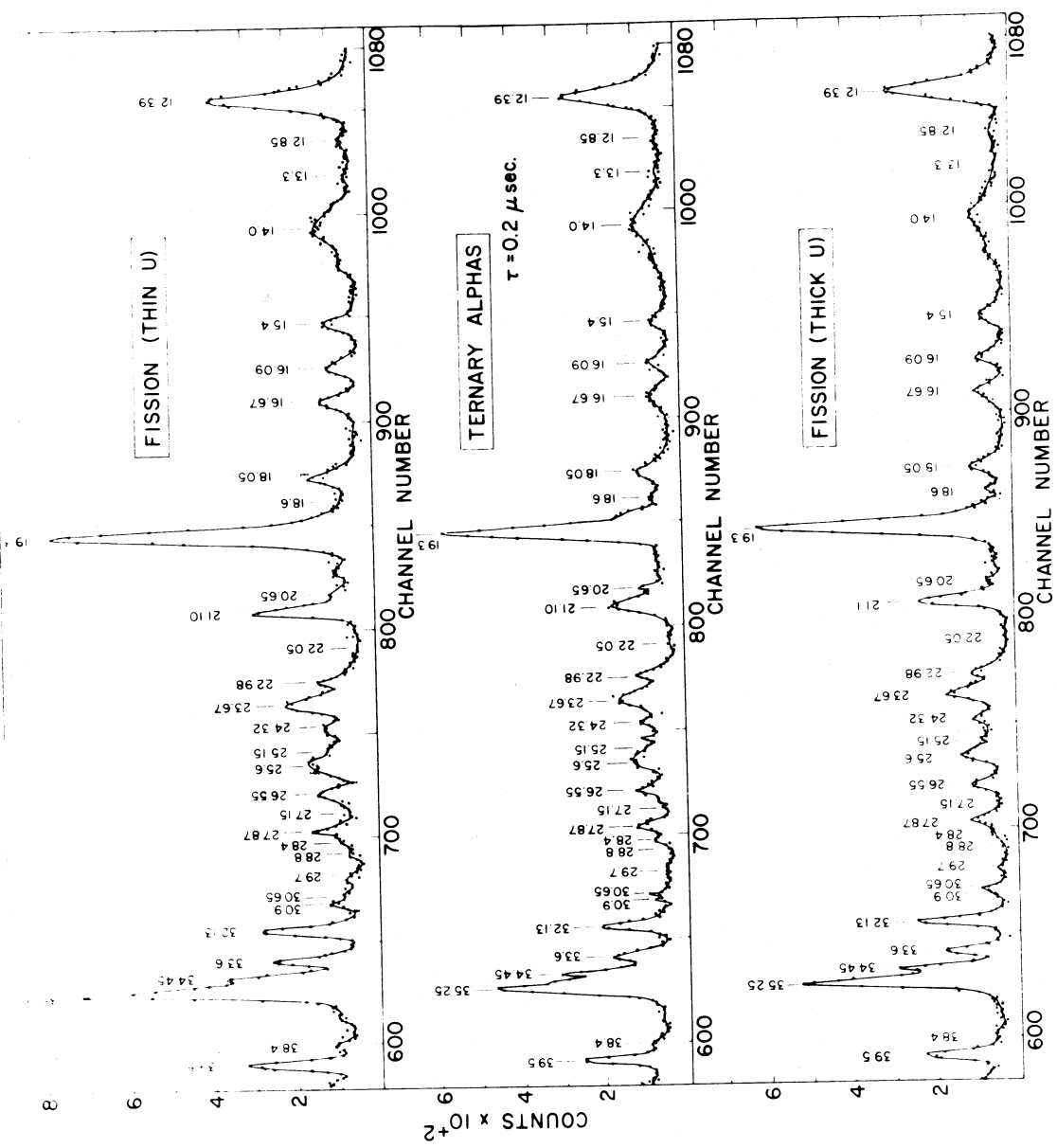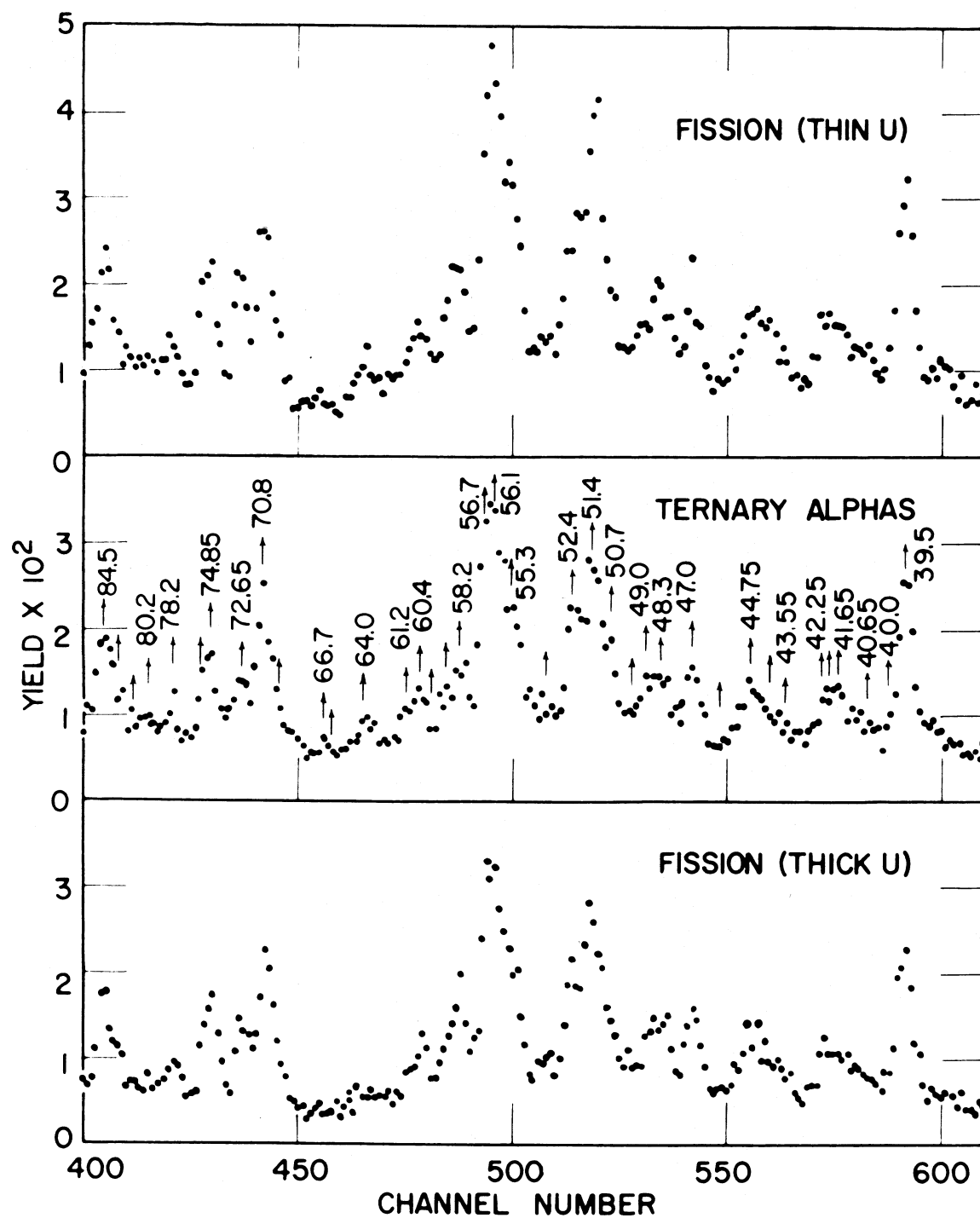
FIG. 12
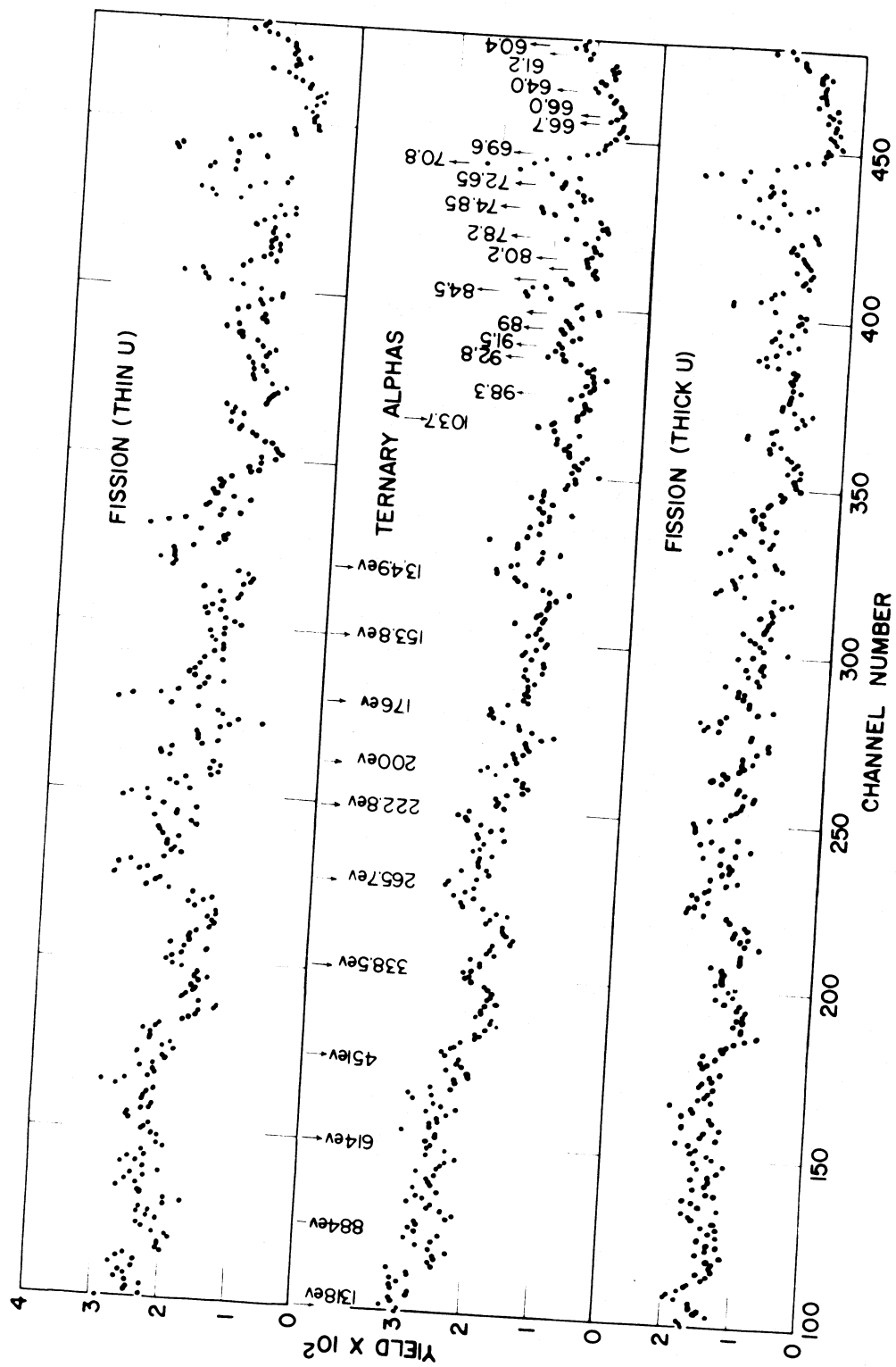
FIG. 13
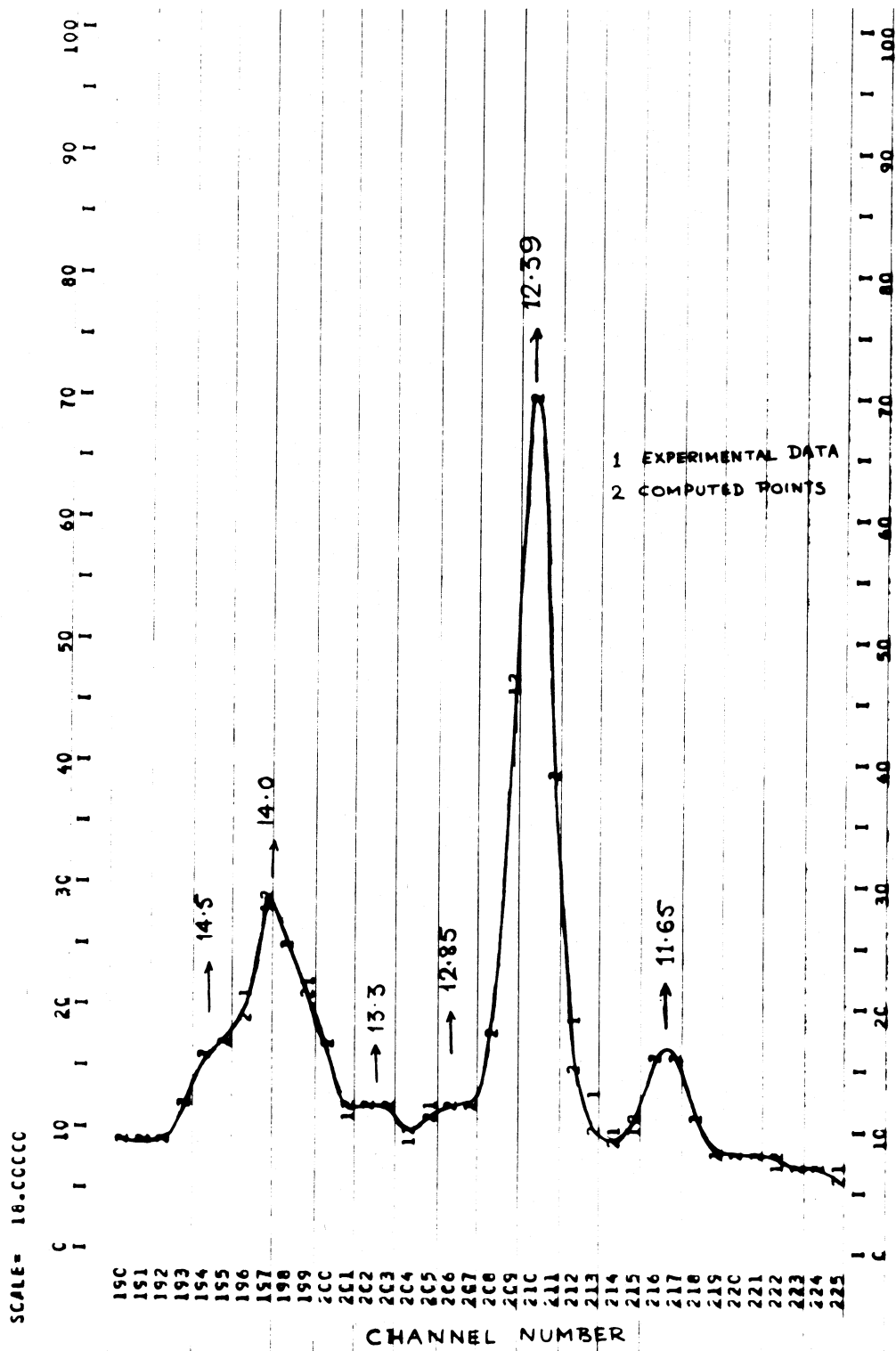
FIG. 14
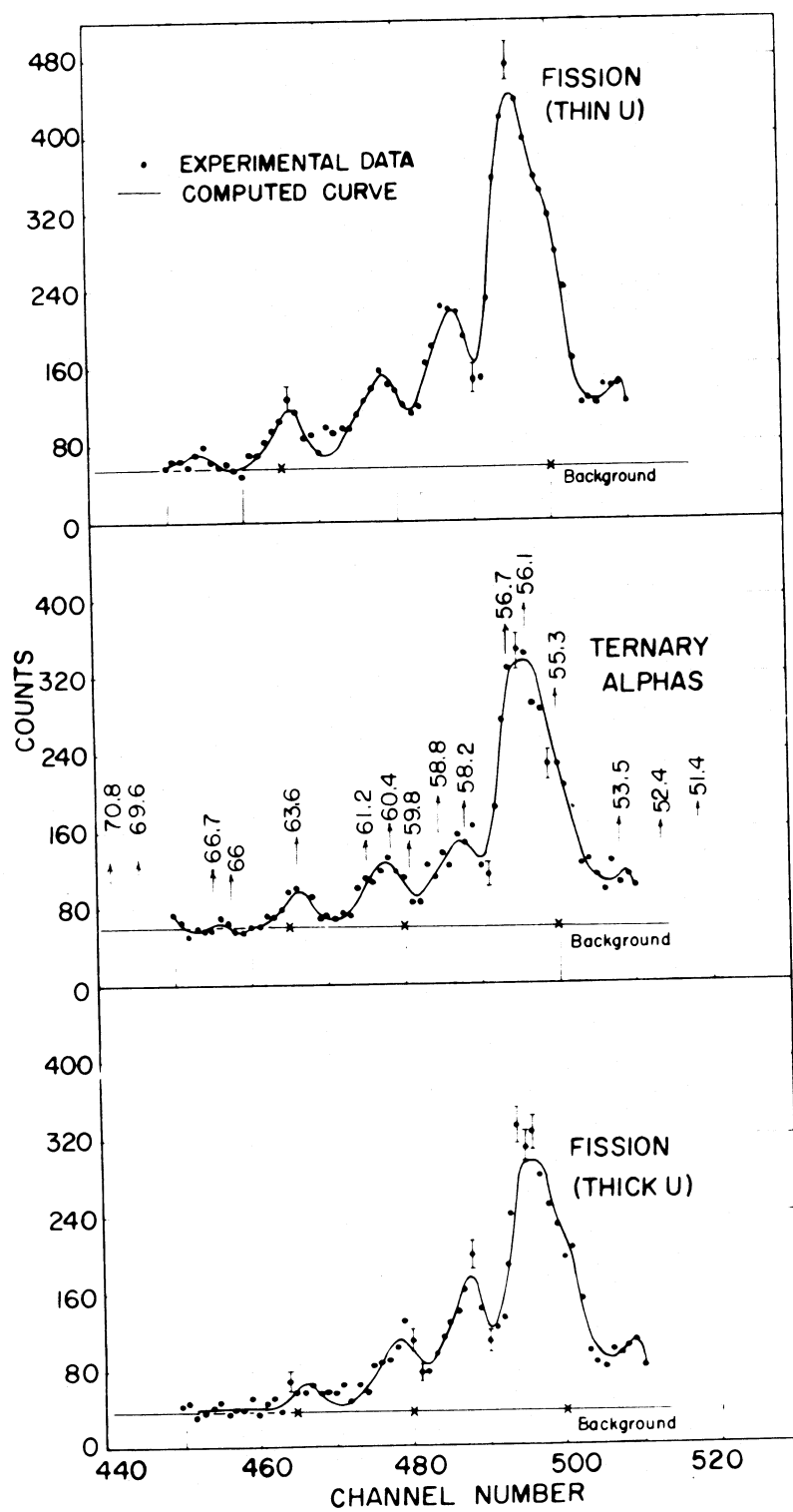
FIG. 15
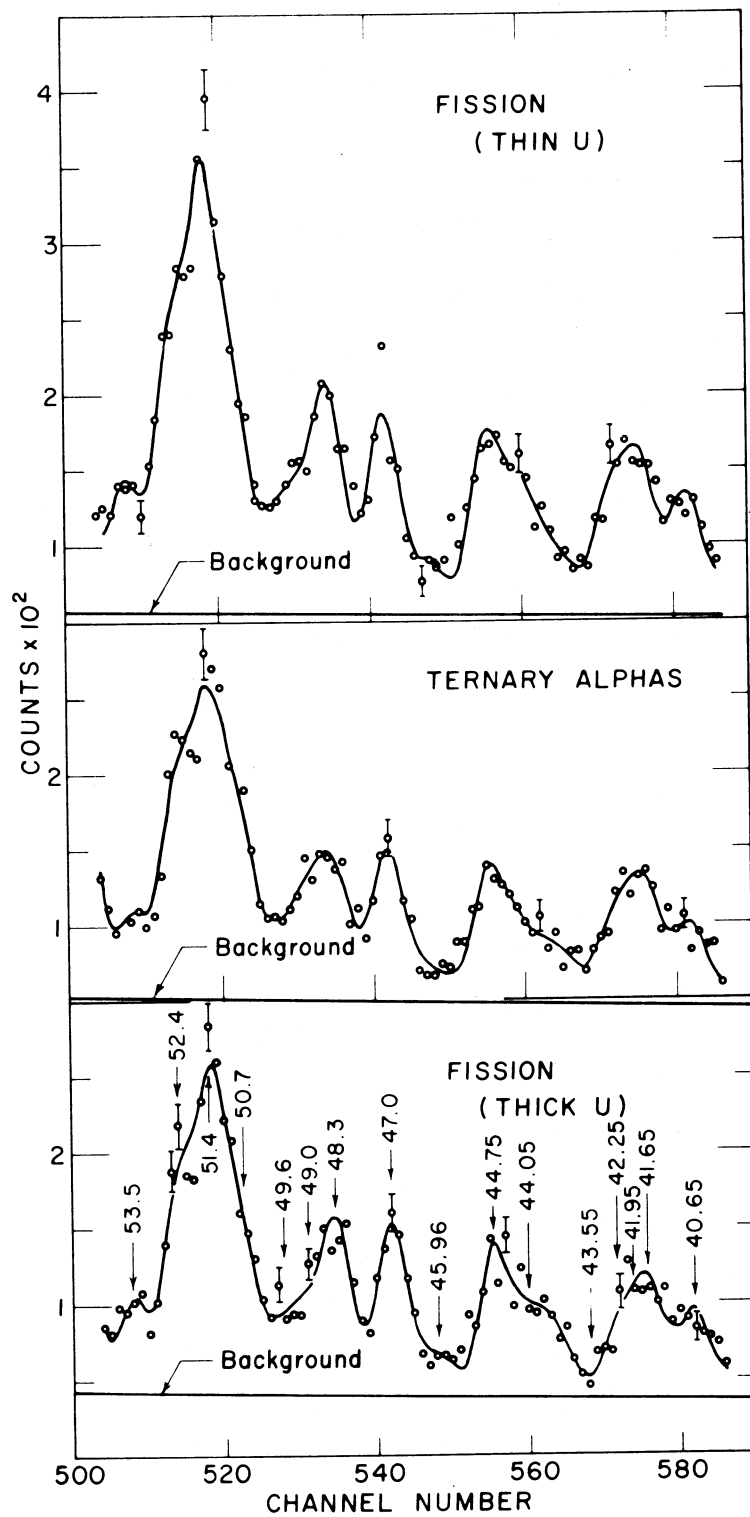
FIG. 16
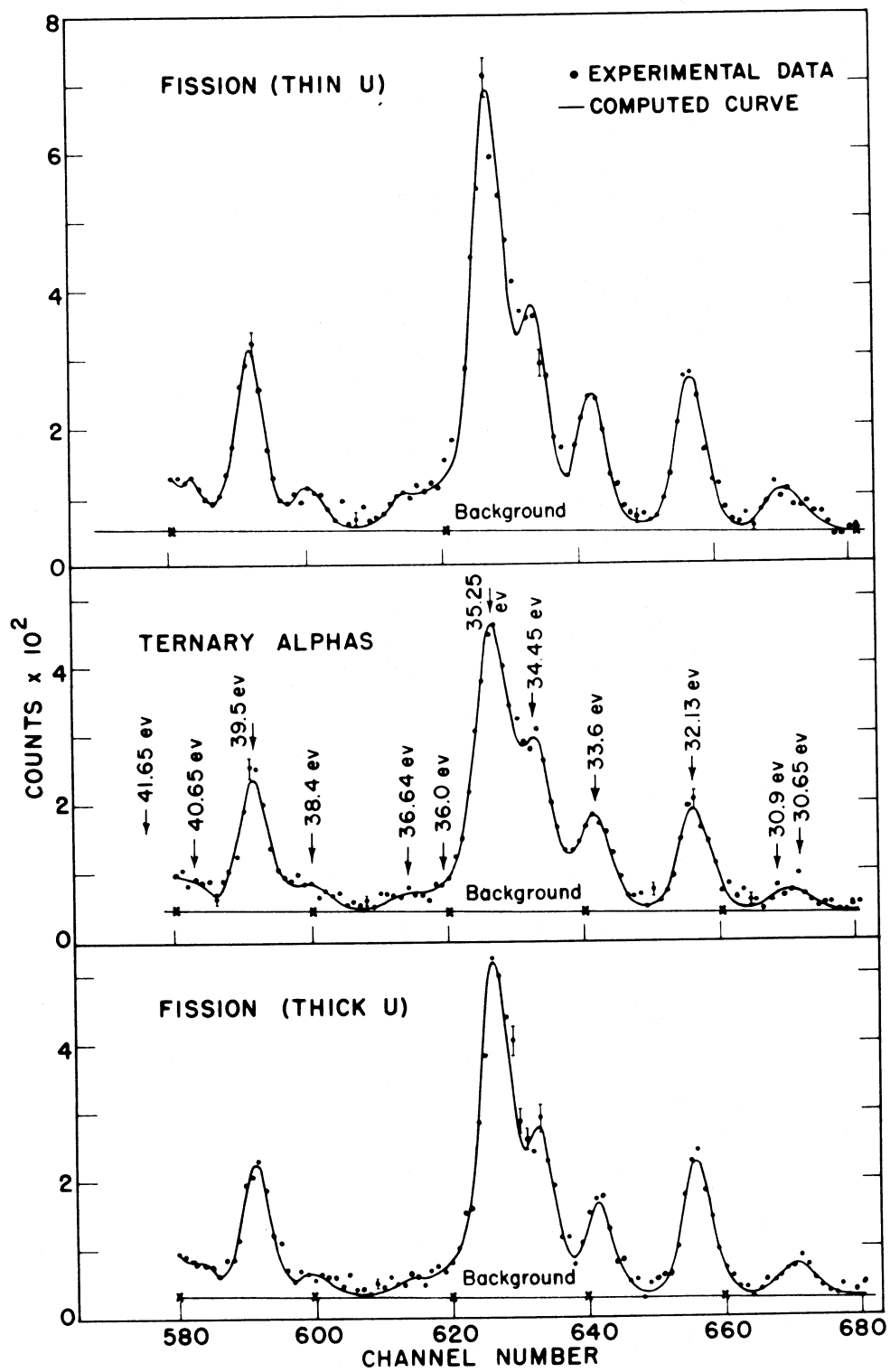
FIG. 17
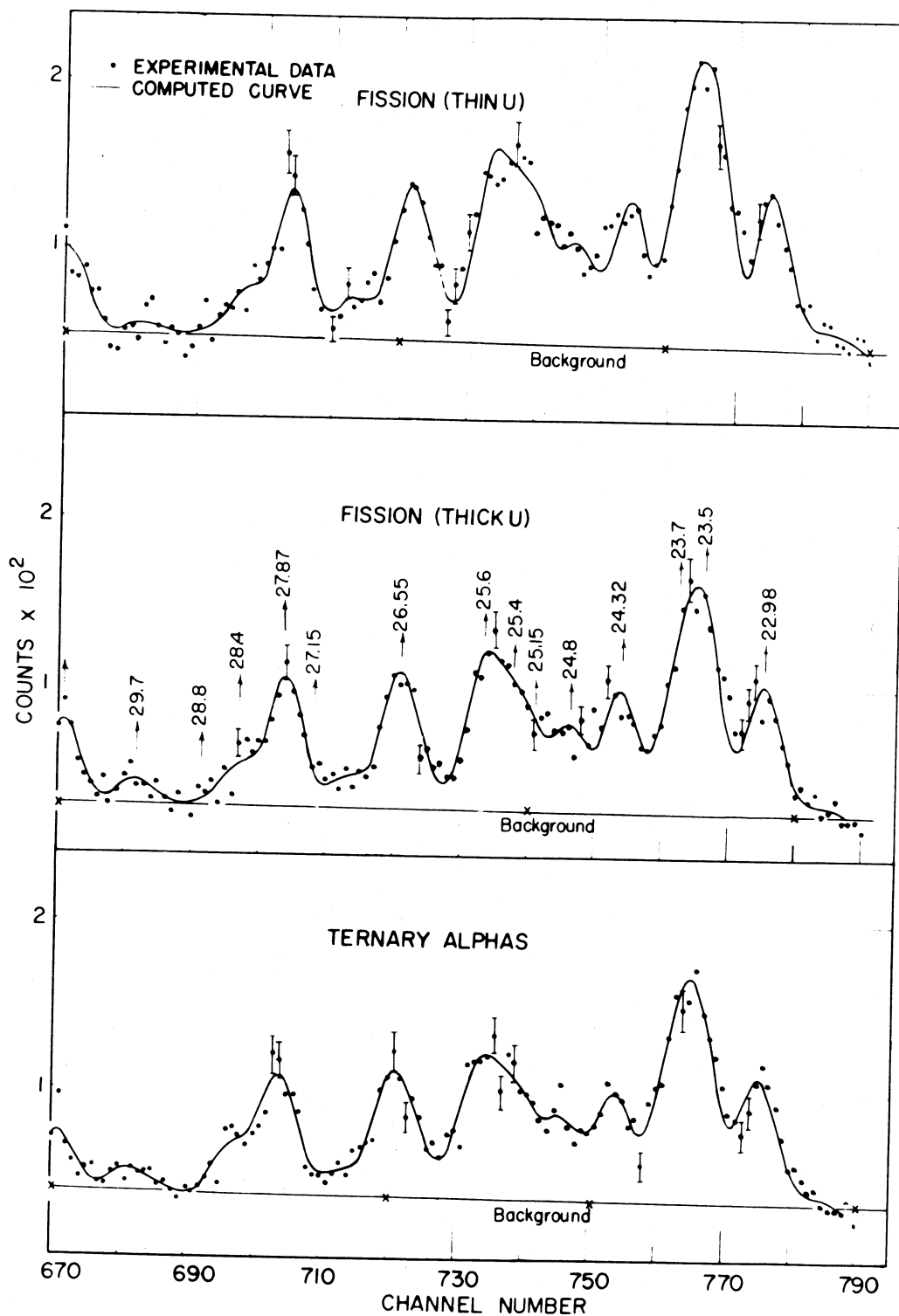
FIG. 18
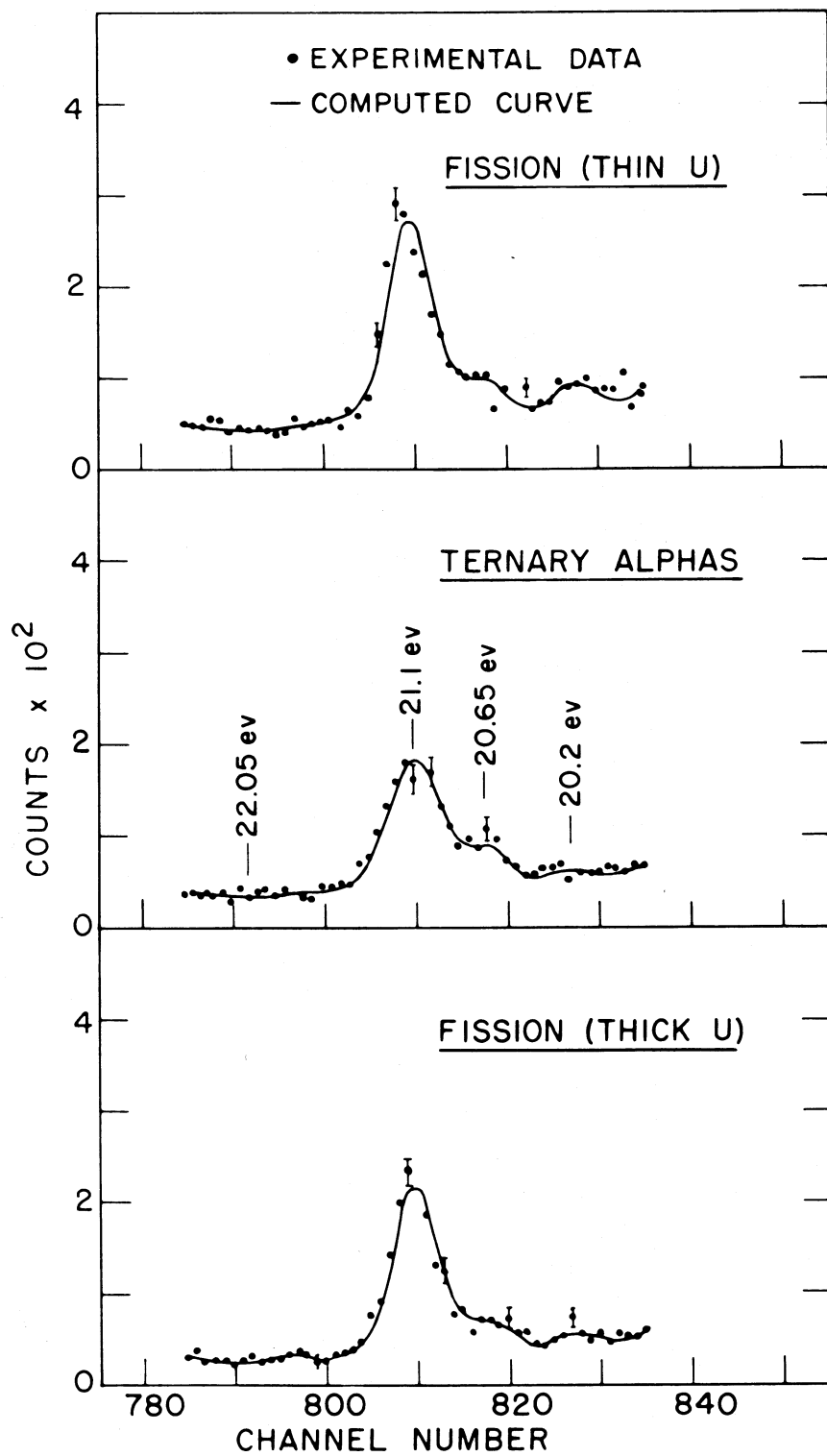
FIG. 19
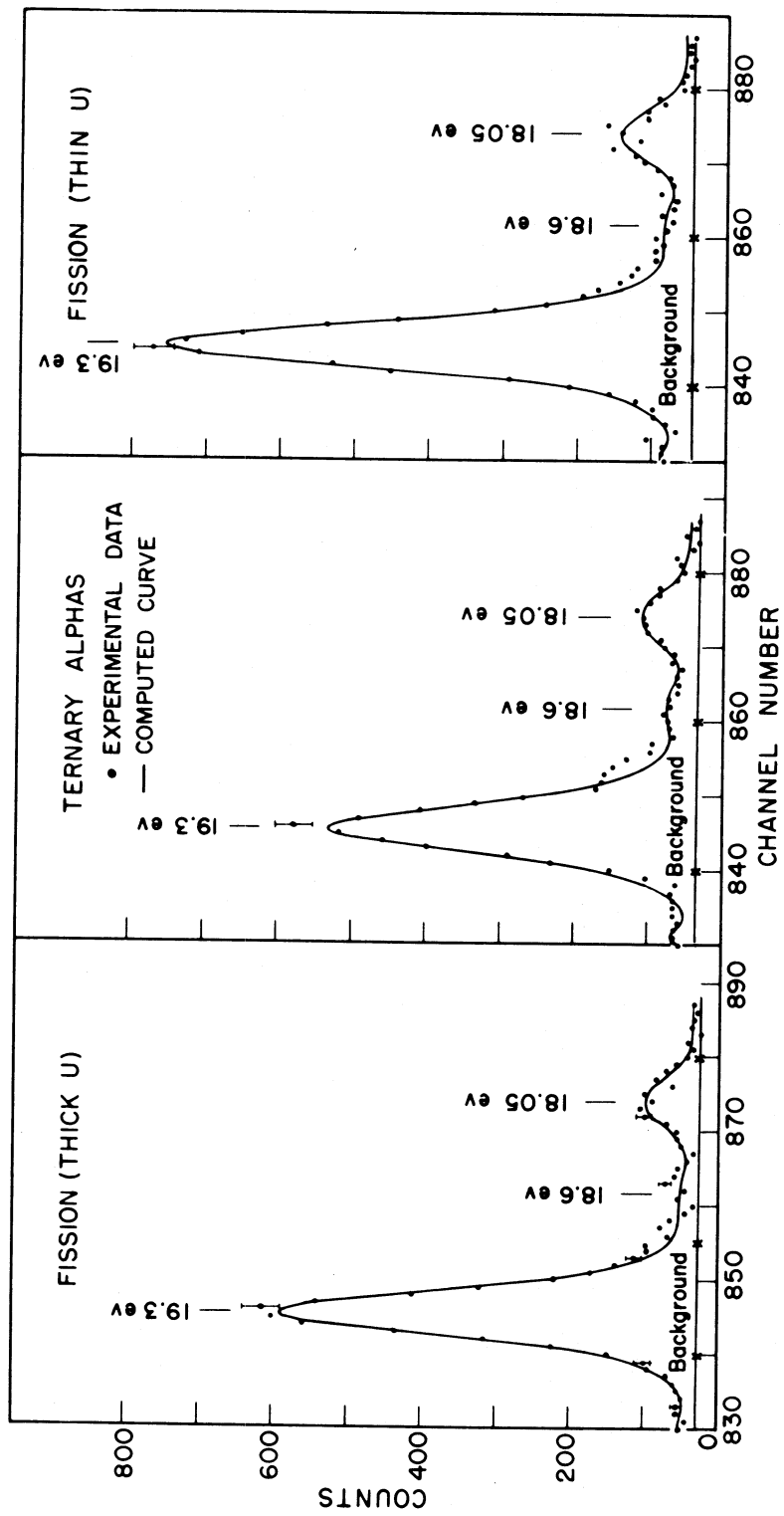
FIG. 20
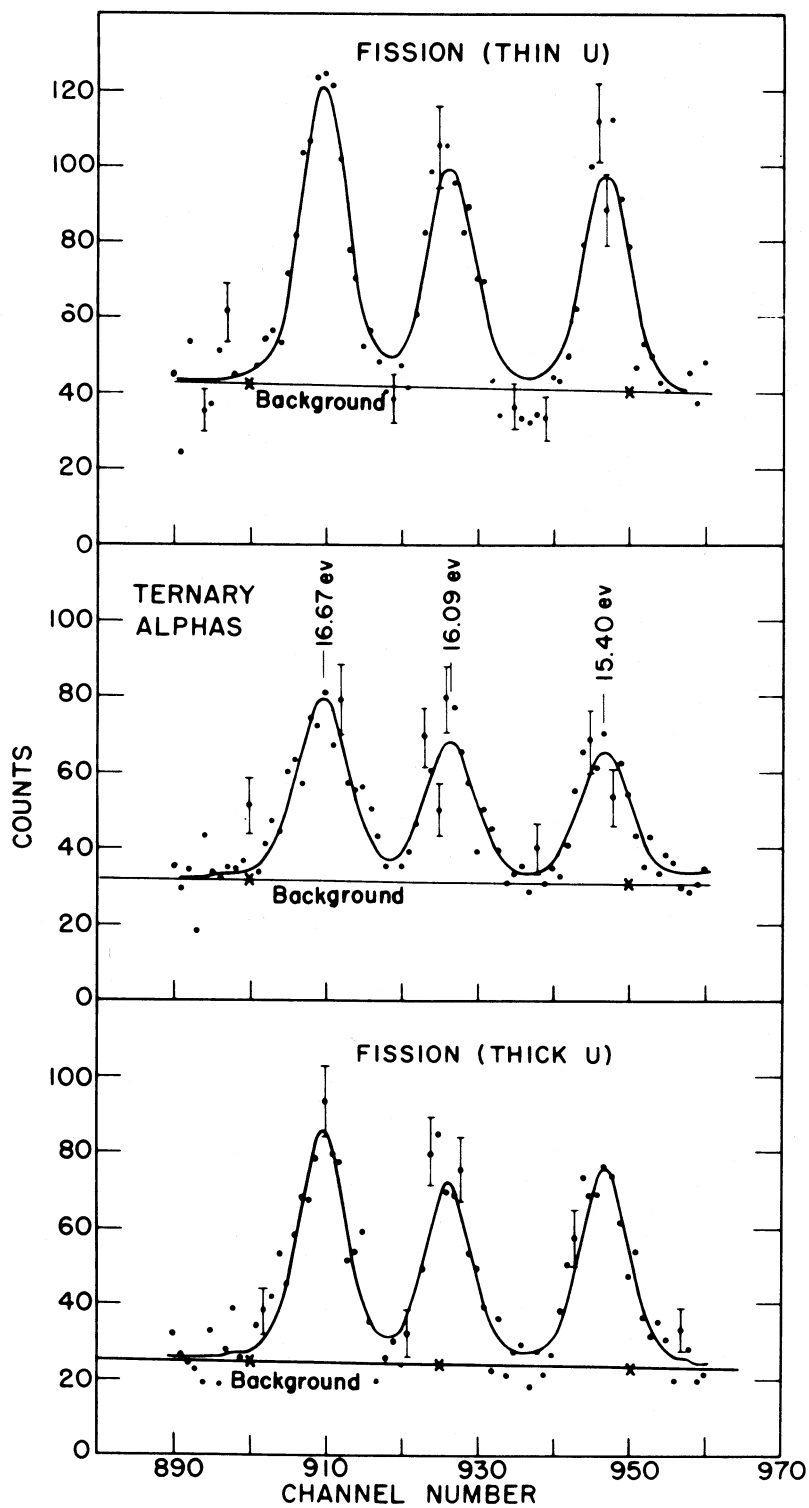
FIG. 21
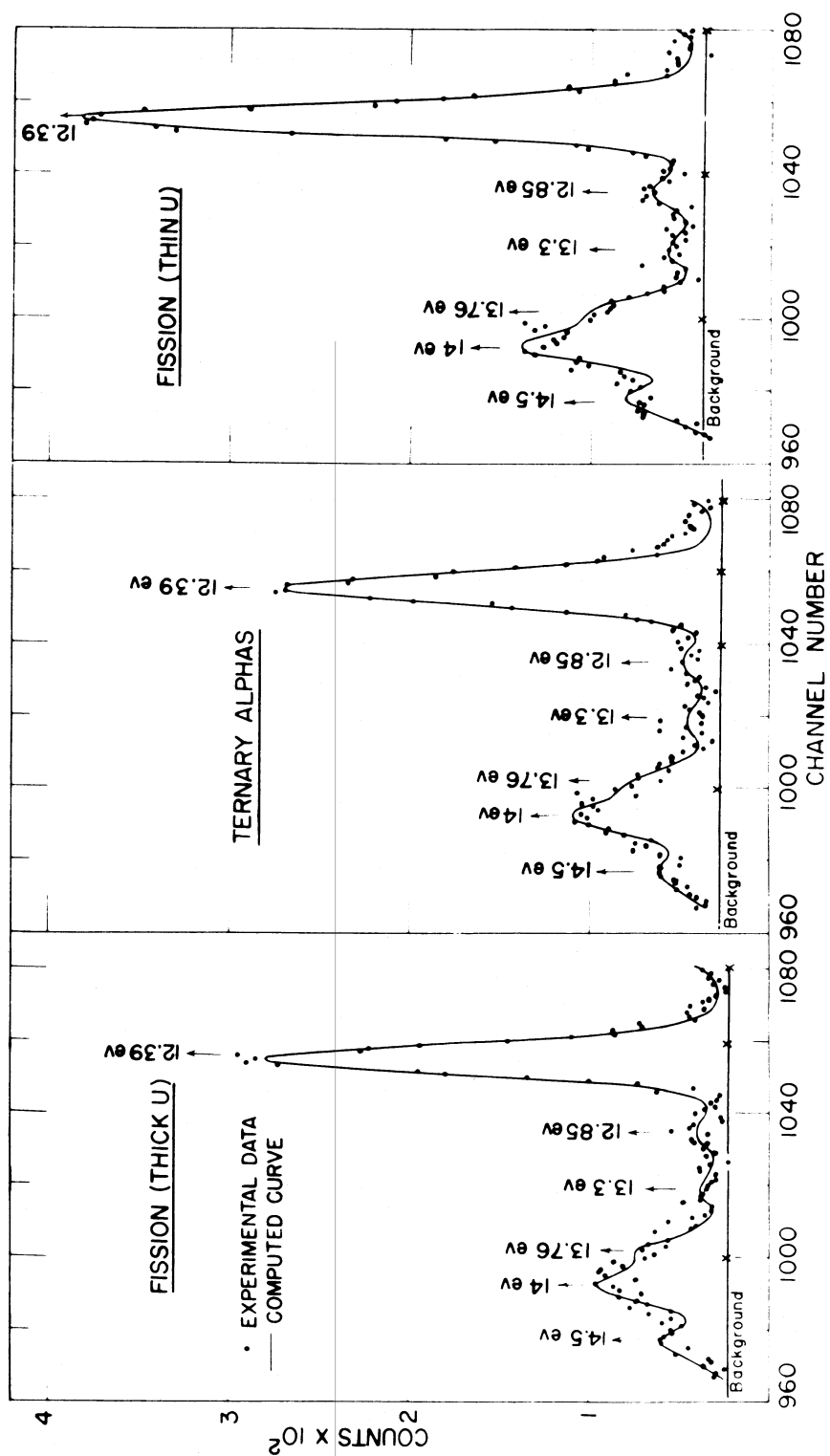
FIG. 22
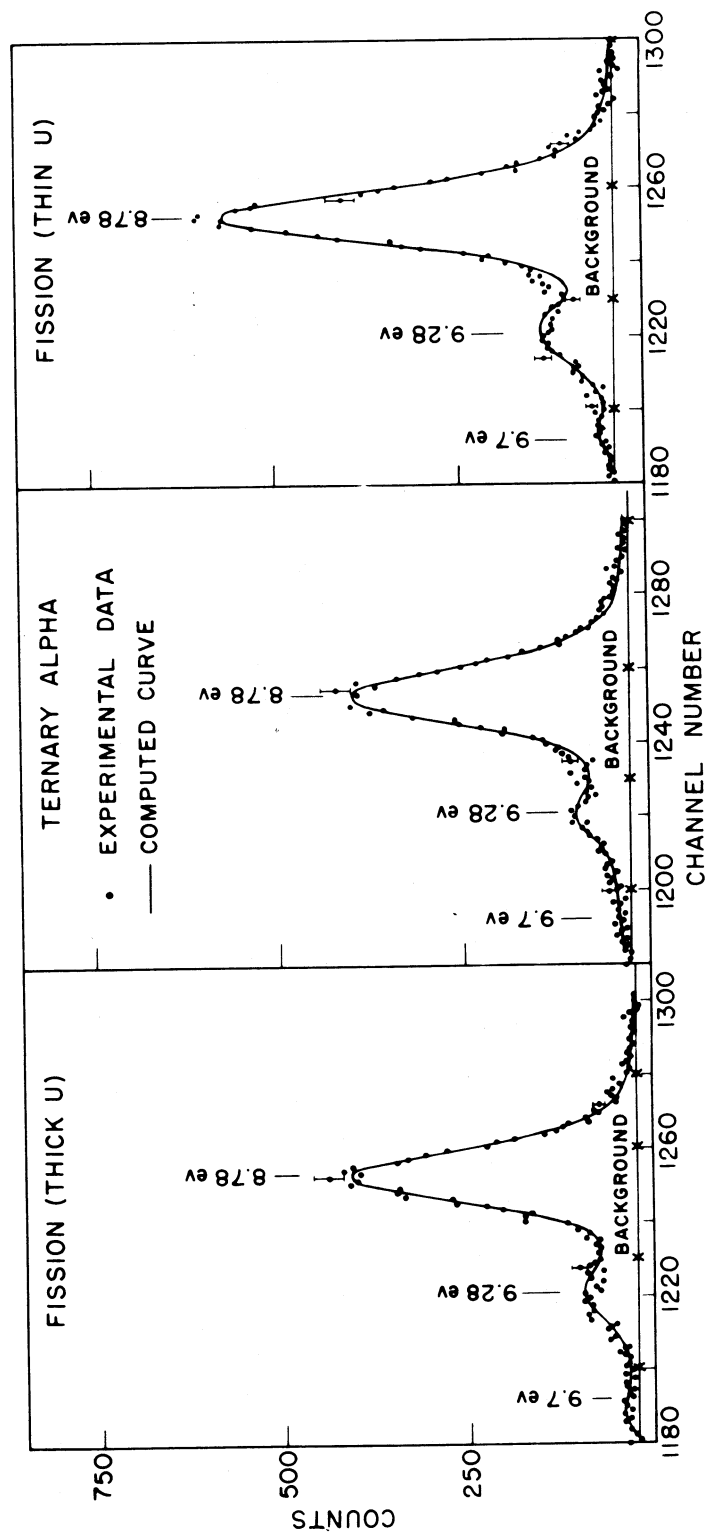
FIG. 23
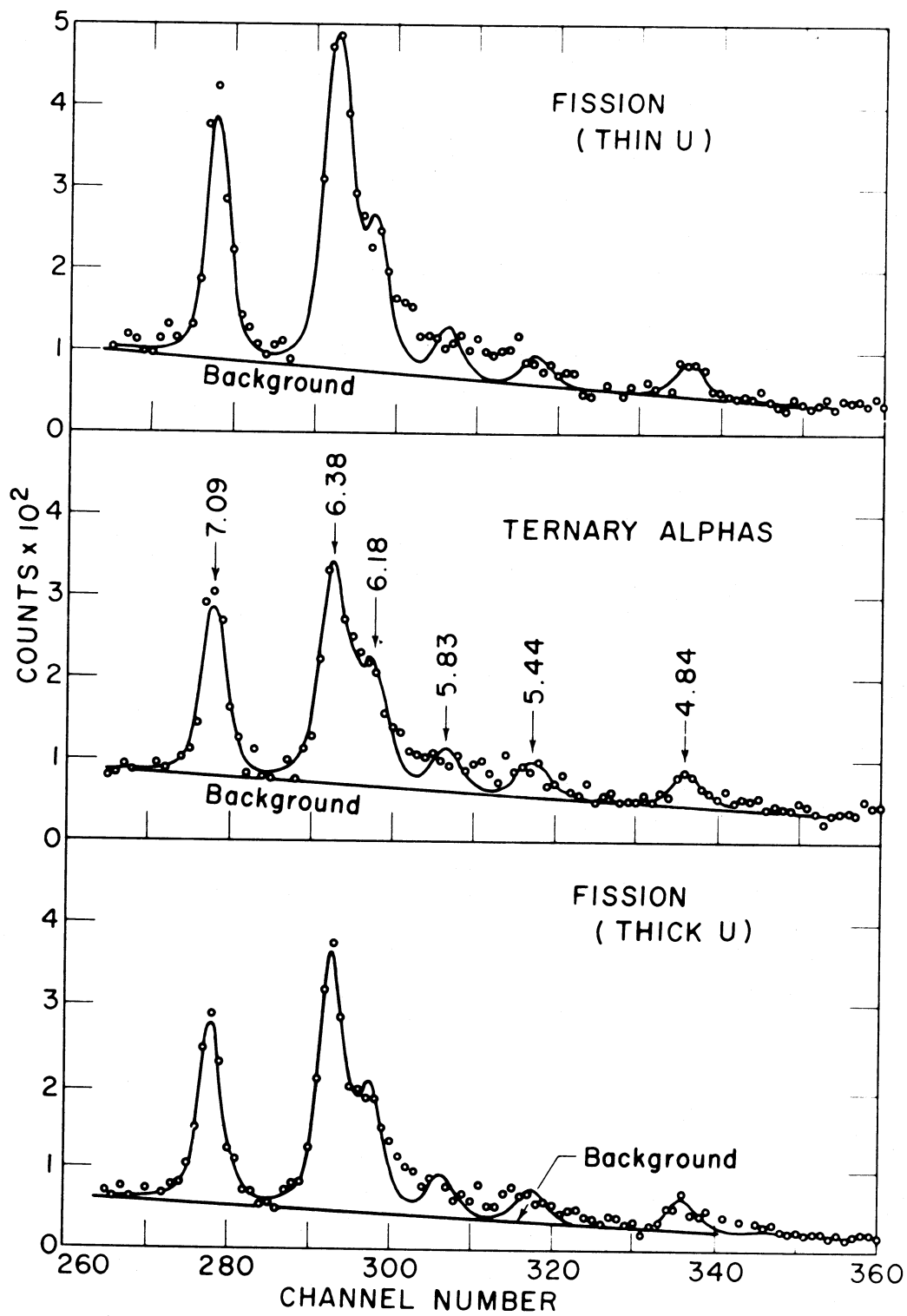
FIG. 24
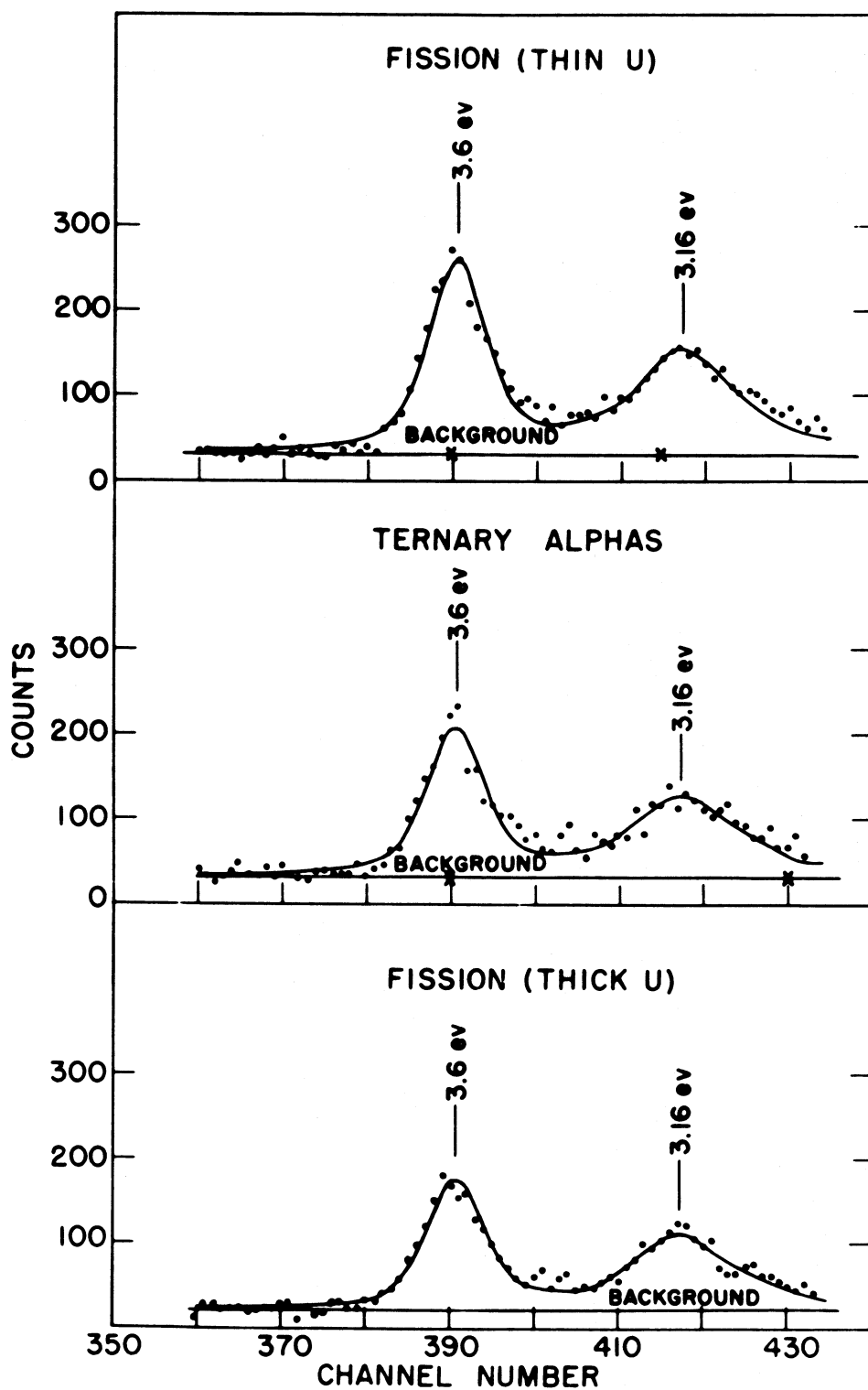
FIG. 25
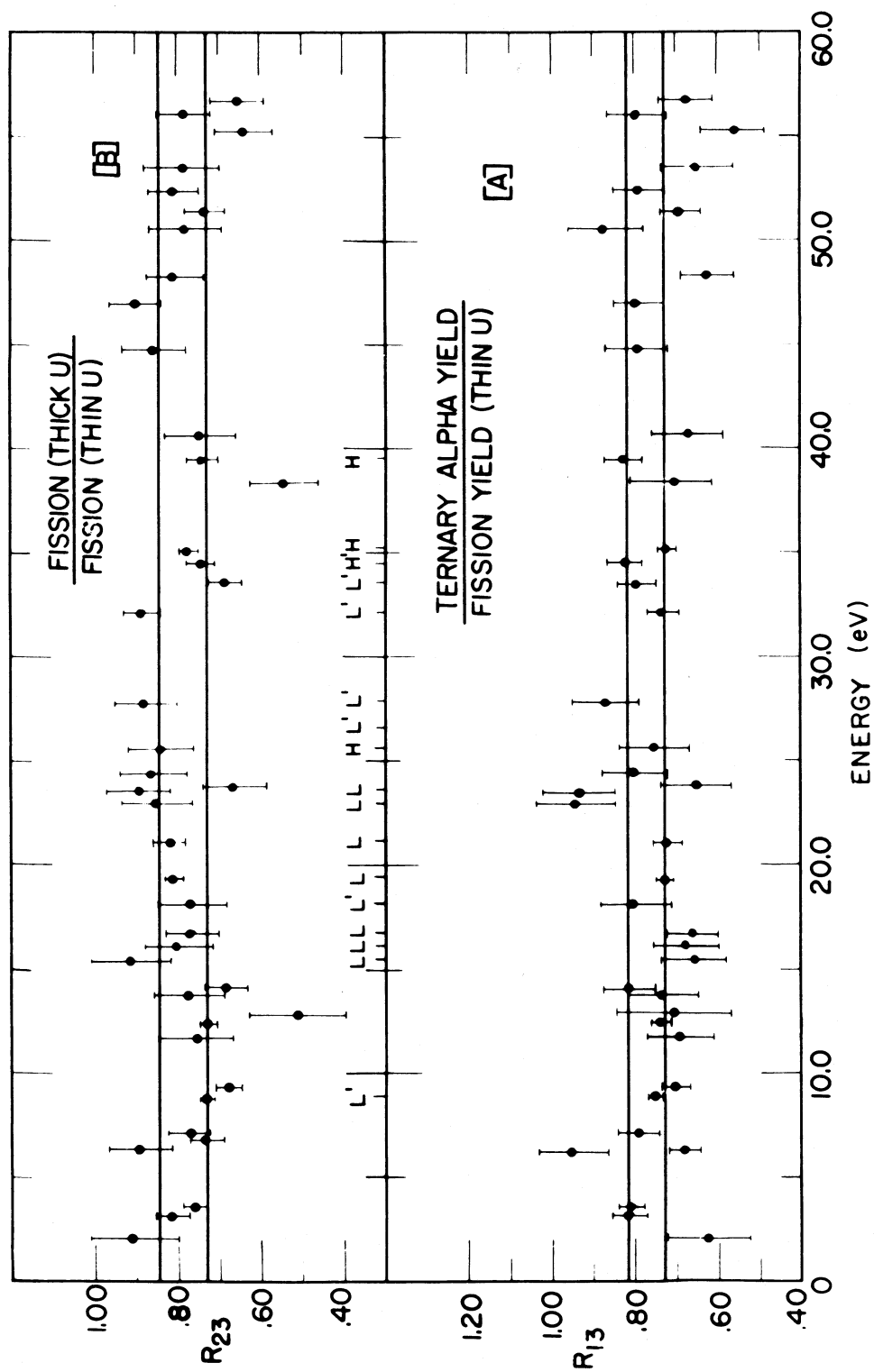
FIG. 26
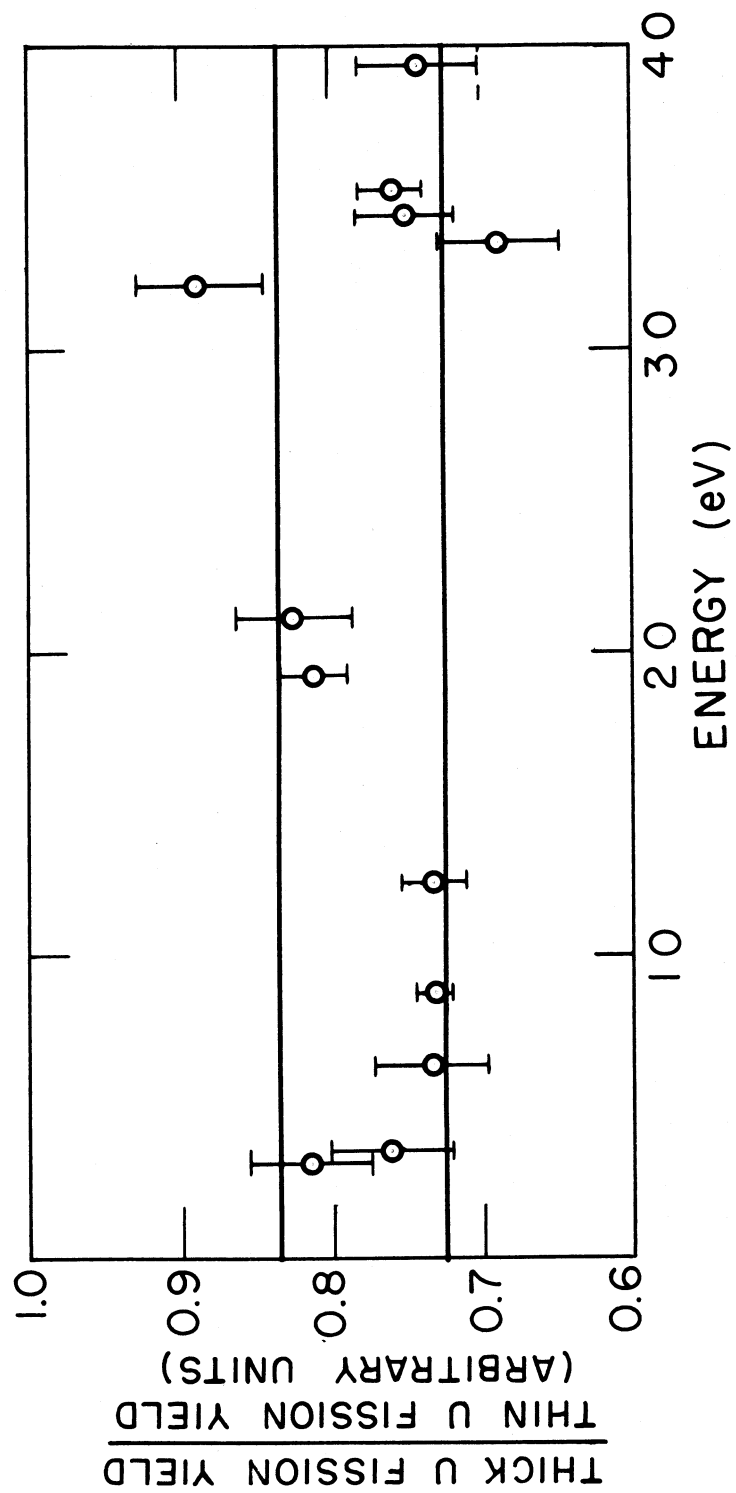
FIG. 27
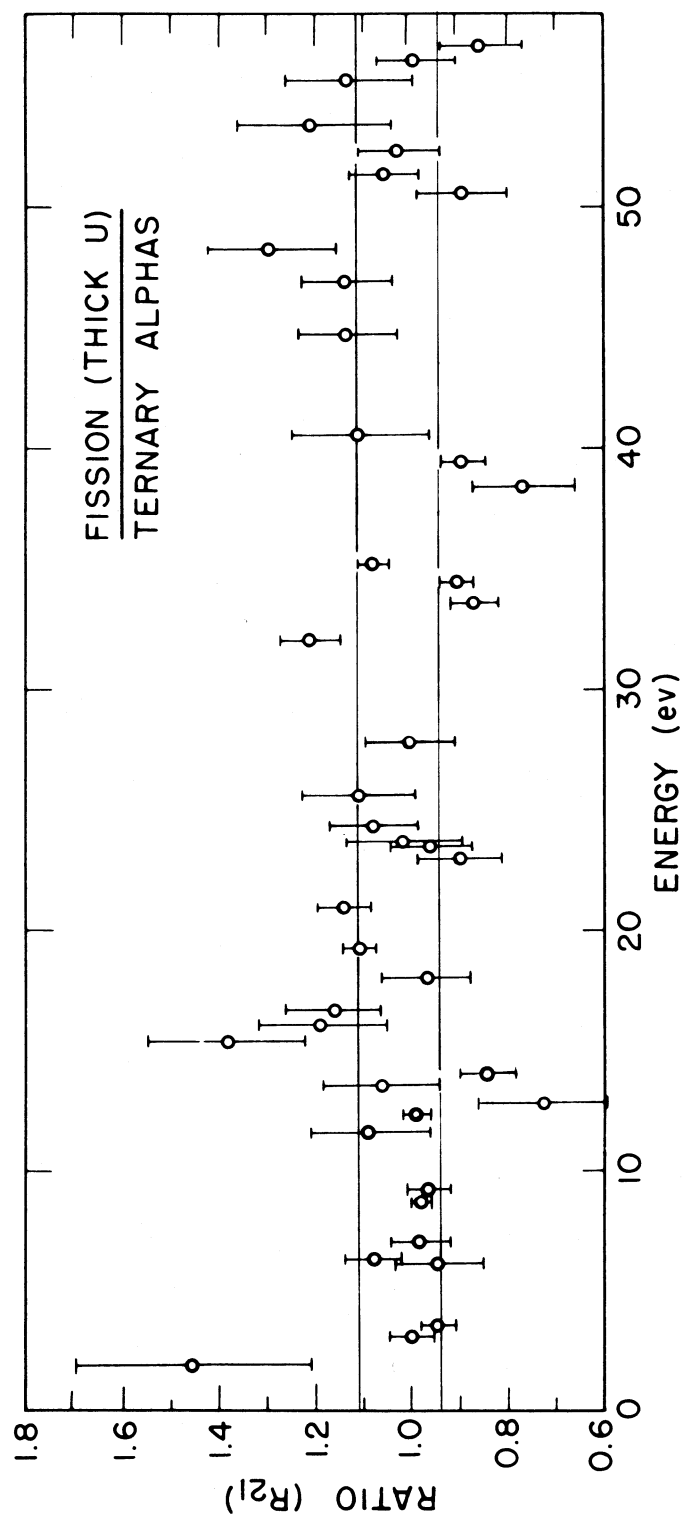
FIG. 28
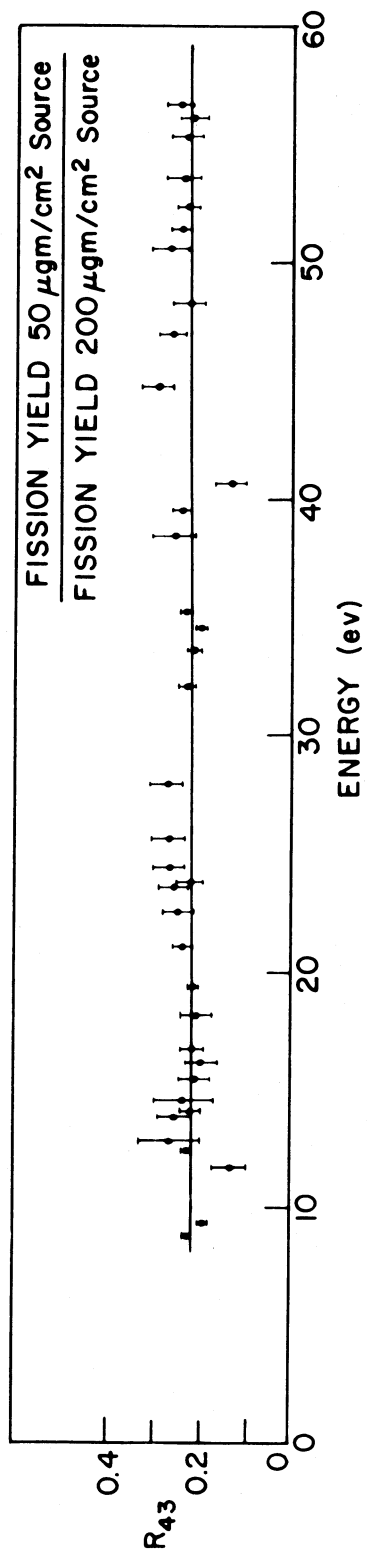
FIG. 29
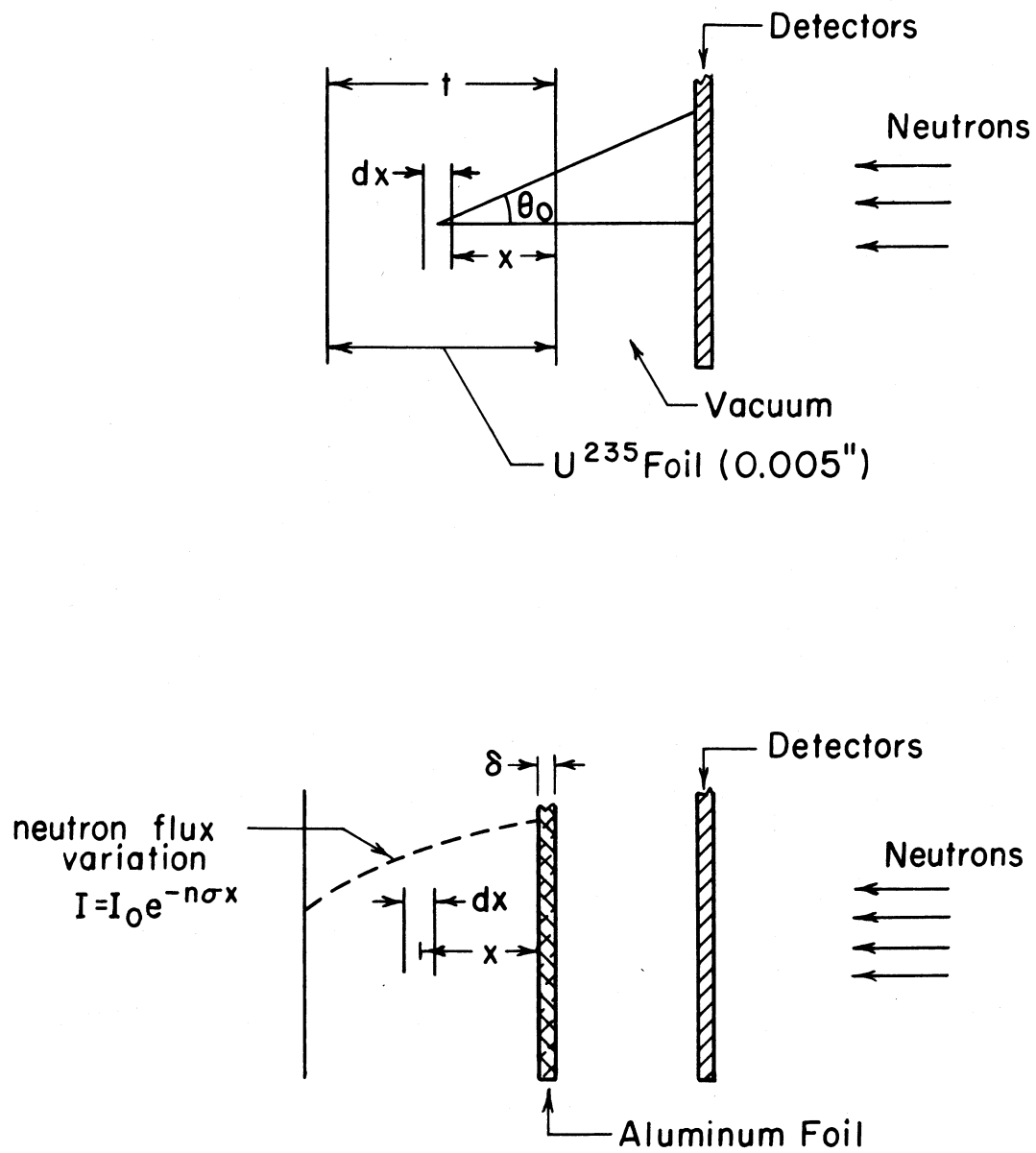
Detectors

Neutrons

t

dx

θ_0

x

Vacuum

U^{235}Foil (0.005")

Detectors

Neutrons

δ

neutron flux
variation
$I = I_0 e^{-n\sigma x}$

dx

x

Aluminum Foil

FIG. A-1

FIG. A-2

CHANNEL NUMBER

COUNTS x 10²

FIG. A-3

FIG. A-4

FIG. A-5

DETECTOR

DETECTOR
SOURCE
DISTANCE $2\frac{1}{2}$"

COUNTS X 10^2

CHANNEL NUMBER
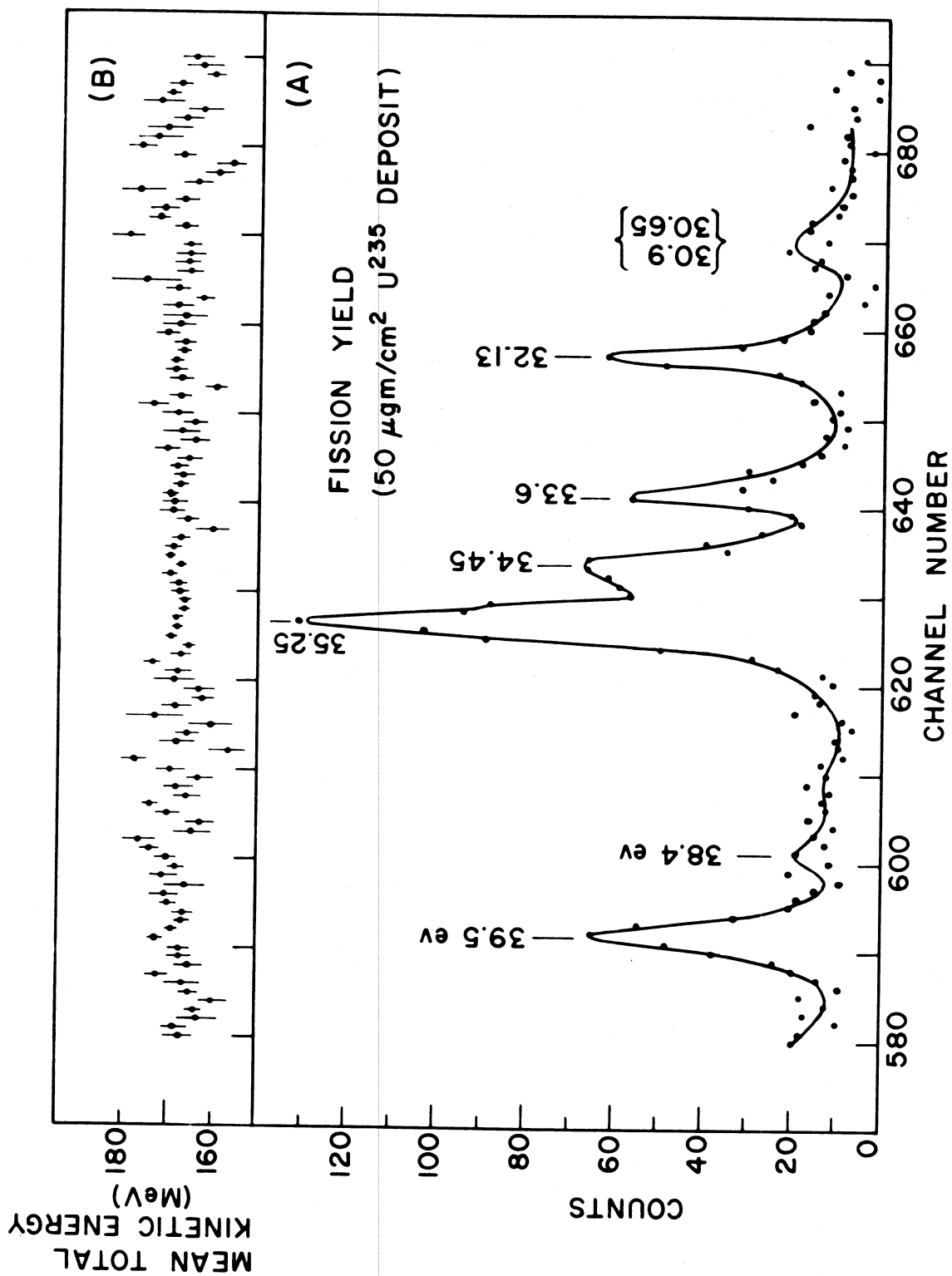
FIG. A-6

FIG. A-7

(a)

(b)

FIG. A-8

TERNARY ALPHAS

(A)

(B)
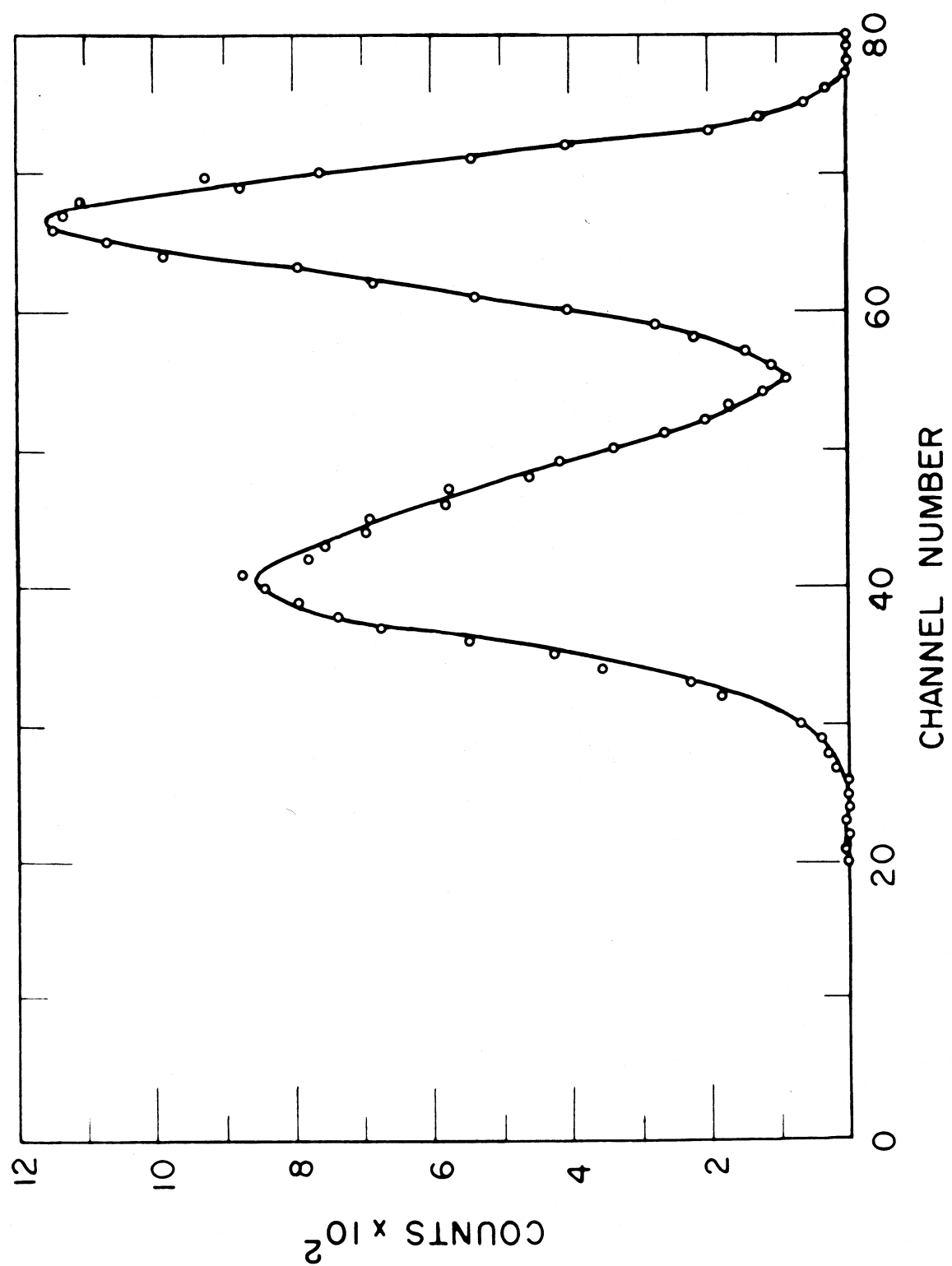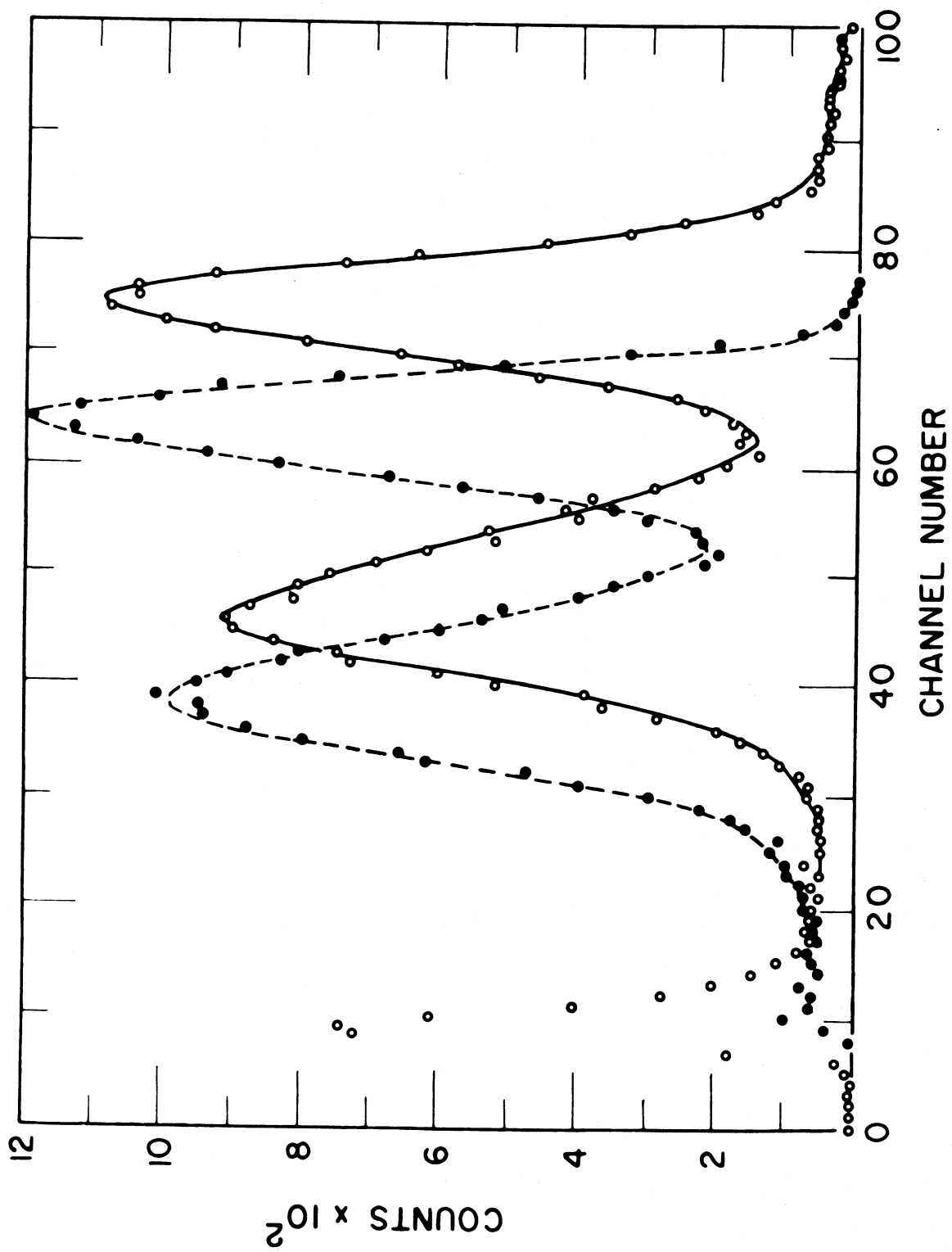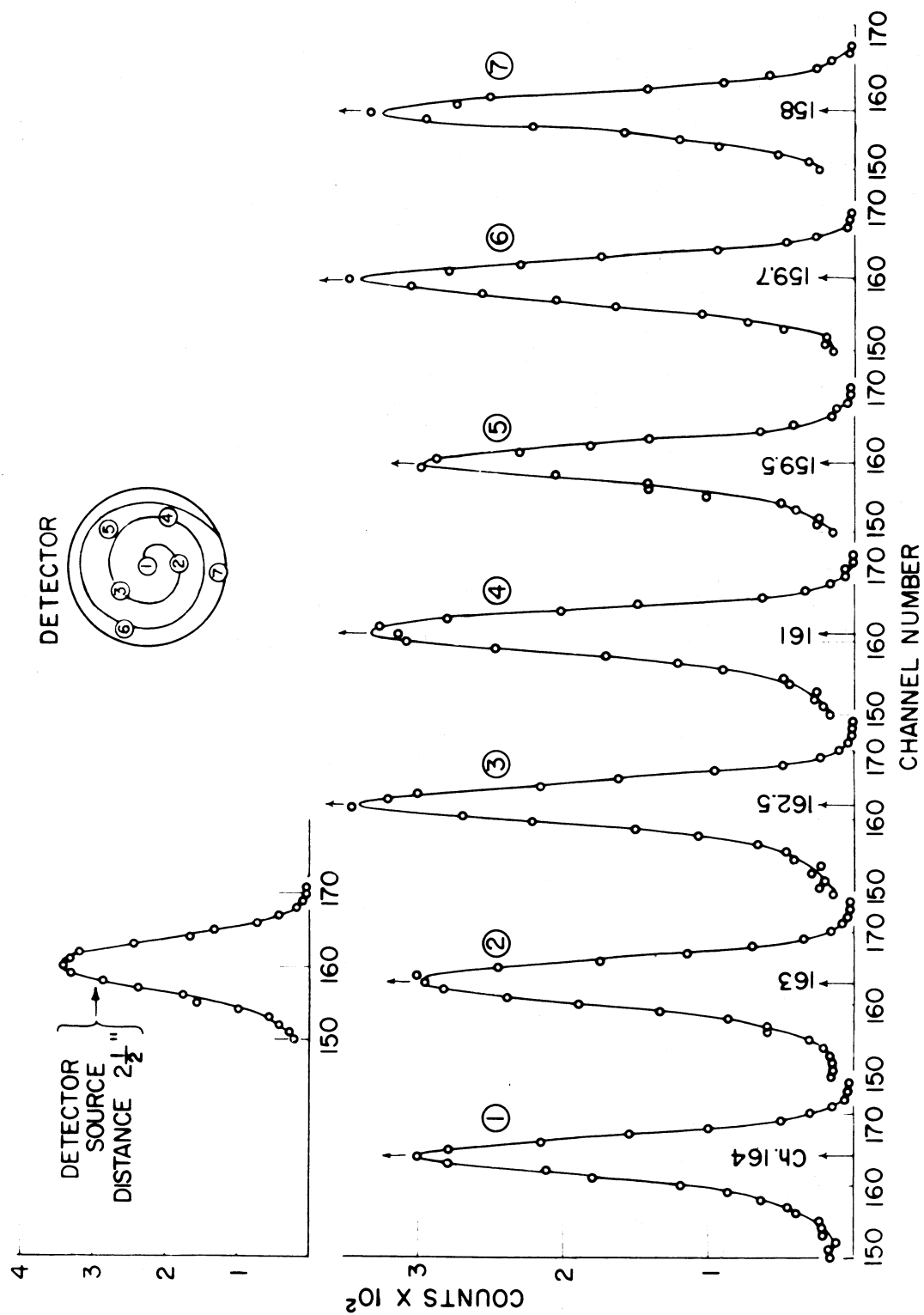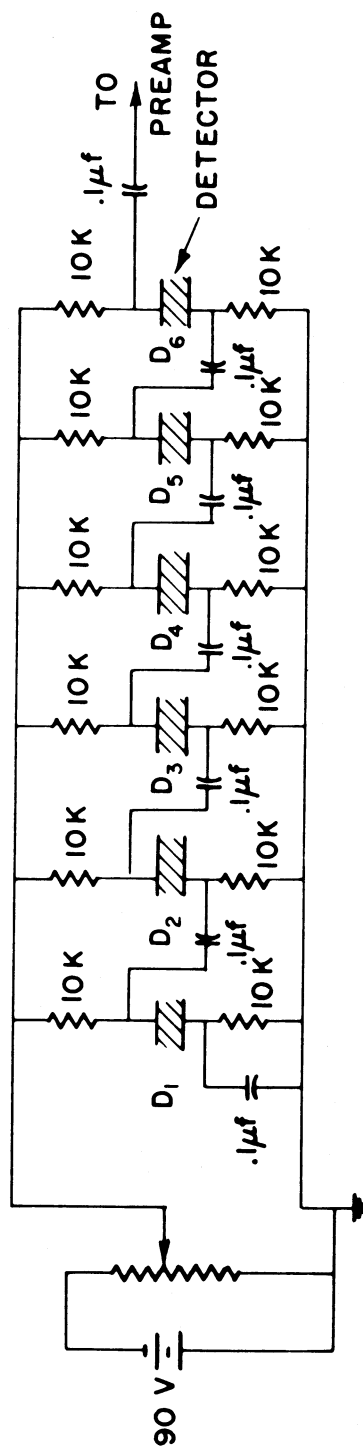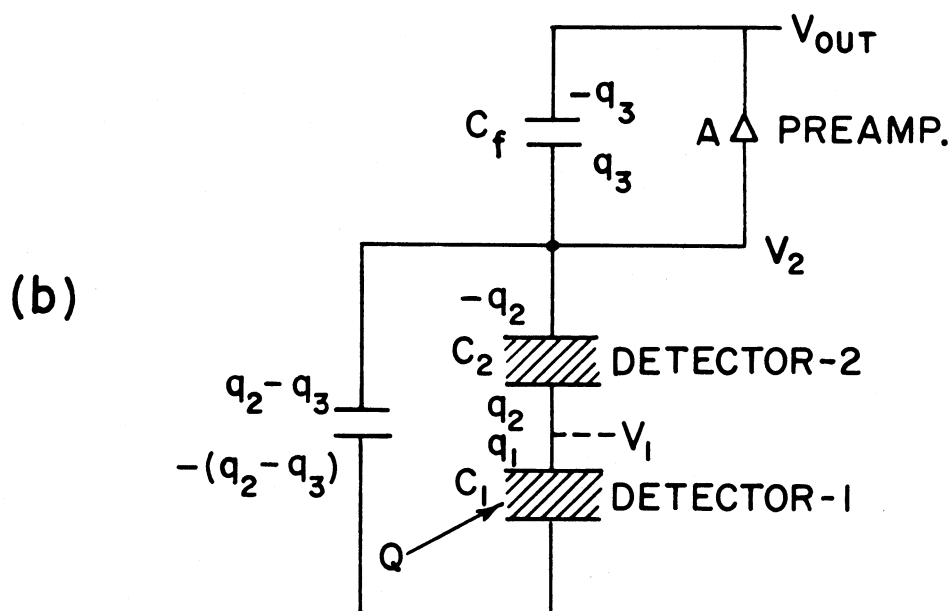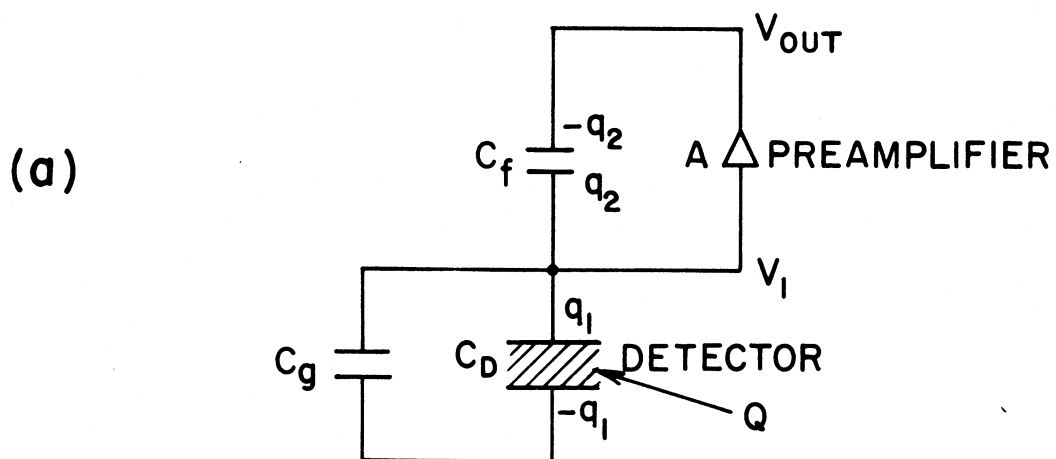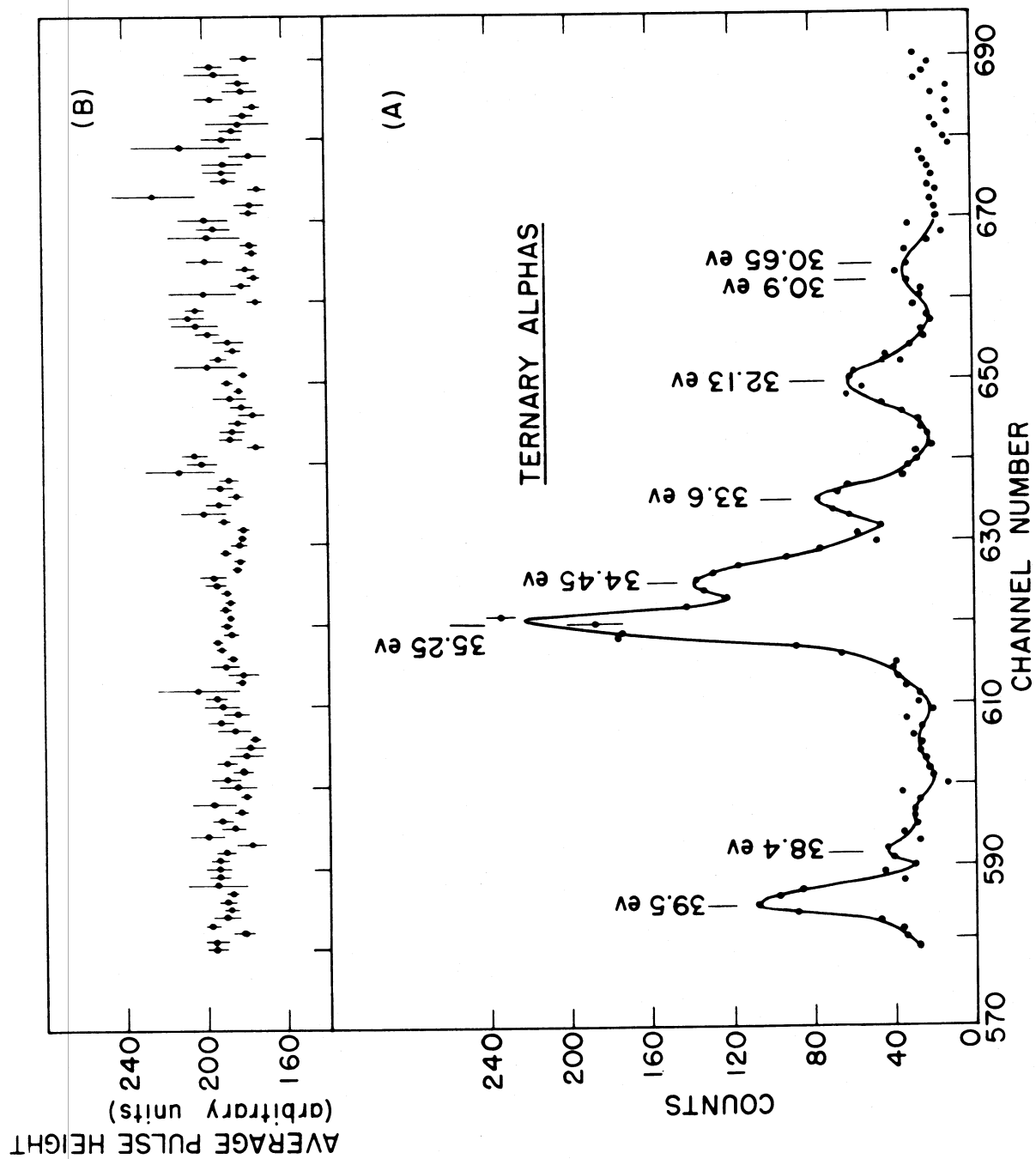
FIG. A-9
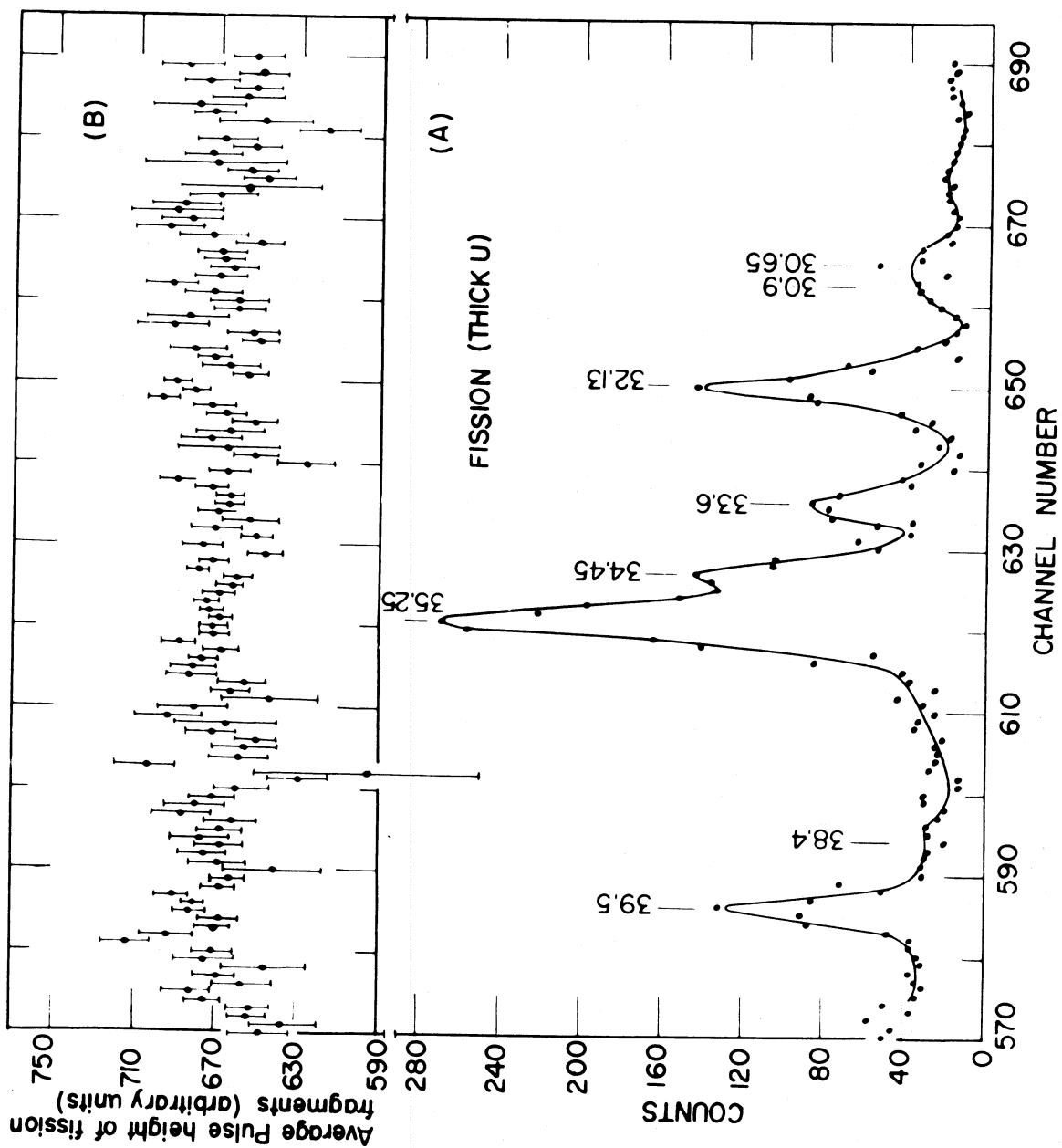
FIG. A-10

FIG. A-11

PICK-UP REJECTION CIRCUIT

FIG. A-12